

1-1-2012

Experimental And Numerical Invetigation Of Dependence Of Soil Thermal Conductivity On Temperature Water Content, And Soil Texture

Behnam Jowkar-Baniani
Ryerson University

Follow this and additional works at: <http://digitalcommons.ryerson.ca/dissertations>

 Part of the [Mechanical Engineering Commons](#)

Recommended Citation

Jowkar-Baniani, Behnam, "Experimental And Numerical Invetigation Of Dependence Of Soil Thermal Conductivity On Temperature Water Content, And Soil Texture" (2012). *Theses and dissertations*. Paper 1501.

This Thesis is brought to you for free and open access by Digital Commons @ Ryerson. It has been accepted for inclusion in Theses and dissertations by an authorized administrator of Digital Commons @ Ryerson. For more information, please contact bcameron@ryerson.ca.

EXPERIMENTAL AND NUMERICAL INVESTIGATION OF DEPENDENCE OF SOIL THERMAL CONDUCTIVITY ON TEMPERATURE, WATER CONTENT, AND SOIL TEXTURE

by

Behnam Jowkar-Baniani

B.Eng. Ryerson University,
Toronto, 2009

A thesis presented to

Ryerson University

In partial fulfillment of
the requirements for the degree of
Master of Applied Science

In the program of
Mechanical and Industrial Engineering

Toronto, Ontario, Canada, 2012

© Behnam Jowkar 2012

AUTHOR'S DECLARATION

I hereby declare that I am the sole author of this thesis. This is a true copy of the thesis, including any required final versions, as accepted by my examiners.

I authorize Ryerson University to lend this thesis to other institutions or individuals for the purpose of scholarly research.

I further authorize Ryerson University to reproduce this thesis by photocopying or by other means, in total or in part, at the request of other institutions or individuals for the purpose of scholarly research.

I understand that my thesis may be made electronically available to the public.

ABSTRACT

Experimental and Numerical Investigation of Dependence of Soil Thermal Conductivity on Temperature, Water content, and Soil Texture

Behnam Jowkar-Baniani

Master of Applied Science, 2012

Program of Mechanical and Industrial Engineering, Ryerson University

Comprehensive set of thermal conductivity data for a loam soil was generated, for temperature variations from 5°C to 92°C and water content variations from dry to saturation, and compared to two other soil textures. The results exhibited similar characteristics as those of the other textures, where a significant change in soil thermal conductivity was. Using the thermal conductivity data sets, a model representing heat and mass transfer in soil was used to study the apparent thermal conductivity due to vapour migration. In addition, a computer simulation of a ground source heat pump system was developed, where the experimental data was used to investigate the impact of water content and soil texture variation on the GSHP performance. It was observed that the GSHP energy consumption varied more prominently when the soil wetness varied from dryness to full saturation and less significantly when the soil type varied from coarse to finer texture.

ACKNOWLEDGEMENTS

The author would like to express his deepest appreciation to Dr. Wey Leong and Dr. Marc Rosen for their guidance and encouragement throughout the project.

The author wishes to thank the engineering support staff at Ryerson University. Particularly Joseph Amankrah, Alan Machin, and Andrew Heim for their advice and assistance during the sample preparation phase of the project.

The author also wishes to thank Dr. Jasmin Schönenberger of Bavarian Environment Agency Laboratory in Marktredwitz, Germany, for providing XRD/XRF analyses of the Richmond Hill fine sandy loam and the Kortright Centre loam and Dr. Jinyuan Liu and Robin Luong of the Department of Civil Engineering, Ryerson University, for using their laboratory to measure the saturated hydraulic conductivity of soils.

Finally, I wish to thank my family and friends for their support over the course of this project.

TABLE OF CONTENTS

AUTHOR’S DECLARATION	ii
ABSTRACT	iii
ACKNOWLEDGEMENTS	iv
TABLE OF CONTENTS	v
LIST OF FIGURES	xi
LIST OF TABLES	xiv
NOMENCLATURE	xvi
CHAPTER 1 INTRODUCTION.....	1
1.1 Motivation.....	1
1.2 Scope and Objectives.....	3
1.3 Outline of the Thesis.....	4
CHAPTER 2 BACKGROUND AND LITERATURE REVIEW	5
2.1 Background.....	5
2.1.1 Underground Thermal Energy Storage	5
2.1.2 Heat and Moisture Transfer in Soil	7
2.2 Literature Review	8
2.2.1 Impact of Heat and Moisture Transfer on Soil Thermal Conductivity	9
2.2.2 Impact of Soil Composition on Soil Thermal Conductivity.....	12

2.2.3	Heat and Moisture Transfer in Thermal Energy Storage	
	(TES) Applications.....	14
CHAPTER 3 APPROACH AND METHODOLOGY		18
3.1	Experimental Analysis of Soil Thermal Conductivity.....	18
3.1.1	Experimental Limitations	20
3.2	Study of the Effect of Vapour Migration on Soil Thermal Conductivity.....	20
3.3	Implementation of Results	21
CHAPTER 4 EXPERIMENTAL INVESTIGATION OF SOIL THERMAL CONDUCTIVITY		22
4.1	Measurement of Soil Thermal Conductivity	22
4.1.1	Data Collection Procedure.....	22
4.2	Properties of Soil under Investigation.....	23
4.3	Experimental Techniques and Procedures	28
4.3.1	Preparation of Soil Samples	28
4.3.2	Soil Sample Preparation Procedure	29
4.3.2.1	Dry Soil Sample Preparation	29
4.3.2.2	Barely-to-Moderately Moist Soil Sample Preparation	30
4.3.2.3	Highly-to-Fully Saturated Soil Sample Preparation	31
4.4	Measurement of Saturated Soil Hydraulic Conductivity	32

4.4.1	Soil Sample Preparation	32
4.4.1.1	Equipment and Supplies	33
4.4.1.2	Soil Compaction Procedure	33
4.4.2	Saturated Hydraulic Conductivity Measurement Procedure	34
4.5	Measurement Error Analysis	35
4.5.1	Methodology in Uncertainty Calculations.....	35
4.5.2	Uncertainty in Derived Variables	37
4.5.3	Measurement Equipment Specifications	38
4.5.4	Plate Temperature Measurement	39
4.5.5	Measurement of Temperature Difference.....	40
4.5.6	Error Associate with the Cold Bath Tank.....	40
4.5.7	Measurement of Electrical Power.....	41
4.5.8	Error in Measurement of Other Dimensions	42
4.5.8.1	Effective Heater Plate Area	42
4.5.8.2	Total Specimen Thickness	43
4.5.8.3	Effective Specimen Thickness.....	44
4.5.8.4	Diameter and Thickness of Sample Container.....	44
4.5.8.5	Silicon Rubber Pad Thickness	44
4.5.8.6	Plate Flatness	44
4.5.9	Heat Flux Measurement	45

4.5.10 Thermal Conductivity Measurement.....	46
4.5.11 Saturated Hydraulic Conductivity Experimental Measurement Uncertainty	46
4.5.11.7 Specimen Thickness	47
4.5.11.8 Measurement of Tube and Test Container Diameter.....	47
4.5.11.9 Measurement of Water Head	47
4.5.11.10 Measurement of Elapsed Time	47
4.5.11.11 Measurement of Hydraulic Conductivity	48
CHAPTER 5 EXPERIMENTAL RESULTS AND DISCUSSION	49
5.1 Results and Discussion of Soil Hydraulic Conductivity.....	49
5.2 Experimental Results of Kortright Centre Soil Thermal Conductivity.....	51
5.2.1 Introduction	51
5.2.2 Experimental Result	52
CHAPTER 6 A STUDY OF THE APPARENT THERMAL CONDUCTIVITY OF SOILS DUE TO VAPOUR MIGRATION.....	56
6.1 Introduction.....	56
6.2 Theory	56
6.3 Methodology	60
6.3.1 Experimental Data	60

6.3.2	Preliminary Evaluation	63
6.4	Results and Discussion	67
6.4.1	Ottawa Sand Results	67
6.4.2	Richmond Hill Results	70
CHAPTER 7 COMPUTER SIMULATION OF A GROUND SOURCE		
HEAT PUMP SYSTEM USING EXPERIMENTAL SOIL THERMAL		
CONDUCTIVITIES FOR THREE SOIL TEXTURES.....		
7.1	Introduction.....	72
7.2	Description of the GSHP under Investigation	73
7.3	Simulation Details.....	75
7.4	TRNSYS Simulation Result	82
CHAPTER 8 CONCLUSIONS AND RECOMMENDATIONS		
8.1	Summary of Results.....	92
8.2	Conclusions.....	94
8.3	Recommendations.....	95
APPENDIX A: DETAILED PARAMETERS OF HEAT AND MASS		
TRANSFER EQUATIONS.....		
97		
APPENDIX B: EXPERIMENTAL THERMAL CONDUCTIVITY		
RESULTS 99		
APPENDIX C: GRAIN SIZE DISTRIBUTION AND MINERAL		
COMPOSITION OF RICHMOND HILL SOIL		
106		

REFERENCES	110
------------------	-----

LIST OF FIGURES

Figure 2.1: A solar energy storage using double U-tube Borehole Thermal Energy Storage (BTES) system [5].....	6
Figure 3.1: Guarded hot plate apparatus (GHPA) used to measure soil thermal conductivity [4].	19
Figure 3.2: A specimen container: (a) closed and (b) open	19
Figure 3.3: Variation in simulation result with change in simulation time step.	21
Figure 4.1: Soil texture chart [38].	25
Figure 4.2: Falling head test set up [43].	34
Figure 4.3: Variation in the cold bath temperature fluctuation from 5°C to 92°C.	41
Figure 4.4: Guarded Hot Plat (GHP) apparatus schematic diagram.	43
Figure 5.1: Variation in thermal conductivity of Kortright Centre soil with temperature and volumetric water content.	52
Figure 5.2: Variation in thermal conductivity of Ottawa sand with temperature and volumetric water content.	53
Figure 5.3: Variation in thermal conductivity of Richmond Hill soil with temperature and volumetric water content.	53
Figure 6.1: Experimental λ_{eff} data for Ottawa sand [4].	60
Figure 6.2: Variation in Ottawa sand thermal conductivity due to pure conduction.	61
Figure 6.3: Apparent thermal conductivity due to vapour migration ($\lambda_{app,exp} = \lambda_{eff} - \lambda_c$).	62
Figure 6.4: Comparison of theoretical and experimental values for λ_{app} , of Ottawa sand, for two temperatures.	66

Figure 6.5: Comparison between theoretical and experimental values for ε , of Ottawa sand, for two temperatures.	69
Figure 6.6: Impact of soil texture on the phase conversion factor ε , at VWC = 0.085 [m ³ /m ³] and 0.1706 [m ³ /m ³], for Ottawa sand and Richmond Hill fine sandy loam soil respectively, for a range of temperatures.	71
Figure 7.1: An overview of the TRNSYS model of the complete HVAC system.....	76
Figure 7.2: Three major components of the HVAC system as modeled in TRNSYS. a) Heat pump-to-ground loop. b) Heat pump-to-buffer tank loop. c) Buffer tank-to-AHU/in-floor heating loop.	77
Figure 7.3: Comparison between actual and simulated heat pump electrical energy consumption for the cooling period from August 23 rd to September 14 th , 2010.	83
Figure 7.4: Comparison between actual and simulated heat pump electrical energy consumption for the heating period from December 1 st to December 20 th , 2010.....	83
Figure 7.5: Variation in the heat pump energy consumption for Ottawa sand with change in volumetric water content.....	84
Figure 7.6: Variation in the heat pump energy consumption for Richmond Hill fine sandy loam with change in volumetric water content.	85
Figure 7.7: Variation in the heat pump energy consumption for Kortright Centre loam with change in volumetric water content.	85
Figure 7.8: Variation in heat pump electrical energy consumption during cooling season (May 01 to October 31) for Ottawa sand at three different water contents.	86
Figure 7.9: Variation in heat pump electrical energy consumption during heating season (November 01 to April 30) for Ottawa sand at three different water contents.	87

Figure 7.10: Variation in heat pump electrical energy consumption during cooling season (May 01 to October 31) for Richmond Hill fine sandy loam at three different water contents.	87
Figure 7.11: Variation in heat pump electrical energy consumption during heating season (November 01 to April 30) for Richmond Hill fine sandy loam at three different water contents.	88
Figure 7.12: Variation in heat pump electrical energy consumption during cooling season (May 01 to October 31) for Kortright Centre loam at three different water contents	88
Figure 7.13: Variation in heat pump electrical energy consumption during heating season (November 01 to April 30) for Kortright Centre loam at three different water contents.....	89
Figure 7.14: Monthly variation in amount of rainfall for the city of Toronto from 2009 to 2011, starting with January 2009 as month 1 [50].	90

LIST OF TABLES

Table 4.1 : Kortright Centre soil texture composition by percent weight.....	24
Table 4.2: Major elements and element oxides for Kortright Centre soil specimen.....	26
Table 4.3: Kortright Centre mineral composition.	27
Table 4.4: Calculated values for permanent wilting point, field capacity and full saturation, for the Kortright Centre soil sample.	28
Table 5.1: Experimental result of saturated hydraulic conductivity.	49
Table 5.2: Comparison between the present and previous [42] experimental values of saturated hydraulic conductivity.....	50
Table 6.1: Values of experimental phase conversion factor ε for Ottawa sand for several values of soil temperature T and volumetric water content θ	67
Table 6.2: Experimental phase conversion factor for Richmond Hill fine sandy loam soil.	70
Table 7.1: Detailed specifications of the HVAC equipment under investigation [48].	74
Table 7.2: TRNSYS Component Description.....	78
Table 7.3: Simulated data for Ottawa Sand.	79
Table 7.4: Simulated data for Richmond Hill soil.	79
Table 7.5: Simulated data for Kortright Centre soil.....	79
Table 7.6: Cooling degree day comparison between actual and simulated data for Aug. 23 – Sep. 14/2010.....	80
Table 7.7: Heating degree day comparison between actual and simulated data for Dec. 01-20/2010.....	81
Table 7.8: Total HDD and CDD for the actual and simulated data.	81

Table 7.9: Variation in the GSHP energy consumption at three different moisture levels for Ottawa sand, Richmond Hill fine sandy loam, and Kortright Centre loam.	91
Table B.1: Effective thermal conductivity ($\text{W/m}\cdot\text{K}$) of Ottawa sand [4].	100
Table B.2: Thermal conductivity for pure conduction ($\text{W/m}\cdot\text{K}$) of Ottawa sand.....	101
Table B.3: Apparent thermal conductivity due to vapour migration ($\text{W/m}\cdot\text{K}$) of Ottawa sand.	102
Table B.4: Effective thermal conductivity ($\text{W/m}\cdot\text{K}$) of Richmond Hill fine sandy loam soil [4].	103
Table B.5: Apparent thermal conductivity due to vapour migration ($\text{W/m}\cdot\text{K}$) of Richmond Hill fine sandy loam soil.	104
Table C.1: Richmond Hill soil texture composition by percent weight.....	107
Table C.2: Major elements and element oxides for the Richmond Hill soil specimen.....	108
Table C.3: Richmond Hill soil mineral composition.	109

NOMENCLATURE

C	volumetric heat capacity of soil, $\text{J/m}^3 \cdot \text{K}$
C_p	specific heat at constant pressure, $\text{J/kg} \cdot \text{K}$
D_{atm}	diffusion coefficient of water vapour in atmospheric air, m^2/s
D_T	thermal moisture diffusivity, $\text{m}^2/\text{s} \cdot \text{K}$
g	gravitational acceleration, m/s^2
h	height of water column (in Chapter 4) or relative humidity of air (in Chapter 6)
K	unsaturated hydraulic conductivity, m/s
L	latent heat of vaporization of water, J/kg
p	total gas pressure, Pa
R	gas constant, $\text{J/kg} \cdot \text{K}$
t	time, s
T	temperature, K
z	elevation, m

Greek Symbols

ε	phase conversion factor
---------------	-------------------------

η	porosity, m ³ /m ³
λ	thermal conductivity, W/m·K
μ	dynamic viscosity of water, N·s/m ²
θ	volumetric content, m ³ /m ³
ρ	density, kg/m ³
σ	surface tension of water, N/m
ψ	capillary potential, m
∇T	macroscopic temperature gradient, K/m
$(\nabla T)_a$	microscopic temperature gradient, K/m

Subscripts

a	air
app	apparent (due to vapour migration)
c	conduction
eff	effective
exp	experimental
FC	field capacity
k	critical

l	liquid water
m	migrated liquid
pc	phase change
PWP	permanent wilting point
r	reference
s	solid (particle)
T	thermal
v	water vapour
vs	saturated vapour

CHAPTER 1 INTRODUCTION

1.1 Motivation

Energy plays a major role in economic prosperity of a nation. As more countries are evolving economically and joining the developed countries, energy demand is increasing significantly in proportion to the population growth. Currently, many believe that the world is approaching its peak energy production using non-renewable sources [1]. As world population grows, these non-renewable energy reserves will be reduced at significant rate, increasing energy production costs rapidly and significantly. This concern has motivated developed countries to think of new and more sustainable ways of energy production. One example of such a move to sustainable energy production is by utilising thermal energy storage (TES) systems. TES systems can reduce energy costs, by taking advantage of low off-peak electricity costs, as well as reducing overall capital costs by reducing the size of the equipment such as chillers and air handling units. In addition, TES systems can have significant benefits on building heating and cooling systems such as [2]:

- More efficient and effective utilization of equipment
- Conservation of non-renewable fuel sources
- Reduced greenhouse gas (GHG) emissions such as carbon dioxide (CO₂) and chlorofluorocarbons (CFCs)
- Reduced air pollution

Energy demands in the commercial and industrial sector vary on daily, weekly or seasonal bases. These demands can be matched by utilising TES systems. As the result, a variety

of TES techniques have been developed over the past few decades [3]. Some details of these applications follow:

- **Industry:** high-temperature waste heat from various industrial processes can be stored for use in preheating and other heating operations.
- **Solar energy systems:** by storing excess solar energy received on sunny days for use on cloudy days and at nights, TES systems can increase the capacity factor of solar energy systems, making them more viable for thermal energy harvesting.

TES deals with storage of energy by cooling, heating, melting, solidifying or vaporizing a material. The thermal energy becomes available when the process is reversed. In general, TES involves a temporary storage of thermal energy for later use. Examples of TES are storage of solar energy during the day to be used for heating during the night time, storage of ice for space cooling during summer, or storing heat or coolness by running electrical equipment during off-peak hours, to be used during high demand periods. By running the equipment during off-peak hours, TES can help take advantage of low electricity costs, hence reducing the electricity bill. Since solar energy is not available all the time, TES can provide a means to store the energy, to be used as needed.

Some TES systems utilize the underground thermal energy available throughout the year to satisfy their heating and cooling loads. The heat transfer medium (usually a mixture of water and glycol) is pumped underground, where it discharges heat, during summer, and absorbs heat during winter. With increasing energy costs, it is extremely important to ensure the system being designed is as efficient as reasonable and all the significant parameters have been considered during the design phase. For such systems, the ability to store thermal energy underground

depends on several parameters such as variation in ground temperature, soil water content, and soil characteristics. Water content is defined as the amount of water occupying the void spaces (pores) within the soil. As heat is rejected into the soil during summer season, part of the moisture within the soil is converted into vapour, which migrates within the voids in the soil and takes the heat away from the source, which is the buried pipe. Temperature change, moisture migration, and soil texture have been shown to have significant effect on heat transfer rate through soil [4]. Current energy modeling software such as eQUEST and TRNSYS, however, do not consider variation in these parameters, and use constant soil properties. This means that when it comes to designing an underground TES system, current design software codes are not capable of predicting the variation in soil parameters on these systems' performance throughout the year. The objective of this thesis is to investigate the significance of these parameters through experimental analysis and create an analytical model that can be implemented in a computer simulation capable of representing this coupled process of heat and moisture transfer more accurately.

1.2 Scope and Objectives

The main objectives of this research are: to establish comprehensive sets of experimental soil thermal conductivity data over wide ranges of water contents and temperatures, to study the effect of vapour migration on soil thermal conductivity, and lastly, to investigate the real-world impact of variation in soil thermal conductivity on the performance of ground thermal energy storages. To achieve these objectives, the research has been divided into three specific sub-objectives. The first part is to continue the work of Nikolaev [4], by collecting experimental thermal conductivity data of a loam soil, called Kortright Centre soil, over a wide range of

temperatures ($5^{\circ}\text{C} - 92^{\circ}\text{C}$) and water contents (complete dryness to full saturation), using the guarded hot plate methodology. The second part of this research is to utilise the experimental data of Nikolaev [4] to study the apparent thermal conductivity due to vapour migration and improve the accuracy of an existing theoretical model for estimating the apparent thermal conductivity. The last part of this research is to investigate the impact of variation in soil thermal conductivity due to variation in soil water content on the performance of a ground source heat pump (GSHP) system, using an energy system modeling software. A simulation model has been developed for this purpose based on an existing GSHP system of an archetype house at Kortright Centre in Vaughan, Ontario.

1.3 Outline of the Thesis

The thesis is comprised of the following sections. First, background on the research topic is introduced with literature review [Chapter 2]. Next, the approach to achieve the objectives and methodology are explained [Chapter 3]. After that, the experimental methodology and soil sample preparation are explained [Chapter 4]. Then, the experimental uncertainty is also evaluated [Chapter 4]. Next, soil saturated hydraulic conductivity is measured [Chapter 4] and compared to the values of similar soils obtained from literature [Chapter 5]. After that, the experimental results are presented and analyzed [Chapter 5]. Based on gathered experimental data of Ottawa sand and Richmond Hill fine sandy loam soil, data sets are developed for the phase conversion factor, ε , as a function of soil water content and temperature [Chapter 6]. To investigate the impact of variation in soil thermal conductivity on ground thermal energy storages, a simulation model of a GSHP system is developed using TRNSYS [Chapter 7]. Finally, the research is summarized and recommendations are made [Chapter 8].

CHAPTER 2 BACKGROUND AND LITERATURE

REVIEW

2.1 Background

2.1.1 Underground Thermal Energy Storage

A well known application of heat and moisture transfer in soil is in utilising underground thermal energy storage (UTES) systems for building heating and cooling demand. A UTES system consists of several pipes laid underground vertically or horizontally, depending on space limitations. The pipes act as heat exchangers with a glycol mixture circulating inside as the heat transfer medium. The heat is transferred to the soil during summer season, and is absorbed back to the heat transfer fluid during winter season. The buried pipes are usually connected to a HVAC system, such as a heat pump. For example, in the cooling mode, the evaporator loop of the heat pump absorbs heat from the house, and rejects it from the condenser loop of the heat pump to underground through the ground heat exchanger. The heat pump can also be connected to a boiler to provide required supplementary heating demand, and a cooling tower (CT) to provide required supplementary cooling demand of the building. Such systems are sometimes known as boiler-GSHP hybrid and CT-GSHP hybrid as well.

Another UTES configuration is solar panel connected to the buried pipes, where the heat collected from the panels is stored for later use. In this configuration, the collected heat is carried underground by the glycol solution, where it is stored in boreholes. Figure 2.1 illustrates such a system. Pipes going down from the house into the boreholes, extract the stored heat as needed to satisfy the heating load of the house [5]. There have been extensive studies performed on impact

of soil properties on UTES systems performance. These studies have been included in section 2.2.3 of this chapter.

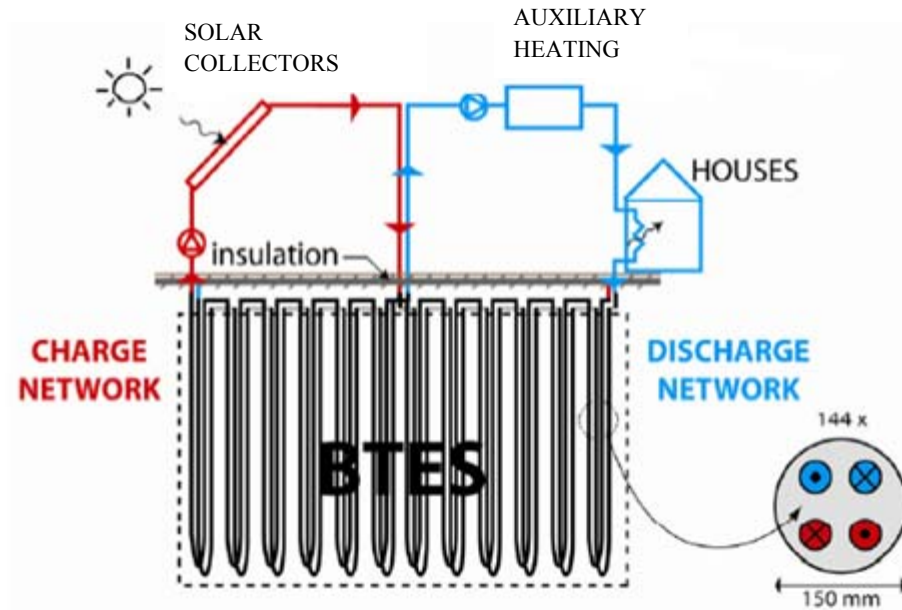


Figure 2.1: A solar energy storage using double U-tube Borehole Thermal Energy Storage (BTES) system [5].

There are several other applications related to heat and moisture transfer in soil, such as underground nuclear waste storage and pesticide contamination. When designing a nuclear waste storage facility, soil type becomes a significant factor. In case of any radioactive leakage, the rate at which the liquid passes through the soil and extent of leakage needs to be evaluated to ensure the liquid waste does not contaminate any underground sources of water. Similarly, when pesticides are used in the agricultural industry, the rate at which the contaminants dissipate through soil depends on soil type. Another application of concept of heat and moisture transfer in soil is in green roof systems. In such application, the rate at which heat is dissipated through the roof will be dependent on soil water content, as well as amount and soil type laid on top of the roof.

2.1.2 Heat and Moisture Transfer in Soil

Soil properties such as temperature, water content and composition have significant impact on heat transfer through soil. The main method of heat transfer through soil is by conduction of heat through soil particles and moisture surrounding them. But as temperature increases within the soil, some of the moisture surrounding the soil particles enhances this heat transfer by migrating away from the heat sink, in the form of water vapour. In addition, soil type plays an important role in heat transfer through soil. A soil with coarse texture, such as sand, has larger void spaces and does not retain moisture as well as a finer soil such as a loam soil does. Hence, the enhancement in heat transfer due to vapour migration through the void spaces would be higher in a coarse soil than a fine soil.

In order to investigate the impact of aforementioned soil properties on heat transfer in soil, the thermal conductivity of several soil types must be obtained, for a range of temperature and water contents. To ensure accuracy and realism, this is often done experimentally. The experimental thermal conductivities of two soil types have been obtained, using the guarded hot plate apparatus (GHPA), by a previous graduate student working on this research [4], for a temperature range of 2 – 92°C, from fully dry to full saturation. The two soil types are known as the Ottawa sand (a sandy soil) and the Richmond Hill soil (a fine sandy loam soil).

This research builds on Nikolaev's [4] research by obtaining the experimental thermal conductivity of a loam type soil, known as the Kortright Centre soil, using the GHPA, to increase the available data base for experimental soil thermal conductivities. A procedure has been developed by Nikolaev [4] to obtain a full range of water contents, where the permanent wilting point (PWP), field capacity (FC), and porosity are used as the starting point. The PWP is defined by the amount of water in the soil sample, occupying the micro-pores around the individual soil

particles, which is defined as the water content at -15 bar of suction pressure. The FC is the maximum water content a particular soil can hold after gravitational drainage, which is typically defined as the water content at -0.33 bar of suction pressure. The porosity is defined as the amount of void spaces that exist among soil particles. When a soil is fully saturated with water, its water content is equal to the porosity of the soil.

In addition to the experimental investigation, a well known theoretical model representing effective soil thermal conductivity as a function of temperature and water content [6], has been modified in order to develop a correlation for a term called the phase conversion factor, ε . According to Luikov [7], a change in soil water content may be considered to be composed of liquid water transfer and phase conversion, which is defined by the phase conversion factor, ε . When moisture transfer occurs in the vapour form alone, $\varepsilon = 1$; when moisture transfer occurs in only liquid form, $\varepsilon = 0$. Hence, the phase conversion factor is modified using the experimental results for the Ottawa sand and the Richmond Hill soil, which can be easily integrated within any energy modeling software.

2.2 Literature Review

Numerous studies of coupled heat and moisture transfer have been reported. The studies have mainly investigated the impact of heat, moisture migration and soil texture on soil thermal conductivity. The works involve theoretical, experimental, as well as numerical models. Other studies have utilised previously developed models to investigate other concepts involving heat and moisture transfer. These works have been described further in the following sections.

2.2.1 Impact of Heat and Moisture Transfer on Soil Thermal Conductivity

Numerous models have been developed throughout the years to investigate and predict the impact of heat and moisture migration on soil thermal conductivity. In an early work, de Vries [6] computed the heat transfer caused by diffusion of water vapour in unsaturated soil, where he found an increase in thermal conductivity due to the diffusion of water vapour.

Reider et al. [8] developed a mathematical model predicting the transient moisture profiles in unsaturated soil samples subjected to a temperature gradient. The developed model, however, only accounts for a temperature range of 2°C to 40°C, for which the heat transfer is dominated by pure conduction. Hence, this model does not accurately simulate a more realistic scenario, where heat transfer is due to both a temperature gradient and moisture migration.

Later on, Thomas [9] developed a theoretical model, based on modifications of the Philip-de Vries model [10], for coupled heat and mass transfer in unsaturated soil which takes into account gravitational effects and which is based on the volumetric liquid content approach. In 1992, Thomas extended his earlier work and developed a second model for coupled heat and mass transfer in unsaturated porous media, based on the capillary potential approach [11]. They used an extension of Darcy's law to unsaturated flow for isothermal problems to develop a one-dimensional numerical solution for this problem. Within the governing heat transfer equations of [9] and [11], for the heat conduction term, the coefficients of effective thermal conductivity λ_{eff} appear to be different. At the same time, Yonge et al. [12] examined coupled heat and mass transfer and determined the coupled heat and water diffusion parameters through a theoretical and experimental technique. They solved the transport equations analytically using dimensionless analysis. Thomas et al. [13] expanded their earlier work and implemented the concept of heat and mass transfer into a more practical work by analyzing a fully coupled heat

and mass transfer model incorporating contaminant gas transfer in an unsaturated medium. The model describes the migration of a contaminant gas through an engineered clay liner of a sanitary landfill site. The model treats migration of water, heat, air, and contaminant gas separately with independent variables such as capillary potential, temperature, pore air pressure, and molar concentration of contaminant gas.

More recently, an article by Reddy [14] introduced a simplified numerical model to analyze heat transfer characteristics of an unsaturated soil bed and have produced similar results obtained in this research. Reddy [14] has also analyzed the effects of various heat transfer processes as well as motion of fluids on heat transfer in a clay bed coupled to a heat pump. His findings show that the effects of convection heat transfer become significant as temperature is increased.

Lee et al. [15] has built on the previously mentioned works, where they have utilized the concept of heat and moisture transfer in unsaturated soil to create a theoretical model to predict the rate of evaporation from the surface of a deformable material. Soil water characteristic curves for a deformable soil were obtained and a column-drying test was conducted to obtain a one-dimensional water flow, heat flow, and evaporation in the surface.

Yu et al. [16] experimentally investigated water transport in porous media at the pore scale, using a thermal probe as a heater and a camera to observe the water vaporization and condensation within the pore. Based on their findings, the water near the heating source evaporates and diffuses far from the source during heating. On condensation, the water releases the heat. As the temperature increases, the distance over which the water vapour migrates before condensation increases.

Dos Santos et al. [17] developed a similar mathematical model to Yonge et al. [12], to analyze coupled heat and mass transfer in soils using a Multi-Tri Diagonal-Matrix Algorithm (MTDMA) to solve the heat and mass transfer governing equations in porous soils. They found that this method avoids numerical instabilities by simultaneously solving the governing equations, allowing the use of large time steps, which are important for long-term simulations of the three-dimensional heat and moisture transfer in soils. These investigations have been expanded further by Prabhu et al. [18] for non-linear two-dimensional coupled heat and mass transfer using the work of Luikov [7], who developed a heat transfer model for the simultaneous solution of heat and mass transfer, which is based on irreversible thermodynamics. These works have been further expanded to investigate thermal and moisture behaviour of wet and dry soils with buried capillary heating system Balghouti et al. [19]. That paper presents the results of an experiment on soil warming, a concept crucial to the greenhouse industry, investigating the effects of thermal energy storage underground. This method is preferred over conventional heating techniques, because it relies on low-temperature energy sources, such as industrial waste heat, geothermal and solar energy [19].

Chen et al. [20] have utilised concepts involving heat and moisture transfer phenomena and has expanded it into investigating salt migration in soils, through experimental analysis. Based on their work, a thermal region has been found in the soil column, along with moisture releasing, transition, and absorbing zones in the soil column. Based on their findings, capillary flow is the dominant mechanism that governs moisture transfer. With moisture transfer, the salt moves from the ground water and accumulates at the top of the column. With the salt accumulation, however, there will be a gradient of salt content, and as the result, the salt will also diffuse due to this gradient.

Heat and moisture transport in soil has been the focus of works of Bittelli et al. [21] as well, who have tried to quantify soil evaporation and soil water content dynamics near the soil surface. Their study was conducted to create a fully coupled numerical model to solve the governing equations for liquid water, water vapour and heat transport in soil, as well as testing the numerical model with detailed measurements of soil temperature, heat flux, water content, and evaporation from the surface [21]. In addition, they have tested different formulations for the soil surface resistance parameter and their effect on soil evaporation. Their model confirmed that vapour transport is the key factor in soil mass and energy transfer. They also found that vapour flow can create sinusoidal variations in soil water content near the surface. While Bittelli et al. [21] focuses on near-surface effect, this thesis focuses on heat and mass transfer effects on heat transfer rate at much lower depths, applicable to many thermal storage applications.

In addition, Olguín et al. [22] have studied heat and mass transfer phenomena during the solidification of high water content materials such as soil, food, tissues and phase change materials (PCMs). They have developed coupled heat and mass transfer equations, by assuming quasi-steady heat conduction in the frozen region.

2.2.2 Impact of Soil Composition on Soil Thermal Conductivity

Several papers have developed analytical models dealing with coupled heat and moisture transfer, by investigating different soil textures. Dos Santos et al. [23] have developed a model dealing with coupled heat and mass transfer in soil and through a building floor, in order to predict ground heat transfer, room temperature and humidity. The methodology used by dos Santos and Mendes is based on the theory of Phillip and de Vries [6], who have used variable

thermo-physical properties for different materials in their investigation. A finite element method was used as well as three dimensional modeling to be able to describe the heat and mass transfer in unsaturated soil and the floor.

Following advances in heat and mass transport in porous medium, Heitman et al. [24] have developed a model that improves the approach for measurement of coupled heat and water transfer in soil cells. They developed an apparatus to provide one dimensional conditions, which permits the measurement of temperature, water content and thermal conductivity under transient boundary conditions. Heitman et al. were able to run a series of experiments using four soil type-initial water content combinations and ten transient boundary conditions. Techniques implemented in these tests allowed observation of transient temperature, water content and thermal conductivity distributions on the same soil samples for all ten boundary conditions [24].

Arfaei Malekzadeh et al. [25] have worked on a fully coupled non-linear heat and mass transfer in unsaturated media and created an analytical solution for the one dimensional case where the coefficients of the system of equations have been assumed to be constant for the entire domain. They have provided three examples to analyze the heat and mass transfer in a semi-finite column of unsaturated soil.

Santander et al. [26] have investigated heat and mass transfer mechanisms in two soil characteristics. They have used the finite volume methodology and experiments to analyze the impact of heat, moisture and soil texture on soil thermal conductivity. They have utilized de Vries model [6] in their investigation as well, and have observed that the de Vries model overestimates moisture migration in soil.

In spite of much research on the impact of heat, moisture transfer, and soil composition on soil thermal conductivity throughout the years, to the best knowledge of this researcher, no one has yet to develop a universal and accurate methodology, to analytically evaluate soil thermal conductivity.

This research builds on and extends works reported earlier [9, 11], in which two similar theoretical models were developed for the apparent thermal conductivity due to vapour migration. These theoretical apparent thermal conductivity models [9, 11] are examined and their validity is verified by comparing them with a set of experimental data. The intension is to develop an accurate model by combining impacts of variation in temperature, water content, and soil characteristics on soil thermal conductivity.

2.2.3 Heat and Moisture Transfer in Thermal Energy Storage (TES) Applications

There has been extensive work done in the literature on underground thermal energy storage, with aforementioned technologies. Some of the studies done on underground thermal energy storage have focused on impact of soil properties on system performance. Florides et al. [27] has developed a numerical model for simulation of energy flows and temperature changes around a borehole heat exchanger. Effect of various parameters such as U-tube diameter, variation of ground thermal conductivity and the specific heat and borehole fill material, on the temperature of the inlet and outlet fluid has been investigated. Based on their findings, the heat transfer rate increases with soil thermal conductivity, however they fail to investigate the effect of moisture migration on heat transfer rate between the U-tubes and the surrounding soil. Similar work has been performed by Jalaluddin et al. [28], where thermal performance of several vertical ground heat exchangers (GHEs) for ground source heat pump systems has been investigated. They have focused on different operations modes of the GHE. Their investigation shows a

change in heat exchange rate with a change in operation mode of the ground heat exchanger. Although their finding can lead to better operation of GSHP systems, their application is specific to operation mode of the GSHP systems. Furthermore, Pertzborn et al. [29] have investigated the impact of weather variation on performance of a boiler-GSHP hybrid system and a Cooling Tower (CT)-GSHP hybrid system. Their finding shows such systems will underperform under extreme weather conditions if the Typical Meteorological Year (TMY)¹ is used during the design phase. Such a finding is significant but it is only a small parameter that is considered when designing a hybrid ground source heat pump system. When designing a GSHP system impact of soil properties on the performance of the system becomes significant and needs to be investigated in detail. More recently, Lu et al. [30] have performed analysis on a ground-sourced heat pump system combined with radiant heat/cooling. Their focus has been on energy conservation benefits of this system compared to traditional systems and the GSHP ability to provide adequate thermal comfort for the occupants of a house. Closer to the work of this research is the study performed by Choi et al. [31] where they have investigated the effect of varying thermal properties of unsaturated soil on the operation of a vertical ground heat exchanger. Their finding shows a 40% reduction in heat exchange rate than saturated conditions. The investigation of Choi et al. is similar to that of this thesis; however, it does not consider variation in temperature and soil composition on performance of the vertical heat exchanger and is thus not extensive enough to be useful and utilized.

Dehdezi et al. [32] have worked on enhancing the thermo-physical properties of soil and its energy storage capability, by modifying a soil with phase change materials (PCM). They have studied the thermo-physical properties of soil modified with different amount of

¹ A collection of weather data for a specific location generated from a data bank, with more than a year in duration.

microencapsulated PCM. Based on their experimental results, increase in amount of PCM within the soil could yield to decrease in soil thermal conductivity, and increase in its volumetric heat capacity. In addition, they have investigated the application of PCM-modified soil through numerical simulation, where they have observed that such enhancement in soil properties could yield to significant reduction in temperature variations in ground, and improvement in GSHP's coefficient of performance (COP).

Furthermore, Wang et al. [33] have studied the changes of soil temperature and water content during the thermal storage process of a Borehole Heat Exchanger (BHE). They have investigated the impact of heat injection temperatures and initial water content on thermal performance of the borehole heat exchanger. Based on their findings, as the heat injection temperature increases, the heat transfer rate of the BHE increases as well. In addition, as water content increases near the heat source, the temperature profile near the BHE deviates from the results predicted by heat conduction, thereby influencing the thermal performance of the BHE. Similarly, Reuss et al. [34] have investigated the impact of heat and moisture transfer in soil, on the thermal performance of underground thermal energy storage systems. They have simulated the combined effect of heat and moisture transfer for temperature up to 90°C, which was validated by laboratory experiments.

Gauthier et al. [35] have extended the concept of heat and moisture transfer into investigating the thermal behaviour of soil heat exchanger-storage systems aimed at reducing the energy consumption of greenhouses. Their system consists of buried pipes circulating air to store and remove heat from soil. They have validated their model by comparing the results to a similar system installed in a commercial type greenhouse. Their investigation shows that variation in

water content becomes negligible as buried pipe length is increased or air velocity within the pipes is decreased.

The works mentioned previously have investigated the impact of change in soil properties on UTES systems performance, yet, to the best knowledge of this researcher, they have not been able to provide a methodology on implementing these impacts when designing such systems. This research will investigate the impact of variation in soil properties such as temperature, water content and texture, on a GSHP system and work on developing a method that takes the impact of these parameters into account, which can be utilised by the industry when designing an underground thermal energy storage system.

CHAPTER 3 APPROACH AND METHODOLOGY

In order to reach the objectives of this research, three approaches have been utilised: experimental analysis of soil thermal conductivity, study of the effect of vapour migration on soil thermal conductivity, and implementation of results. These approaches are further explained below.

3.1 Experimental Analysis of Soil Thermal Conductivity

An experimental approach is desirable since it ensures real results are obtained, as long as a correct procedure is followed. In addition, a database can be developed for thermal conductivities of different soil types using the experimental procedure introduced in this research. This approach enables other researchers to use the results with confidence that they have been obtained experimentally and accurately, in fields relating to heat and moisture transfer. To obtain the results, a guarded hot plate apparatus (GHPA) designed and built by Reid [36] in the Thermofluids Research Laboratory at Ryerson University has been utilised. To ensure the accuracy of the results, a detailed soil sample preparation procedure by Nikolaev [4] has been followed and the experimental error has been determined and included in this thesis.

Figures 3.1 and 3.2 present the GHPA set-up [36] and a specimen container, respectively. The hot and cold plates are 7 inches by 7 inches in dimensions. The hot plate is at the top and cold plate at the bottom, with the specimen container in between. The locking screws are used to move the hot plate up or down so that the specimen container can be removed easily or secured tightly between the hot and cold plates. The plates and heat transfer fluid pipes are insulated with

fiberglass to minimize heat loss to the environment. Oil is used as the heat transfer fluid, since it does not evaporate easily at temperatures up to 100°C.

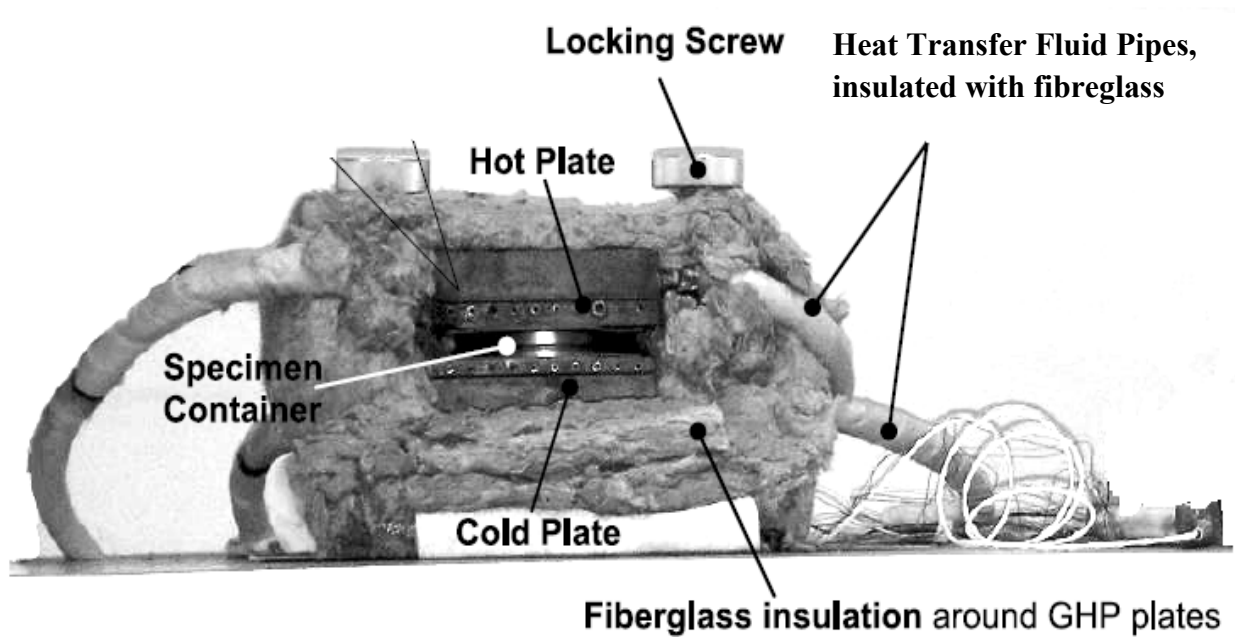


Figure 3.1: Guarded hot plate apparatus (GHPA) used to measure soil thermal conductivity [4].



Figure 3.2: A specimen container: (a) closed and (b) open .

3.1.1 Experimental Limitations

Several experimental limitations existed, which affected the results of the experiments. For instance, due to equipment limitations, the temperature range covered in this research was kept between 5°C and 92°C, inclusively. The water added to each soil sample was tap water, which has dissolved minerals that might affect the experimental results.

Due to a long testing time of the GHPA for achieving steady-state conditions, there might be moisture redistribution in the soil samples under the influence of temperature gradient and gravity, which might also affect the experimental results. In addition, the soil samples were tested at the heating-from-above orientation; therefore, natural convection in the soil samples is considered to be non-existent.

3.2 Study of the Effect of Vapour Migration on Soil Thermal Conductivity

The second approach is to use the experimental results to study the apparent thermal conductivity due to vapour migration. This approach enables a correction factor, called the phase conversion factor ϵ , to be used to “correct” the theoretical apparent thermal conductivity, which can be integrated in any energy simulation software for taking into account the effect of vapour migration on soil thermal conductivity. The experimental values of the phase conversion factor are calculated based on the well known model by de Vries [6] for the Ottawa sand and Richmond Hill soil.

3.3 Implementation of Results

The last approach is to implement the experimental results in a commercially available energy system modeling software. This approach allows the investigation of the actual impact of variation in soil thermal conductivity on the performance of a GSHP system under realistic conditions. As the result, the experimental thermal conductivity data of a sandy, a sandy loam, and a loam soil has been implemented in a TRNSYS model of a GSHP system. Since this research is to investigate the impact of soil thermal conductivity on a GSHP performance, only thermal conductivity values have been changed in the model and the soil volumetric heat capacity was kept constant.

In order to determine the appropriate simulation time step, the simulation of a case was repeated at 15, 30, 60 and 90 minutes, as shown in Figure 3.3. The time step sensitivity analysis shows that the simulation result does not change significantly below 60 minutes. As the result, the simulation time step is kept at 60 minutes for all simulations.

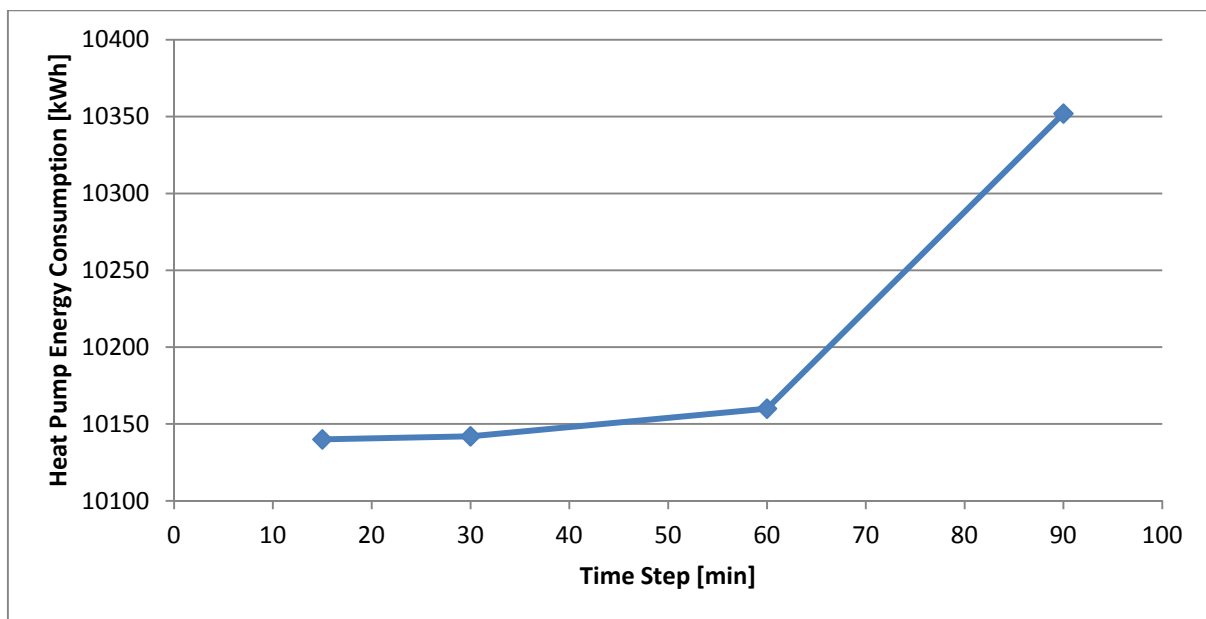


Figure 3.3: Variation in simulation result with change in simulation time step.

CHAPTER 4 EXPERIMENTAL INVESTIGATION OF

SOIL THERMAL CONDUCTIVITY

4.1 Measurement of Soil Thermal Conductivity

In order to observe the complete variation of the sample soil thermal conductivity with water content and temperature, twelve experimental points are considered as follows: one point at dry condition ($\theta = 0$), two points within the barely moist region ($0 < \theta < \theta_{PWP}$), five points within the moderately moist region ($\theta_{PWP} < \theta < \theta_{FC}$), three points within the highly moist region ($\theta_{FC} < \theta < \theta_{FS}$), and one point at full saturation ($\theta = \theta_{FS}$). Based on these points, the samples are prepared, and each sample is tested from 5°C to 92°C, in order to capture variation in soil thermal conductivity at low, medium and high temperature ranges.

The circulating baths are turned on manually and allowed to warm up for approximately 30 minutes. Meanwhile, the hot and cold plates of the GHPA, heat transfer hoses and circulating baths are inspected for proper operation. The specimen container is then clamped between the plates, with silicon rubber pads between the specimen container and plate surfaces.

4.1.1 Data Collection Procedure

Each specimen container is placed between two 0.5mm thick silicon rubber pads (of known thermal conductivity) to provided better surface contact between the plates and the container. At the start of each test, the circulating baths are manually turned on and each bath's temperature is set to maintain a 4°C temperature difference between the hot and cold plates. The baths are allowed approximately 30 minutes to warm up and stabilize. National Instruments

Measurement and Automation software is used at this point to observe temperature stabilization at both plates. Once the hot and cold plates' temperatures are stabilised, the National Instruments LabVIEW version 8.5 is used to collect the data during the experiment. The lab view program consists of two parts. First, the electrical power optimiser program is run to obtain the optimum electrical power going to the heater plate in order to equalize the temperature of the heater plate with the temperature of the guarded hot plate. Initial high and low guesses are given to the program and it uses the initial values for high and low voltage and reduces them until a pre-defined difference is reached (0.0003 V). Once the optimum electrical power is achieved, the second part of the program is run, which collects several data such as voltage and current to the heater plate, hot and cold plate temperatures, shunt voltage and current. Through trial and error, it was observed that in order to obtain enough data to cover the fluctuations in the system and ensure accurate results, the data collection time should be 1800 s, with a sampling rate of 1 Hz. In addition, data is collected three times for each temperature (from 5°C to 92°C) and averaged to increase the accuracy of the experimental data.

4.2 Properties of Soil under Investigation

The soil used for this experiment was obtained from Kortright Centre in Vaughan, Ontario. The soil has a particle density, ρ_s , of 2650 kg/m³ (as for most North American soils), a dry bulk density, ρ_{db} , of 1272 kg/m³, and a porosity, ϕ , of 0.520. Particle density is defined as the ratio of the weight of the solid portion of soil to the total volume of solids, whereas, dry bulk density is defined as the ratio of mass (weight) of the oven dried soil to the total volume of soil [37]. Equations for calculating of the dry-bulk density and porosity have been included in the next section. The soil was collected near the buried horizontal pipes of the GSHP system at the

Kortright Centre, at a depth of approximately 30 cm, to prevent any influence by biological activity and organic matter; as the amount of organic matter increases in soil, its dry bulk density decreases [4]. The soil was sent to the Agriculture and Food Laboratory at the University of Guelph, in order to obtain its composition (percent sand, silt, and clay). The results are presented in Table 4.1. They provided the following main soil compositions (based on mass fraction) for the Kortright Centre soil sample: sand mass fraction, $m_{sa} = 32.2\%$, silt mass fraction, $m_{si} = 49.5\%$, and clay mass fraction, $m_{cl} = 18.3\%$. There are about 4% mass of gravel (particle size $> 2000 \mu\text{m}$) in the soil; but they were removed using sieve for the test samples. Figure 4.1 presents different soil compositions based on sand, silt and clay mass fractions. Based on mass fractions of Kortright Centre soil sample, its texture type falls within the loam region, and it is very close to the silty loam.

Table 4.1 : Kortright Centre soil texture composition by percent weight.

Soil Texture	Particle Size [μm]	Mass Fraction [wt%]
Sand (total)	53 – 2000	32.2
Very Fine Sand	53 – 100	13.3
Fine Sand	100 – 250	12.5
Medium Sand	250 – 500	4.2
Coarse Sand	500 – 1000	1.3
Very Coarse Sand	1000 – 2000	0.9
Silt	2 – 53	49.5
Clay	< 2	18.3

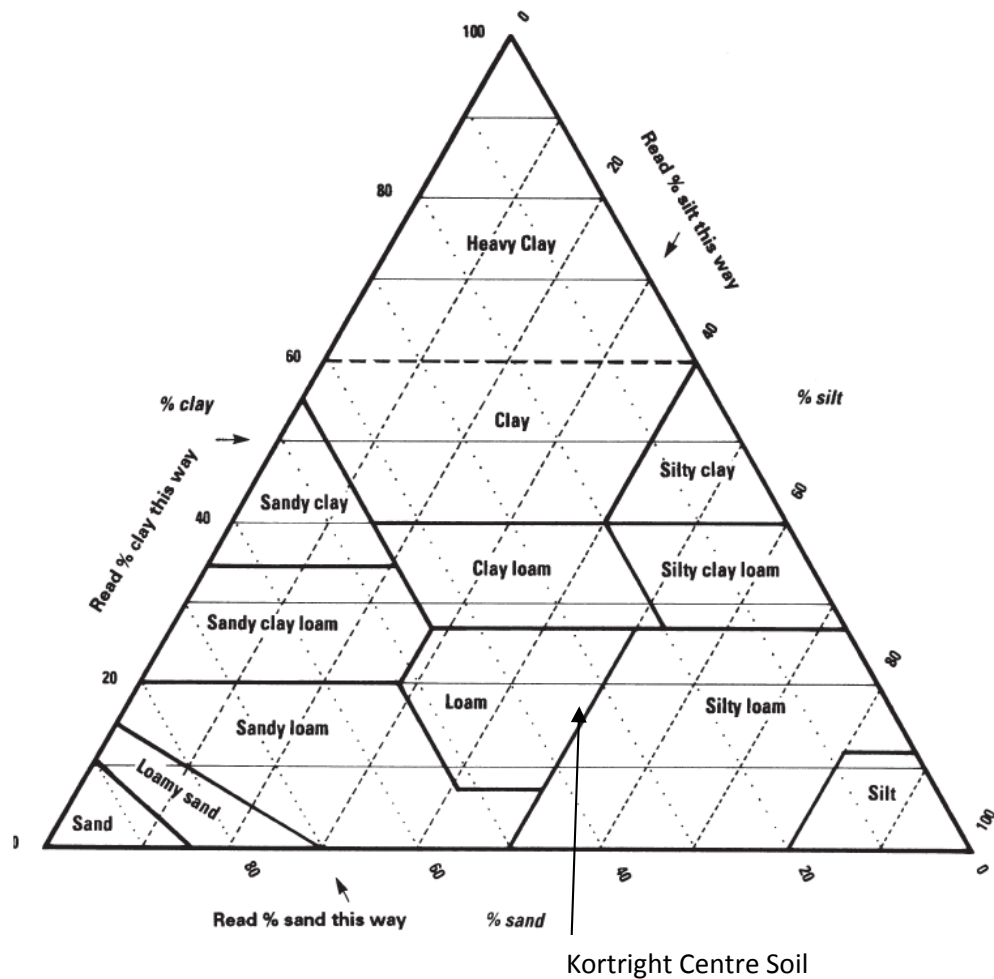


Figure 4.1: Soil texture chart [38].

In addition to the above analysis, a specimen of 130 g (as requested by the laboratory) of the Kortright Centre soil was sent to the Bavarian Environment Agency Laboratory in Marktredwitz, Germany, where the major element oxides, elements, and mineral content of the soil specimen were obtained as presented in Table 4.2 and 4.3 respectively. The absolute error is between 2-3 weight percent.

Table 4.2: Major elements and element oxides for Kortright Centre soil specimen.

Element Content	Composition
LOI [*]	3.65 [wt%]
SiO ₂	67.7 [wt%]
Al ₂ O ₃	13.72 [wt%]
Fe ₂ O ₃	5.05 [wt%]
MgO	0.12 [wt%]
MnO	1.56 [wt%]
CaO	1.93 [wt%]
Na ₂ O	2.07 [wt%]
K ₂ O	2.92 [wt%]
TiO ₂	0.71 [wt%]
P ₂ O ₅	0.2 [wt%]
Ce	60 [mg/kg]
Cr	61 [mg/kg]
Nb	11 [mg/kg]
Ni	31 [mg/kg]
Sr	245 [mg/kg]
V	80 [mg/kg]
Zn	64 [mg/kg]
Zr	337 [mg/kg]

* LOI = Loss of Ignition. It represents the amount (weight percent) of carbon elements within the specimen, which is lost by heating the specimen for 1.5 hours in an oven at 1050°C.

Table 4.3: Kortright Centre mineral composition.

Mineral Content	Composition [wt%]
Quartz	39
K-Feldspar (microcline-dominated)	10
Plagioclase (albite-dominated)	25
Actinolite	4
Chlorite	4
Clay Minerals (illite-dominated)	18

Using the physical properties obtained for the Kortright Centre soil, it is possible to estimate the volumetric water content at the permanent wilting point, θ_{PWP} , and the field capacity, θ_{FC} , which are required for the planning stage of the experiment. They are used as the starting point to create the experimental points for the water content range, as described in section 4.1. A simple way to estimate these two values has been developed by [39], and [40], which demonstrated that the ratios of:

$$\frac{\theta_{FC}}{\phi} = \frac{1}{2} \quad (4.1)$$

$$\frac{\theta_{PWP}}{\phi} = \frac{1}{4} \quad (4.2)$$

are good approximations, based on measured correlations on several soil samples. Table 4.4 provides the values for volumetric water content at permanent wilting point and field capacity,

and full saturation for the Kortright Centre soil, based on the approximate approach (Eqs. (4.1) and (4.2)).

Table 4.4: Calculated values for permanent wilting point, field capacity and full saturation, for the Kortright Centre soil sample.

Volumetric Water Content	[m³/m³]
θ_{PWP}	0.130
θ_{FC}	0.260
θ_{FS}	0.520

4.3 Experimental Techniques and Procedures

Soil thermal conductivity is strongly influenced by the soil volumetric water content and temperature. Hence, in order to obtain reliable experimental results, properties such as soil volumetric water content, dry bulk density and soil particle density have to be measured as accurately as possible. The sample preparation procedure has been obtained from Horton et al. [41], which subjects the pre-moist soil sample to heating and cooling cycles to obtain uniform water distributions. The procedure has been summarized in the following section.

4.3.1 Preparation of Soil Samples

The soil sample preparation procedure has been divided into three categories: dry, barely-to-moderately saturated, and highly-to-fully saturated samples [4]. Lumps of dry soil samples have been ground down to loose soil particles for better compaction. A microwave oven has been used to provide the heating cycles in order to distribute moisture evenly within the soil sample.

4.3.2 Soil Sample Preparation Procedure

The following procedure has been derived from the work of Nikolaev [4] and followed for the preparation of the Kortright Centre soil samples.

4.3.2.1 Dry Soil Sample Preparation

The following procedure is for dry soil sample preparation:

1. The soil sample is dried in an oven for 24 hours at a temperature of 105°C.
2. An arbitrary sample is chosen and its mass and volume are measured.
3. The soil sample is then poured into an electroplated steel container with the following dimensions: diameter: 149.42 mm, depth: 24.77 mm, wall thickness: 0.20 mm. To prevent formation of air gaps within the soil sample, the soil is poured into the experimental container in layers and well compacted with a 1 kg weight dropped over a height of about 10 cm for 5 times.
4. The dry bulk density, ρ_{db} , of the soil sample is determined by:

$$\rho_{db} = \frac{M_{ds}}{V_c} \quad (4.3)$$

where M_{ds} is the mass of the oven dry soil, and V_c is the volume of the experimental container.

5. The porosity (fraction of voids within the soil sample) is calculated by:

$$\phi = 1 - \frac{\rho_{db}}{\rho_s} \quad (4.4)$$

where ρ_s is the density of soil solid particles and is measured by mixing a known mass of soil in water and recording the volume change of the water.

6. The container is closed, the weight and thickness of the filled container are measured and it is ready for the experiment.

4.3.2.2 Barely-to-Moderately Moist Soil Sample Preparation

The following procedure is for preparation of those samples that are barely moist; with the volumetric water content, θ , below the permanent wilting point, θ_{PWP} . The volumetric water content is the fraction of total volume of water within the soil sample. Barely-to-moderately moist soil samples are prepared as follow:

1. The oven dry soil sample, with known mass, is poured into a sample container of known volume V_c . The following equations are used to obtain the desired volumetric water content θ :

$$V_w = V_c \theta \quad (4.5)$$

$$M_w = V_c \theta \rho_w \quad (4.6)$$

where V_w and M_w are volume and mass of water respectively. To ensure uniform moisture distribution within the sample, the dry soil and water are poured into a ziploc bag for mixing.

2. The ziploc bag is sealed, its weight measured, and placed into a microwave oven.
3. The bag is reheated for 5-10 times, for 1 minute each time, and left for 10 minutes to cool, at which point the next heating cycle starts. After the last heating/cooling cycle, the

sample is left in a constant temperature environment for 6 hours, and the cycle was repeated to ensure uniform moisture distribution.

4. The weight of the bag is re-measured, since some moisture could have escaped during the reheating process. The volumetric water content of the sample is recalculated, which is then used as the actual volumetric water content.
5. The soil sample is poured into an experimental container in layers and well compacted, as described previously, and the lid is closed. To prevent any moisture from escaping the container during the experiment, the experimental container is sealed using the Permatex 1372 high temperature, non-hardening, foam-a-gasket sealant.
6. The container is left at room temperature for 48 hours for the sealant to set and for the moisture to distribute evenly.
7. The weight of the container is measured and it is ready for experiment.
8. After the experiment, the sealed container is weighted again to check for any moisture loss.

The same procedure is also used to prepare moderately moist soil samples, i.e., $\theta_{PWP} < \theta < \theta_{FC}$.

4.3.2.3 Highly-to-Fully Saturated Soil Sample Preparation

The following procedure is for samples with volumetric water content greater than the field capacity, i.e., $\theta > \theta_{FC}$.

1. The dry soil (of mass M_{ds}) and water (of mass M_w) are poured into the ziploc bag.
2. The ziploc bag is sealed and weighted. The sample is mixed inside the bag

3. The soil sample is poured into an experimental container (of mass M_c), heavily compacted to prevent air gaps, and sealed.
4. The sealed container is left at room temperature for the sealant to set.
5. The weight of the sealed container is measured and it is ready for experiment.
6. After the experiment the container is weighed again to check for moisture loss.

4.4 Measurement of Saturated Soil Hydraulic Conductivity

Soil hydraulic conductivity is one of the parameters required to calculate the apparent thermal conductivity of the experimental soil. It describes the ease with which water can pass through pores in soil, and is influenced by soil water content and temperature as well. After extensive literature review, an analytical model of soil hydraulic conductivity used by Eching et al. [42] was found. In the paper, they have measured hydraulic conductivity of soils with similar soil compositions to two soils (Richmond Hill soil and Kortright Centre soil) under investigation in this research. In order to use the analytical model in this study, an experiment was conducted to obtain the values of saturated hydraulic conductivity for all three soil types, which were then compared with those presented in [42]. The soil sample preparation and experimental procedure for this test are explained in the following section.

4.4.1 Soil Sample Preparation

The hydraulic conductivity measurement described in this section follows the falling head test set up, shown in Figure 4.2. A large tank, at known height and filled with water, is connected to the test container by a transparent plastic tube with known diameter. Water is released from the tank, which goes through the tube and the sample container, and is collected at

the bottom. The following procedure was obtained from Dahiya et al. [43]. It includes soil compaction procedure as well as saturated hydraulic conductivity measurement.

4.4.1.1 Equipment and Supplies

1. Standard compaction mould with a diameter of 101.6 mm and height of 116.3 mm
2. Standard base plate and collar
3. Compaction rammer, 2.5 kg with a 51 mm diameter striking face and a 305 mm drop
4. Mixing tray, approximately 600 mm by 600 mm
5. Mixing trowel and scoop
6. Steel straight edge
7. Drying oven set at 105°C
8. Clean water, preferably distilled or demineralised

4.4.1.2 Soil Compaction Procedure

1. Place the soil in the tray and break up any lumps of soil being careful not to break any individual soil particles.
2. Place sufficient soil in the assembly (mould, base plate, and collar) such that the compacted specimen will occupy approximately 1/3 of the mould. Usually this means filling the mould to the 2/3 mark with loose soil.
3. Compact the soil in the mould by 25 uniformly distributed blows of the rammer. For each blow the rammer is allowed to fall freely for a distance of 305 mm.
4. Repeat steps 2 and 3 twice more giving a compacted thickness of soil of approximately 125 mm.

5. Remove the collar and the base plate and carefully trim the compacted soil with the straight edge until it is even with the top of the mould. Trimming should begin at the Centre of the specimen and proceed towards the outside.

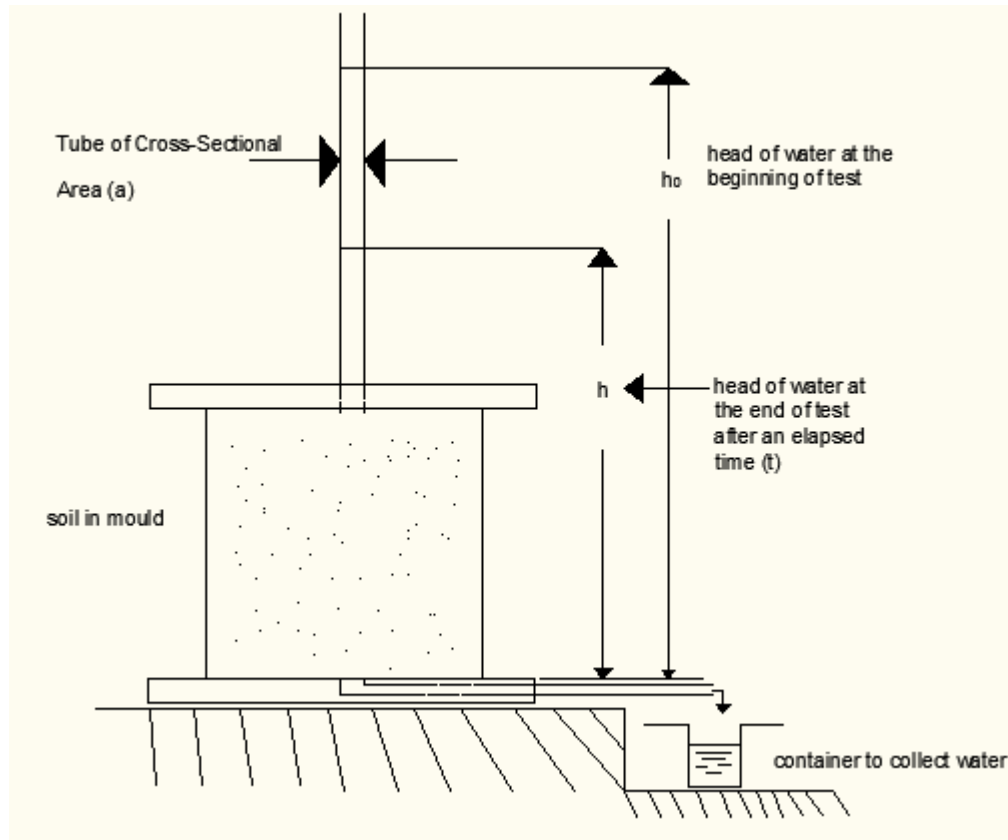


Figure 4.2: Falling head test set up [43].

4.4.2 Saturated Hydraulic Conductivity Measurement Procedure

1. Connect the prepared mould (see previous section) to the system as shown in Figure 4.2.
2. Allow water to pass through the system under a constant head for a sufficient time to ensure that no air remains in the system.
3. Collect the water which has passed through the soil and note the temperature but do not start recording the time at this point. When the temperature is relatively constant and the seepage appears to be regular and steady, the actual test can begin.

4. Take the initial reading of head of water in the tube above the soil specimen.
5. Start the timer.
6. After an interval of time, read and record the fallen head of water in the tube above the soil specimen and record the time. The interval of time will depend upon the type of soil being tested but should be such that the change in head will be in the order of one to two meters.

4.5 Measurement Error Analysis

The overall uncertainty in an experiment is a combination of several sources. These sources include equipment calibration, data acquisition, and data reduction. In order to have a good confidence on the experimental results, one must quantify these uncertainties and ensure they are within an acceptable range. The methodology to calculate the uncertainties for the experimental results introduced in this thesis has been derived from Reid [36].

4.5.1 Methodology in Uncertainty Calculations

The total error in any measurement is comprised of two components and is given by:

$$\delta_i = \beta + \varepsilon_i \quad (4.7)$$

where δ_i is the total error, β is the bias error, and ε_i is the precision error. The bias error is assumed to be constant for repeated measurements, and therefore, it represents a fixed deviation from the true value, which is estimated by calibration and independent measurements. The precision error, however, is based on statistical estimate and is given by the standard deviation σ .

The best estimate of σ is what is known as standard error, or precision index S_x , for N repeated measurements of a parameter x , and is given by:

$$S_x = \sqrt{\frac{\sum_{i=1}^N (x_i - \bar{x})^2}{N-1}} \quad (4.8)$$

where \bar{x} is the mean of the x_i measurements.

The total bias error of parameter x is calculated by combining all the individual parameters using the root-sum-square (RSS) method. Hence, the total bias error is given by:

$$B_x = \sqrt{B_1^2 + B_2^2 + \dots + B_j^2} \quad (4.9)$$

And the total precision index of the parameter is given by:

$$S_x = \sqrt{(S_x)_1^2 + (S_x)_2^2 + \dots + (S_x)_j^2} \quad (4.10)$$

By combining the bias and precision errors, Eqs. (4.9) and (4.10) respectively, the overall uncertainty U , of the desired parameter can be obtained. The RSS method, with 95 percent confidence level, is used again to combine these two errors:

$$U_{0.95} = \sqrt{(B_x)^2 + (t'S_x)^2} \quad (4.11)$$

where t' is the t multiplier for 95% confidence ($\alpha = 0.05$) and N-1 degrees of freedom. For a certain confidence interval, $1-\alpha$, the t -multiplier is the probability such that the unknown value is within $-t_{\alpha/2}$ and $+t_{\alpha/2}$ under a t -distribution graph with N-1 degrees of freedom.

4.5.2 Uncertainty in Derived Variables

To determine the uncertainty in results, a relationship between the dependent and independent variables must be obtained. This dependence is indicated by sensitivity coefficient, θ [4]. For a given function, Y :

$$Y = f(X_1, X_2, \dots, X_k) \quad (4.12)$$

The sensitivity coefficient is given by:

$$\theta_i = \frac{\partial Y}{\partial X_i} \quad (4.13)$$

The bias error and precision index of the result is then determined by the following expressions respectively:

$$B_Y = \left[\sum_{i=1}^k (\theta_i B_i)^2 \right]^{\frac{1}{2}} \quad (4.14)$$

$$S_Y = \left[\sum_{i=1}^k (\theta_i S_i)^2 \right]^{\frac{1}{2}} \quad (4.15)$$

The overall uncertainty for the derived variable Y can then be obtained as

$$U_{0.95} = \left[(B_Y)^2 + (t' S_Y)^2 \right]^{\frac{1}{2}} \quad (4.16)$$

where t' is the t multiplier for 95% confidence and $N-1$ degrees of freedom.

4.5.3 Measurement Equipment Specifications

A. National Instrument Data Acquisition Card:

B. Temperature Measurement:

i. Platinum Resistance Thermometer (PRT)

- a. Model: Azonix Corporation Model 12001A-1262A, laboratory grade
- b. Repeatability and accuracy: 0.006°C (4)

ii. Platinum Resistance Temperature Detector (RTD)

- a. Model: OMEGAFILM RTD element series F, catalog no. F3105
- b. Nominal resistance: $100\ \Omega$ at 0°C
- c. Repeatability: $< 0.01^{\circ}\text{C}$

C. NEMIC-LAMBDA Programmable Power Supply

i. Model: ZUP 10-20

a. Constant Voltage

Range: $0 - 10\text{V}$ with 2.8 mV resolution

Stability: $\pm 0.01\% + 2\text{ mV}$ ($T_{\text{ambient}} = 25^{\circ}\text{C} \pm 5^{\circ}\text{C}$)

b. Constant Current:

Range: $0 - 20\text{ A}$ with 6 mA resolution

Stability: $\pm 0.02\% + 5\text{ mA}$ ($T_{\text{ambient}} = 25^{\circ}\text{C} \pm 5^{\circ}\text{C}$)

D. Standard Micrometers

- i. Range: $0 - 25.4\text{ mm}$ and $0 - 200\text{ mm}$
- ii. Precision error: 0.0254 mm

4.5.4 Plate Temperature Measurement

The overall bias errors for hot plate, cold plate, as well as heater plate temperature measurements are determined as follows [36]:

The bias error for hot and cold plate measurement is evaluated from the fluid temperature change, the conduction error due to lead wires, and the calibration of the RTD, which is given by:

$$B(T_h) = [(0.0017\Delta T)^2 + (4 \times 0.0016)^2 + 0.0283^2]^{\frac{1}{2}} \quad (4.17)$$

$$B(T_c) = [(0.0033\Delta T)^2 + (4 \times 0.018)^2 + 0.0283^2]^{\frac{1}{2}} \quad (4.18)$$

The heater plate measurement bias error is due to heater plate temperature non-uniformity due to the HFM, the conduction error of the thermocouple lead wire, and the calibration of the thermocouple, given by:

$$B(T_{htr}) = [(0.0011\Delta T)^2 + 0.0011^2 + 0.034^2]^{\frac{1}{2}} \quad (4.19)$$

For a ΔT of 4°C, the bias errors for the cold plate, the hot plate, and the heater plate were obtained to be $\pm 0.0785^\circ\text{C}$, $\pm 0.0298^\circ\text{C}$, and $\pm 0.0343^\circ\text{C}$ respectively.

The bias error of the mean temperature, T_m between the hot plate and the cold plate was obtained as:

$$\frac{B(T_m)}{T_m} = \left[\left(\frac{0.00586}{T_m} \right)^2 + 2.89 \times 10^{-6} \left(\frac{\Delta T}{T_m} \right)^2 \right]^{\frac{1}{2}} \quad (4.20)$$

The mean temperature bias error was determined to be 0.448%.

4.5.5 Measurement of Temperature Difference

The bias limit for measuring the temperature difference between the hot and cold plate is determined by the following expression:

$$\frac{B(\Delta T)}{\Delta T} = \left[\left(\frac{B(T_h)}{\Delta T} \right)^2 + \left(\frac{B(T_c)}{\Delta T} \right)^2 \right] \quad (4.21)$$

The bias error of the temperature difference between the hot and cold plates was 2.10% for $\Delta T = 4^\circ\text{C}$.

4.5.6 Error Associate with the Cold Bath Tank

Due to the age of the refrigeration system in the cold bath tank used to maintain the temperature of the cold plate, the fluctuation of the cold bath temperature was noticed to be higher at low temperatures, up to about 40°C . Figure 4.3 shows the variation in the cold plate temperature fluctuation from 5 to 92°C .

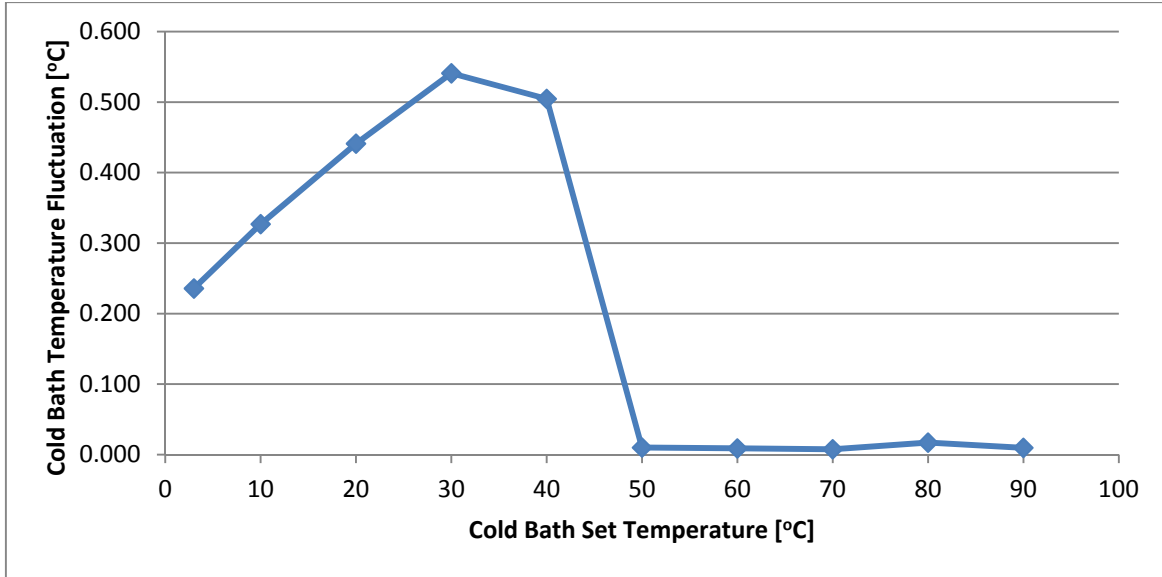


Figure 4.3: Variation in the cold bath temperature fluctuation from 5°C to 92°C.

This significant change in the cold bath temperature fluctuation will impact the measurement of the temperature difference across the soil specimen at low temperatures, which in turn will impact the measurement of the overall soil thermal conductivity. Hence the error associated with the cold bath temperature fluctuation must be considered in the overall measurement error of the soil thermal conductivity. However the error associated with the fluctuation can be reduced by taking measurement over a long period of time (such as 30 minutes), in order to cover at least three cycles of the fluctuation giving a very close to ‘true’ average value of the cold-plate temperature.

4.5.7 Measurement of Electrical Power

NEMIC-LAMBDA power supply (Model ZUP 10-20) was used to supply power to the heater plate. A piece of constantan wire ($R_{sh} = 0.36 \, \Omega \pm 1.4\%$) was connected in series to the heater plate to form a shunt resistance. The current to the heater plate was determined using the shunt resistance. By determining the voltage drop across the heater plate, V , and the shut

resistance, V_{sh} , it was possible to determine the electrical power supplied to the heater plate using the following expression:

$$VI = V \left(\frac{V_{sh}}{R_{sh}} \right) \quad (4.22)$$

From RSS method, the bias error for measuring electrical power to the heater plate was determined by:

$$\frac{B(VI)}{VI} = \left[\left(\frac{B(V)}{V} \right)^2 + \left(\frac{B(V_{sh})}{V_{sh}} \right)^2 + \left(\frac{B(R_{sh})}{R_{sh}} \right)^2 \right]^{\frac{1}{2}} \quad (4.23)$$

The bias error of the heater plate power was determined to be 1.4%

4.5.8 Error in Measurement of Other Dimensions

Other dimensions that needed to be measured during this research included the effective surface area of the heater plate A_{hp} , the distance between the hot plate and the cold plate L , the diameter D , and height H , of the specimen container. A micrometer with precision error of ± 0.0254 mm was used for measurement of dimensions smaller than 25.4 mm and another for dimensions up to 200 mm [36].

4.5.8.1 Effective Heater Plate Area

The effective heater plate area (Figure 4.4) is defined as a plate having same side dimensions as the heater plate plus one-half the nominal 0.80 mm width of the gap between the

plate and the hot plate [4]. The uncertainty of this area was taken as one-half of the gap area.

Thus, the effective heater plate area was calculated as [36]:

$$A_{hp} = 5.929 \times 10^{-3} \text{ m}^2 \pm 1.2 \times 10^{-4} \text{ m}^2$$

Therefore the uncertainty of the heater plate area was 2.02%.

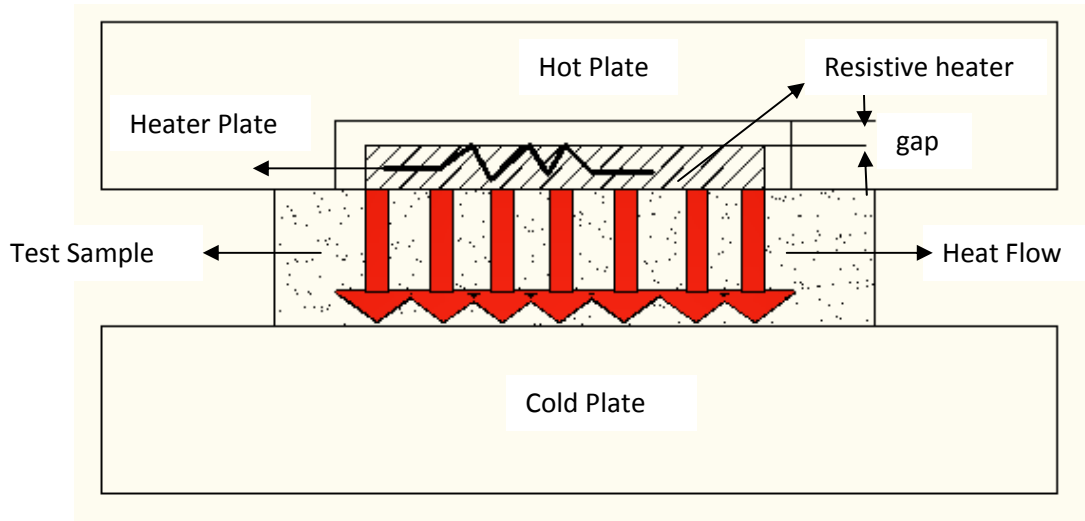


Figure 4.4: Guarded Hot Plat (GHP) apparatus schematic diagram.

4.5.8.2 Total Specimen Thickness

The distance between the hot plate and cold plate was determined as the sum of the soil specimen in the test container, the thickness of the container base and lid, and the thickness of the rubber pads at both outer surfaces of the test container [36]. The total specimen thickness was calculated to be:

$$L = 26.13 \text{ mm} \pm 0.025 \text{ mm}$$

This gives an uncertainty of 0.0972%.

4.5.8.3 *Effective Specimen Thickness*

The effective specimen thickness is the thickness of the soil layer within the sample container, H , and was calculated to be:

$$H = 24.37 \text{ mm} \pm 0.11 \text{ mm}$$

This gives an uncertainty of 0.435%

4.5.8.4 *Diameter and Thickness of Sample Container*

The diameter and thickness of the sample container were determined as:

$$D = 144.48 \text{ mm} \pm 0.09 \text{ mm} \text{ (0.0640\% uncertainty)}$$

$$\text{Specimen container thickness (lid and cover)} = 0.23 \text{ mm} \pm 0.025 \text{ mm}$$

4.5.8.5 *Silicon Rubber Pad Thickness*

The thickness of each silicon rubber pad was determined as:

$$L_{srp} = 0.68 \text{ mm} \pm 0.025 \text{ mm} \text{ (3.676\% uncertainty)}$$

4.5.8.6 *Plate Flatness*

To obtain the plate flatness measurement uncertainty, thickness of gaps between a steel straight edge and plate surface was checked using a precision feller gauge set [36]. Maximum deviation was in the order of $\pm 0.05 \text{ mm}$ over the plate's surface.

4.5.9 Heat Flux Measurement

The heat transfer from the heater plate to the cold plate is defined by:

$$q = q_{hp} + q_{HFM} \quad (4.24)$$

where q_{hp} is the electrical power to the heater plate and q_{HFM} is the heat transfer from the guarded hot plate to the heater plate via the heat flux meter, defined as [36]:

$$q_{hp} = VI \quad (4.25)$$

$$q_{HFM} = \alpha e \quad (4.26)$$

Therefore, the heat flux through the specimen is determined by:

$$q'' = \frac{q}{A_{hp}} = \frac{VI + \alpha e}{A_{hp}} \quad (4.27)$$

Since the temperature difference between the guarded hot plate and the heater plate is very small, due to the optimal electrical power supplied to the heater plate, the *emf* reading (e) from the heat flux meter is essentially zero. Therefore the bias error associated with the heat flux is only determined from uncertainties in calculating the heater plate area A_{hp} and the power to the heater plate q_{hp} :

$$\frac{B(q'')}{q''} = \left[\left(\frac{B(A_{hp})}{A_{hp}} \right)^2 + \left(\frac{B(VI)}{VI} \right)^2 \right]^{\frac{1}{2}} \quad (4.28)$$

The bias error of the heat flux was calculated to be 2.46%.

4.5.10 Thermal Conductivity Measurement

The thermal conductivity is determined from Fourier's law as:

$$\lambda = q'' \frac{dx}{dT} \quad (4.29)$$

Here, dx in above equation represents the specimen thickness, H , and dT is the temperature difference across the specimen thickness, ΔT . Hence, the bias error associated with the soil thermal conductivity measurement is determined from uncertainty in measurement of the heat flux, q'' , specimen thickness, H , and temperature difference across the specimen, ΔT :

$$\frac{B(\lambda)}{\lambda} = \left[\left(\frac{B(q'')}{q''} \right)^2 + \left(\frac{B(H)}{H} \right)^2 + \left(\frac{B(\Delta T)}{\Delta T} \right)^2 \right]^{\frac{1}{2}} \quad (4.30)$$

As stated previously, the error associated with the cold bath temperature fluctuation must be considered when determining the bias error of the thermal conductivity. Hence, the bias error of the soil thermal conductivity was determined to be 6.00% at highest cold bath temperature fluctuation, and 5.56%, at lowest cold bath temperature fluctuation.

4.5.11 Saturated Hydraulic Conductivity Experimental Measurement Uncertainty

The hydraulic conductivity measurement was associated with several uncertainties such as specimen thickness, tube diameter, d , measurement of water head (h_o and h), test container diameter, D , and elapsed time.

4.5.11.7 Specimen Thickness

Specimen thickness is the thickness of the soil layer within the test container. The specimen thickness was determined to be:

$$L = 12 \text{ cm} \pm 0.05 \text{ cm} (0.417\% \text{ uncertainty})$$

4.5.11.8 Measurement of Tube and Test Container Diameter

The diameters of the tube and test container were measured to be:

$$d = 0.6 \text{ cm} \pm 0.005 \text{ cm}$$

$$D = 11.4 \text{ cm} \pm 0.05 \text{ cm}$$

4.5.11.9 Measurement of Water Head

The water pressure heads, h and h_o , were measured to be:

$$h_o = 2 \text{ m} \pm 0.0005 \text{ m} (0.0250\% \text{ uncertainty})$$

$$h = 1 \text{ m} \pm 0.0005 \text{ m} (0.0500\% \text{ uncertainty})$$

4.5.11.10 Measurement of Elapsed Time

The elapsed time for the water level to drop from h_o to h was measured using a regular stop watch as:

$$t = 8369 \text{ s} \pm 0.05 \text{ s} (0.000597\% \text{ uncertainty}) \text{ for Richmond Hill soil,}$$

$$t = 2.13 \text{ s} \pm 0.05 \text{ s} (2.35\% \text{ uncertainty}) \text{ for Ottawa Sand}$$

$$t = 8120 \text{ s} \pm 0.05 \text{ s} (0.000616\% \text{ uncertainty}) \text{ for Kortright Centre soil}$$

4.5.11.11 Measurement of Hydraulic Conductivity

The saturated hydraulic conductivity was calculated using the following expression [43]:

$$K_s = \frac{2.3aL}{At} \log\left(\frac{h_o}{h}\right) \quad (4.30)$$

where a is the tube cross-sectional diameter, L is the specimen thickness, A is the specimen cross-sectional area, t is the elapsed time, and h_o and h are the water pressure head at the initial and final time.

Therefore, the bias error associated with the measurement of hydraulic conductivity is determined as the RSS of the errors associated with the tube cross-sectional diameter, the specimen thickness, the specimen cross-sectional area, the elapsed time, and the water pressure head. Using Eqs. (4.13) and (4.14):

$$\frac{B(K_s)}{K_s} = \left[\left(\frac{B(a)}{a} \right)^2 + \left(\frac{B(A)}{A} \right)^2 + \left(\frac{B(L)}{L} \right)^2 + \left(\frac{B(t)}{t} \right)^2 + \left(\frac{B(h_o)}{h_o \log\left(\frac{h_o}{h}\right)} \right)^2 + \left(\frac{B(h)}{h \log\left(\frac{h_o}{h}\right)} \right)^2 \right] \quad (4.31)$$

The bias error of saturated hydraulic conductivity measurement for Richmond Hill soil, Ottawa sand, and Kortright Centre soil was calculated to be 0.991%, 2.55%, and 0.995% respectively.

CHAPTER 5 EXPERIMENTAL RESULTS AND DISCUSSION

5.1 Results and Discussion of Soil Hydraulic Conductivity

Experimental results for saturated hydraulic conductivity, K_s , of Ottawa sand, Richmond Hill fine sandy loam, and Kortright Centre loam have been presented in Table 5.1.

Table 5.1: Experimental result of saturated hydraulic conductivity.

Soil Type	Saturated Hydraulic Conductivity, K_s [m/s]
Ottawa Sand	5.71×10^{-3}
Richmond Hill Fine Sandy Loam	2.75×10^{-6}
Kortright Centre Loam	5.34×10^{-6}

Hydraulic conductivity describes the ease with which water can pass through the pore spaces within the soil. The higher the hydraulic conductivity, the higher is the rate of water moving through the pore spaces. Hence, hydraulic conductivity is highly dependent on soil texture. A soil with high sand content has more “voids” within pores and therefore it would be easier for water to pass through. Conversely, a soil with high clay content has finer particles and therefore harder for water to move through its pore spaces. This impact of soil texture can be seen by looking at the experimental results obtained for saturated hydraulic conductivity of three

soils under investigation. Ottawa sand has 99% sand content and hence it has very high saturated hydraulic conductivity. On the other hand, Richmond Hill and Kortright Centre soils have higher silt and clay content and therefore they have lower saturated hydraulic conductivity.

As mentioned previously, the saturated hydraulic conductivity measurement was compared with saturated hydraulic conductivity of similar soils presented in Eching et al. [42]. The difference between the experimental results and those obtained from [42] are presented in Table 5.2².

Table 5.2: Comparison between the present and previous [42] experimental values of saturated hydraulic conductivity.

Soil Type	Present Experiment K_s [m/s]	Previous Experiment K_s [m/s]	Difference [%]
Richmond Hill Sandy Loam	2.75×10^{-6}	2.80×10^{-6} (Hanford sandy loam)	1.82
Kortright Centre Loam	5.34×10^{-6}	5.43×10^{-6} (Panoche loam)	1.69

² The saturated hydraulic conductivity of Ottawa sand has not been added to Table 5.2, since its soil composition is different from that presented in Eching et al. [42].

The differences between the present and previous experimental results for Richmond Hill and Kortright Centre soils are about the overall experimental uncertainty of 1%. Hence, it would be reasonable to implement the analytical hydraulic conductivity model used by Eching et al. [42] for Richmond Hill and Kortright Centre soils for the evaluation of a theoretical soil apparent thermal conductivity model, as described in Chapter 6.

5.2 Experimental Results of Kortright Centre Soil Thermal Conductivity

5.2.1 Introduction

Measurement of the thermal conductivity of Kortright Centre loam soil was conducted using the guarded hot plate apparatus in Ryerson University's Thermofluids Research Laboratory to study the impact of variation in soil water content and temperature on soil thermal conductivity. The results were obtained for a temperature range of 5 to 92°C, at 10°C intervals, with $\Delta T = 4^\circ\text{C}$ between the hot and cold plate, from complete dryness to full saturation. This temperature difference was selected through a series of preliminary analysis [4] to provide an optimum temperature difference for maximizing the sensitivity of measuring equipment and minimizing the temperature gradient across the specific thickness of soil samples.

5.2.2 Experimental Result

The variation in thermal conductivity of Kortright Centre loam soil with volumetric water content for each temperature is presented in Figure 5.1³. The effect of temperature and water content are clearly visible in the graph, and follow a similar pattern to the results obtained by Nikolaev [4] for Ottawa sand and Richmond Hill soil thermal conductivities, as shown in Figures 5.2 and 5.3 respectively.

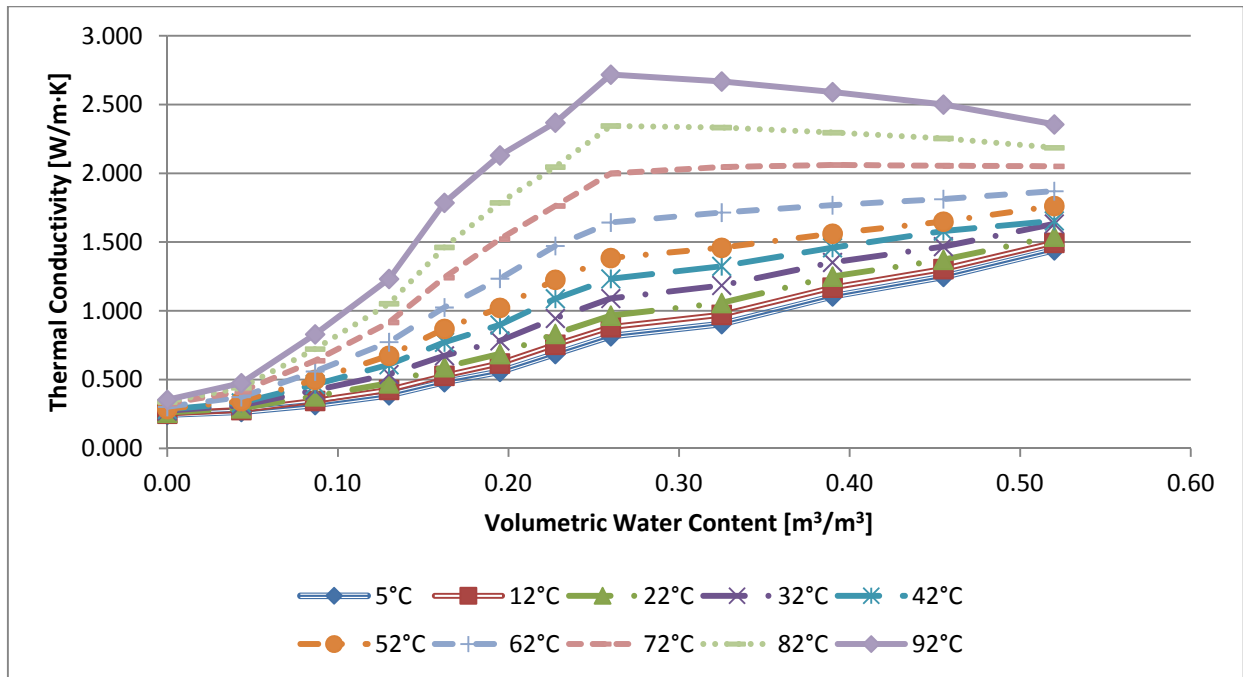


Figure 5.1: Variation in thermal conductivity of Kortright Centre soil with temperature and volumetric water content.

³ For tabulated data please refer to Appendix B.

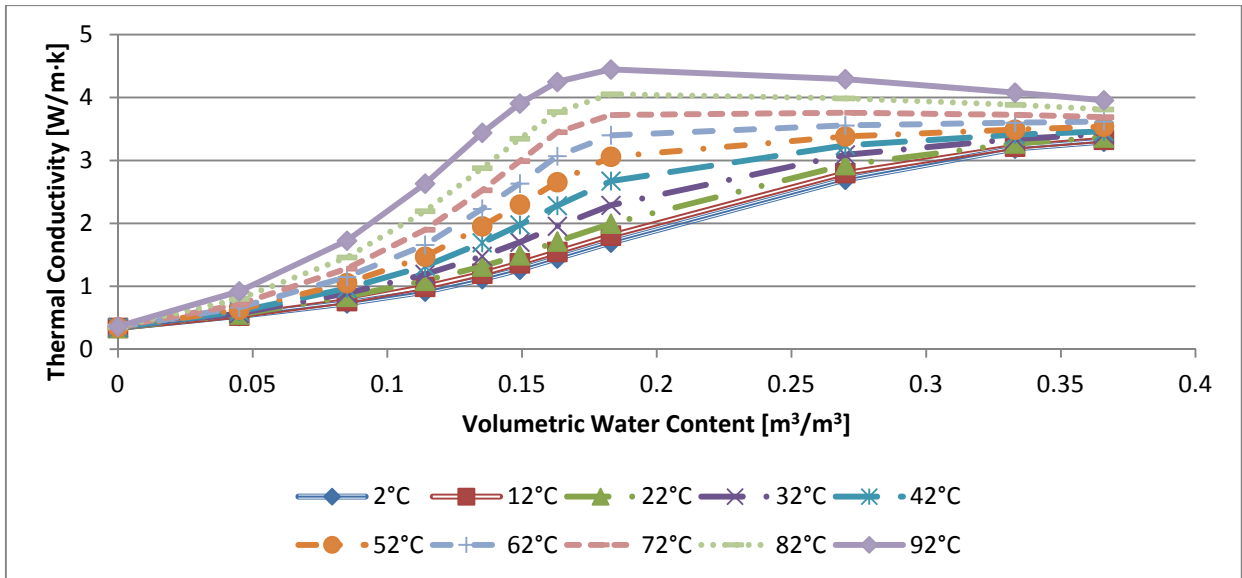


Figure 5.2: Variation in thermal conductivity of Ottawa sand with temperature and volumetric water content.

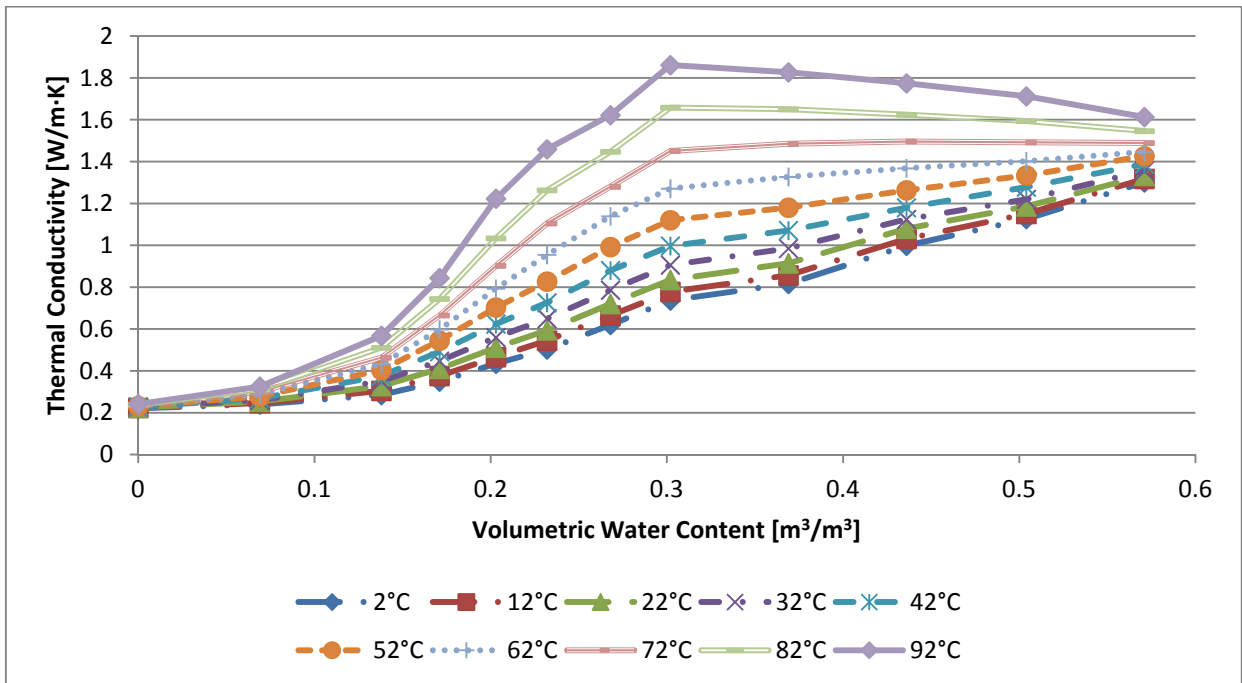


Figure 5.3: Variation in thermal conductivity of Richmond Hill soil with temperature and volumetric water content.

As Figure 5.1 shows, soil thermal conductivity is dependent on soil water content and temperature. At low temperatures, up to approximately 30°C, heat transfer is mainly dominated by pure conduction and vapour migration does not have any effect, which is evident by small variation in soil thermal conductivity. As temperature increases, especially at temperatures above 40°C, vapour migration becomes more significant. At high temperatures, heat transfer between soil particles is enhanced due to moisture occupying void spaces between soil particles. As temperature is increased, moisture between soil particles absorbs and transfers the heat away in the form of water vapour. In fact, the increase in soil thermal conductivity from 32 to 92°C is approximately 359 percent greater than the one from 5 to 32°C.

Figure 5.1 also shows a clear dependency of soil thermal conductivity to variation in soil water content. At low moisture levels (below permanent wilting point) soil thermal conductivity increases at a slow rate. The slow rate is due to the fact that at this stage, the soil particles are barely covered by water and the voids between particles are still occupied by air pockets. As moisture level is increased beyond the permanent wilting point, however, heat transfer between soil particles is increased rapidly, which is evident by the steep increase in soil thermal conductivity. In particular, at 92°C and at field capacity, soil thermal conductivity is approximately 15 percent greater than that at full saturation. At this stage, water is starting to fill the voids between soil particles and thereby enhancing the heat transfer between soil particles. At this stage, heat transfer is enhanced even further as temperature is increased, as vapour migration dominates the heat transfer process. As soil water content is increased beyond the field capacity, the increase in heat transfer rate is reduced. This is due to the fact that at this stage, most of the voids between soil particles are filled with water. As the result, heat transfer due to moisture migration is reduced. In fact, as the temperature exceeds approximately 70°C, the thermal

conductivity slowly decreases with increase in water content. This may be explained by the fact that since most of void spaces between soil particles are filled with water, water vapour cannot migrate away from the heat source, thereby reducing the heat transfer rate.

Kortright Centre soil has lower thermal conductivity than Ottawa sand by an average of approximately 50 percent from completely dry to full saturation, for all temperatures. Compared to Richmond Hill soil, however, Kortright Centre soil has higher thermal conductivity by an average of approximately 26 percent. Such difference in thermal conductivities may be explained by the variation in soil composition between each soil type. In order to better understand the impact of soil type on soil thermal conductivity, more soil types, such as silt and clay need to be examined. In addition, Kortright Centre soil thermal conductivity increases by an average of 500 percent, from completely dry to full saturation, and by approximately 170 percent from 5°C to 92°C. This observation suggests that soil thermal conductivity may be more dependent on variation in water content than temperature.

CHAPTER 6 A STUDY OF THE APPARENT THERMAL CONDUCTIVITY OF SOILS DUE TO VAPOUR MIGRATION

6.1 Introduction

Extensive work has been published on the concept of coupled heat and moisture transfer in soil, yet, to the best knowledge of the author, none of the previously published work on this concept has been able to develop a universally accepted methodology for evaluating soil thermal conductivity. In this chapter, two models developed by Thomas [9] and Thomas and King [11] are examined and extended, to develop a more accurate method of evaluating soil thermal conductivity. To this extent, the experimental values of the phase conversion factor, ε , are obtained, using the experimental results of Ottawa sand and Richmond Hill soil, in order to allow the use of the soil apparent thermal conductivity equation (Eq. 6.3) to obtain a more accurate expression for soil thermal conductivity as a function of temperature and water content.

6.2 Theory

The flow of water in saturated and unsaturated soil is described by Darcy's law [9]. There are two approaches, as described by Thomas [9] to predict unsaturated flow. The first approach is in terms of pore capillary potential ψ , and second is in terms of volumetric water content θ . The disadvantage of the second approach is that it cannot readily be extended to include saturated flow; nonetheless it is widely used in coupled heat and mass transfer work. When soil is subjected to both a temperature and moisture-content gradients, fluid flow takes place due to

thermal effects [9], in the form of vapour and liquid transfer. Near saturation and at very low saturation levels, there is little coupling of these processes, so vapour transfer is negligible. For large ranges of water content, however, the coupling becomes significant, with the maximum coupling expected to occur when the moisture moves mainly in the liquid phase [9]. Thomas derived a model for coupled heat and mass transfer using the work of de Vries [6], leading to the following governing heat transfer equation [9]:

$$C \frac{\partial T}{\partial t} = \nabla \cdot (\lambda_{eff} \nabla T) + \nabla \cdot \left(\frac{K_\varepsilon}{D_T} \nabla \theta_l \right) + L \rho_l \frac{\partial(\varepsilon K)}{\partial z} \quad (6.1)$$

where the parameter K_ε is defined in Appendix A and λ_{eff} is the effective thermal conductivity of soil, given by:

$$\lambda_{eff} = \lambda_c + \lambda_{app} \quad (6.2)$$

Here, λ_c is the soil thermal conductivity for pure heat conduction and λ_{app} is the apparent thermal conductivity due to vapour migration, expressible as

$$\lambda_{app} = L \varepsilon \rho_l D_T \quad (6.3)$$

This is the enhanced thermal conductivity which is examined in this study. In Eq. (6.3), D_T is the thermal moisture diffusivity, defined as follows [44]:

$$D_T = D_{Tl} + D_{Tv} \quad (6.4)$$

where

$$D_{Tl} = K \frac{\partial \psi}{\partial T} \quad (6.5)$$

$$D_{Tv} = f(\theta_a) D_{atm} \frac{p}{p - p_v} \frac{\rho_v}{\rho_l} \frac{(\nabla T)_a}{\nabla T} \frac{1}{p_{vs}} \frac{\partial p_{vs}}{\partial T} \quad (6.6)$$

The model developed by Thomas and King [11] has also employed the extension of the Darcy's law to unsaturated flow. There is a difference, however, because the final model is derived for coupled heat and mass transfer. The governing differential equation for heat transfer developed by [11] is as follows:

$$\rho_l C_{T\psi} \frac{\partial \psi}{\partial t} + \rho_l C_{TT} \frac{\partial T}{\partial t} = \nabla \cdot (\lambda_{eff} \nabla T) + \nabla \cdot (\rho_l K_{T\psi} \nabla \psi) \quad (6.7)$$

where the parameters $C_{T\psi}$, C_{TT} , and $K_{T\psi}$ are defined in Appendix A. The effective thermal conductivity λ_{eff} in Eq. (6.7) consists of two components (like Eq. (6.2)), but the apparent thermal conductivity is as given below [11]:

$$\lambda_{app} = L \rho_l K_{v2} \quad (6.8)$$

where

$$K_{v2} = f(\theta_a) \frac{D_{atm}}{\rho_l} \frac{p}{p - p_v} \frac{(\nabla T)_a}{\nabla T} \left(h \frac{\partial \rho_{vs}}{\partial T} - \frac{\rho_v \psi g}{R_v T^2} \right) \quad (6.9)$$

The following parameters are common between Eq. (6.6) and Eq. (6.9) [9, 11, 6]:

$$f(\theta_a) = \begin{cases} \theta_a + \theta_l = \eta, & \theta_l \leq \theta_{lk} \\ \theta_a + \theta_a \frac{\eta - \theta_a}{\eta - \theta_{lk}}, & \theta_l > \theta_{lk} \end{cases} \quad (6.10)$$

$$D_{atm} = 21.7 \times 10^{-6} (T / 273.16)^{1.88} \quad (6.11)$$

$$p_v = p_{vs} h = p_{vs} \exp(\psi g / R_v T) \quad (6.12)$$

$$\rho_v = \rho_{vs} h = \rho_{vs} \exp(\psi g / R_v T) \quad (6.13)$$

$$\frac{(\nabla T)_a}{\nabla T} = \frac{1}{3} \left[\frac{2}{1 + BG} + \frac{1}{1 + B(1 - 2G)} \right] \quad (6.14)$$

$$G = \begin{cases} 0.333 - 0.298(\eta - \theta_l) / \eta, & \theta_{FC} < \theta_l < \eta \\ 0.013 + (0.32 - 0.298(\eta - \theta_{FC}) / \eta)(\theta_l / \theta_{FC}), & 0 < \theta_l < \theta_{FC} \end{cases} \quad (6.15)$$

$$B = (\lambda_a + \lambda_v) / \lambda_l - 1 \quad (6.16)$$

$$\lambda_v = D_{atm} \frac{p}{p - p_v} h L \frac{\partial \rho_{vs}}{\partial T} \quad (6.17)$$

Walker et al. [45] state that θ_k in Eq. (6.10) is best equated to $\eta/4$ for soils with high clay contents and $\eta/8$ for very sandy soils. Note that p_{vs} in Eqs. (6.6) and (6.12) and ρ_{vs} in Eqs. (6.9), (6.13) and (6.17) are the saturation pressure and the density of saturated vapour, respectively. These parameters can be expressed as polynomial functions of temperature by fitting their values, as determined from steam tables. Similarly, the density of liquid water ρ_l can be expressed as a polynomial function by fitting density values of saturated liquid from steam tables. The thermal conductivities of air λ_a and liquid water λ_l are readily obtainable as a function of temperature from heat transfer texts and other property data sources.

Thomas and King [11] suggest that the vapour flow area factor $f(\theta_a)$ in Eq. (6.9) be equal to the porosity η at all water contents. However, in order to ensure that K_{v2} becomes zero at fully saturated condition (i.e., $\theta_l = \eta$), $f(\theta_a)$ in Eq. (6.10) is used for K_{v2} in this study, because there is no vapour migration at the fully saturated state.

6.3 Methodology

6.3.1 Experimental Data

Figure 6.1⁴ shows measurements of λ_{eff} obtained by Nikolaev [4] for Ottawa sand (C190). This soil is natural silica sand with 99% quartz content, a particle density of 2650 kg/m³, and particles with diameters varying from 0.59 to 0.84 mm. It is compacted to a dry bulb density of 1680 kg/m³, giving a porosity $\eta = 0.366$. Its permanent wilting point and field capacity are approximated to be $\theta_{PWP} = \eta/4$ and $\theta_{FC} = \eta/2$ [46] which are 0.092 and 0.18 m³/m³, respectively.

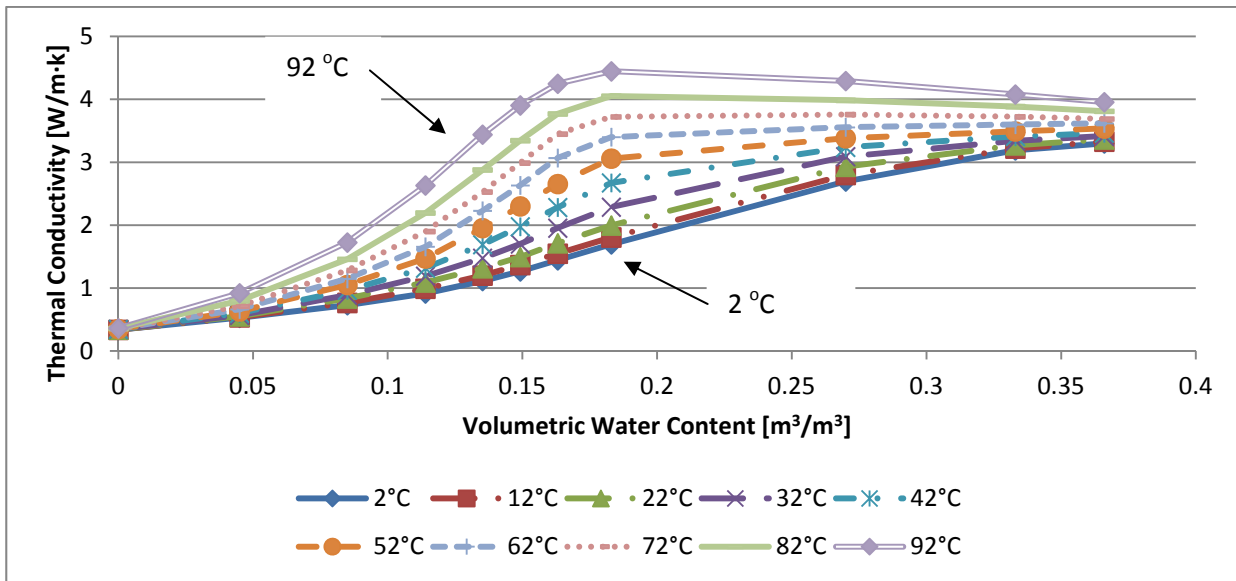


Figure 6.1: Experimental λ_{eff} data for Ottawa sand [4].

Figure 6.1 clearly shows the change in the effective thermal conductivity with temperature and volumetric liquid water content. Therefore, in order to be able to evaluate the two models of apparent thermal conductivities due to vapour migration, as expressed by Eqs. (6.3) and (6.8), the values of the apparent thermal conductivity must first be extracted from the

⁴ Data is tabulated in Table B-1 in Appendix B.

data in Figure 6.1. This step is accomplished by creating a surface fitting the data for 2, 12 and 22°C, together with the data at dry and saturation states for all temperatures. These selected data represent the soil thermal conductivity for pure heat conduction with a reasonable assumption that the apparent thermal conductivity due to vapour migration plays a very minor role at low temperatures. The resulting surface curve fitting equation, which is a function of θ_l and T , serves to predict the soil thermal conductivity of pure heat conduction for other temperatures ($T > 22^\circ\text{C}$) from dry to saturation states.

Figure 6.2⁵, developed from Nikolaev's data in Figure 6.1 using a surface fitting program called TableCurve3D, shows some of the predicted values of the soil thermal conductivity for pure heat conduction. Finally the apparent thermal conductivity due to vapour migration, as shown in Figure 6.3⁶ for four selected temperatures, can be obtained by subtracting the values in Figure 6.2 from the data values in Figure 6.1.

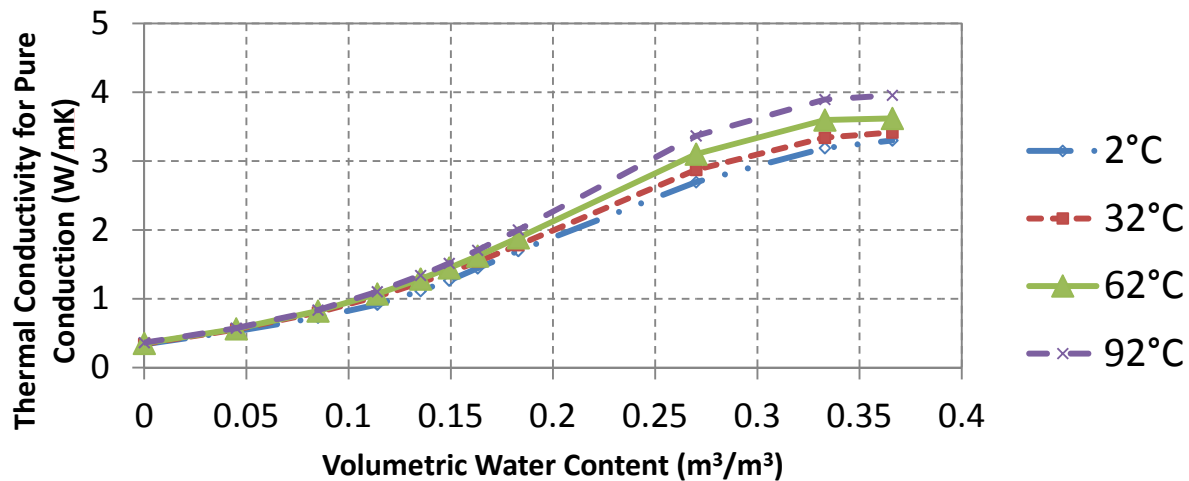


Figure 6.2: Variation in Ottawa sand thermal conductivity due to pure conduction.

⁵ The full set of data is tabulated in Table B-2 in Appendix B.

⁶ The full set of data is tabulated in Table B-3 in Appendix B.

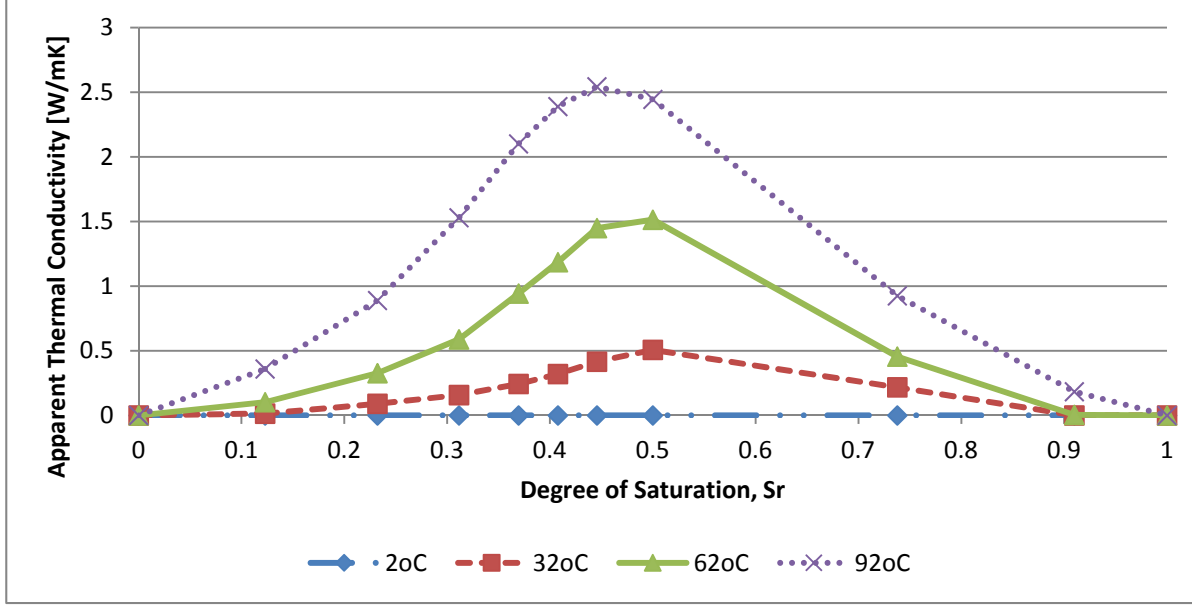


Figure 6.3: Apparent thermal conductivity due to vapour migration ($\lambda_{app,exp} = \lambda_{eff} - \lambda_c$).

By comparing the data in Figures 6.1 and 6.3, it is seen that the fractions of apparent thermal conductivity can be as high as 60% of the effective soil thermal conductivity, depending on the volumetric liquid content and temperature, especially at around θ_{FC} and high temperature. Hence, the apparent thermal conductivity can play an important role in heat diffusion in soils.

The results from Table B-3 in Appendix B can now be used to verify the validity of the two λ_{app} models developed Thomas [9] and Thomas and King [11]. In order to calculate the apparent thermal conductivity using Eq. (6.3), the phase conversion factor ε needs to be calculated as a function of θ_l and T .

6.3.2 Preliminary Evaluation

Since Eqs. (6.6) and (6.9) appear to be similar, a preliminary evaluation on them is performed. In order to apply Eqs. (6.6) and (6.9), the following ψ - θ_l and K - θ_l relationships (for Ottawa sand) [11] are used:

$$\psi(\theta_l, T) = \frac{\sigma(T)}{\sigma(T_r)} \psi_r(\theta_l) \quad (6.18)$$

$$K(\theta_l, T) = \frac{\mu(T_r)}{\mu(T)} K_r(\theta_l) \quad (6.19)$$

where σ and μ are the surface tension and the dynamic viscosity of water, respectively, as functions of temperature given below:

$$\sigma(T) = 0.1171 - 0.0001516T \quad (6.20)$$

$$\mu(T) = 661.2 \times 10^{-3} (T - 229)^{-1.562} \quad (6.21)$$

Also, the experimental reference capillary potential and unsaturated hydraulic conductivity functions for a medium sand at $T_r = 293.15$ K [11, 42] are used:

$$\psi_r(\theta_l) = (-2.41 - 0.002 \theta_l^{-1.75}) / g \quad (6.22)$$

$$K_r = K_s \left[\frac{(\theta - \theta_r)}{(\theta_s - \theta_r)} \right]^l \times \left[1 - \left(1 - \left[\frac{(\theta - \theta_r)}{(\theta_s - \theta_r)} \right]^{\frac{1}{m}} \right)^m \right]^2 \quad (6.23)$$

where K_s is the saturated hydraulic conductivity, obtained experimentally as described in Chapter 4, θ_r is the residual water content, θ_s is the saturated water content, and l and m are non-dimensional parameters [42] as follows:

$$K_s = 0.0057086 \text{ m/s}$$

$$\theta_r = 0.032 \text{ m}^3/\text{m}^3$$

$$\theta_s = 0.366 \text{ m}^3/\text{m}^3$$

$$l = 0.5$$

$$m = (1 - (1/n))$$

$$n = 7.339$$

For Richmond Hill soil, most of the equations introduced before are the same except that of capillary potential. Eq. (6.24) represents this parameter:

$$\psi = \psi_s \left(\frac{\theta}{\theta_s} \right)^{-b} \quad (6.24)$$

where, using a curve fitting software, called TableCurve2D, and the experimental data of Endo et al. [47], the values for ψ_s and b are obtained:

$$\psi_s = -1.085 \text{ m}$$

$$b = 3.554$$

The hydraulic conductivity equation for the Richmond Hill soil is the same as that for Ottawa sand (Eq. 6.23), except the values for the following parameters have changed:

$$K_s = 2.753 \times 10^{-6} \text{ m/s}$$

$$\theta_r = 0.01 \text{ m}^3/\text{m}^3$$

$$\theta_s = 0.571 \text{ m}^3/\text{m}^3$$

$$l = 0.5$$

$$m = (1 - (1/n))$$

$$n = 1.632$$

The ψ - θ_l relation used by Thomas [9] is based on different soil porosity than that used in this thesis. Hence, the volumetric water content must be normalized first before Eq. (6.22) can be used.

$$S_r = \frac{\theta}{\eta_{Ottawa}} \quad (6.25)$$

$$\theta = \eta_{Thomas} \times S_r \quad (6.26)$$

where the parameter S_r is the degree of saturation, η_{Ottawa} is the Ottawa sand porosity (0.366) and η_{Thomas} is the porosity used in [11] (0.389).

It is important to mention that the above relationships for ψ - θ_l (Eqs. (6.22) and (6.24)) and K - θ_l (Eq. (6.23)) were the closest and best the author could obtain from literature. If better relations can be obtained from experiment or literature in future, the results for the phase conversion factor, ε , should be re-evaluated. It is confirmed that Eqs. (6.6) and (6.9) yield the same values over the temperature and volumetric liquid water content ranges covered in this study using Eqs. (6.18) - (6.23).

Since there is no readily available model for the phase conversion factor in Eq. (6.3), a logical step is to equate Eqs. (6.3) and (6.8) to obtain the theoretical phase conversion factor, as follows:

$$\varepsilon = \frac{K_{v2}}{D_T} = \frac{D_{Tv}}{D_T} \quad (6.27)$$

with the assumption that Eqs. (6.3) and (6.10) are equivalent. Figure 6.4 shows the results of Eq. (6.3) using the theoretical ε expression of Eq. (6.27). It can be seen that values of λ_{app} are poorly predicted at both low and high temperatures of 22 and 92°C, respectively. Therefore the λ_{app} model of Eq. (6.3) or (6.8) using the theoretical ε expression of Eq. (6.27) cannot produce results similar to the experimental λ_{app} data.

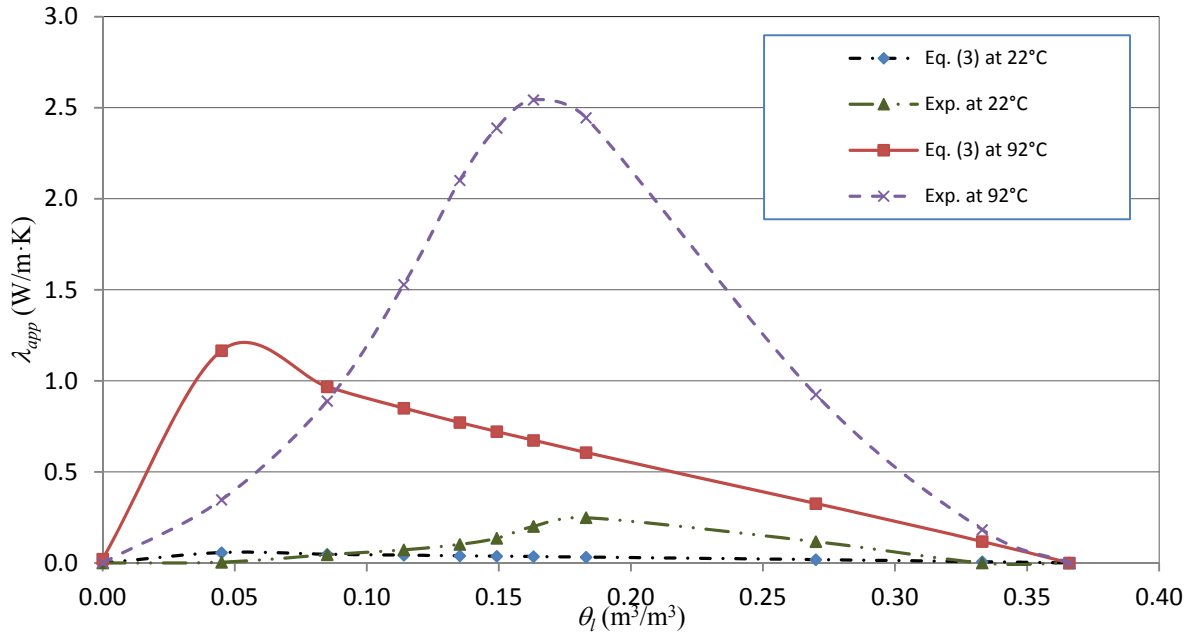


Figure 6.4: Comparison of theoretical⁷ and experimental values for λ_{app} , of Ottawa sand, for two temperatures.

⁷ Equation 3 in Figure 6.4 represents Equation (6.8) in the thesis.

6.4 Results and Discussion

6.4.1 Ottawa Sand Results

As shown in the previous section, when the theoretical phase conversion factor is used, calculated values of λ_{app} with Eq. (6.3) do not agree well with the experimental data in Table B-3, which implies that Eq. (6.8) is also the same. However Eq. (6.3) provides an opportunity to be “corrected” or “calibrated” using the experimental data. As a result, the experimental phase conversion factor is sought, using the following equation:

$$\varepsilon = \frac{\lambda_{app, exp}}{L \rho_l D_T} \quad (6.28)$$

where $\lambda_{app, exp}$ is the experimental apparent thermal conductivity from Table B-3. The results have been presented in Table 6.1.

Table 6.1: Values of experimental phase conversion factor ε for Ottawa sand.

T [°C]	θ [m ³ /m ³]										
	0	0.045	0.085	0.114	0.1352	0.1492	0.1631	0.183	0.27	0.333	0.366
2	0	0	0	0	0	0	0	0	0	0	0
12	0	0	0	0	0.001	0.002	0.002	0.001	0	0	0
22	0	0.073	0.183	0.027	0.010	0.006	0.004	0.002	0	0	0
32	0	0.162	0.277	0.046	0.018	0.011	0.007	0.004	0	0	0
42	0	0.351	0.381	0.065	0.027	0.016	0.010	0.005	0	0	0
52	0	0.400	0.448	0.083	0.035	0.021	0.013	0.006	0	0	0
62	0	0.402	0.492	0.100	0.041	0.024	0.015	0.007	0	0	0
72	0	0.395	0.536	0.119	0.047	0.027	0.016	0.007	0	0	0
82	0	0.377	0.556	0.139	0.052	0.029	0.017	0.007	0	0	0
92	0	0.278	0.534	0.165	0.062	0.033	0.018	0.007	0	0	0

Figure 6.5 shows theoretical and experimental values of ε at two temperatures; the values are clearly different. The phase conversion factor becomes significant at high temperatures and low to medium water contents, whereas at high water contents (i.e., $\theta_l > \theta_{FC}$), the factor is close to zero for all temperatures. The theoretical values peak at around $0.05 \text{ m}^3/\text{m}^3$ ($S_r = 0.12$); however, the experimental values peak at around $\theta_{PWP} = 0.092 \text{ m}^3/\text{m}^3$ ($S_r = 0.23$). This observation seems reasonable as there is a continuous film of water around soil particles at the permanent wilting point, which provides the maximum exposure of water surface for evaporation.

According to Luikov [7], the total differential change in soil liquid mass is equal to the sum of the migrated liquid mass (m) and the condensed or evaporated liquid mass (pc):

$$d(\rho_l \theta_l) = d(\rho_l \theta_l)_m + d(\rho_l \theta_l)_{pc} \quad (6.29)$$

The phase conversion factor is then defined as:

$$\varepsilon = \frac{d(\rho_l \theta_l)_{pc}}{d(\rho_l \theta_l)} \quad (6.30)$$

which enables the evaporation of soil liquid mass to be expressed within clearly defined limits as ε varies from 0 to 1. The obtained experimental data in Table 6.1 are within the limits as expected.

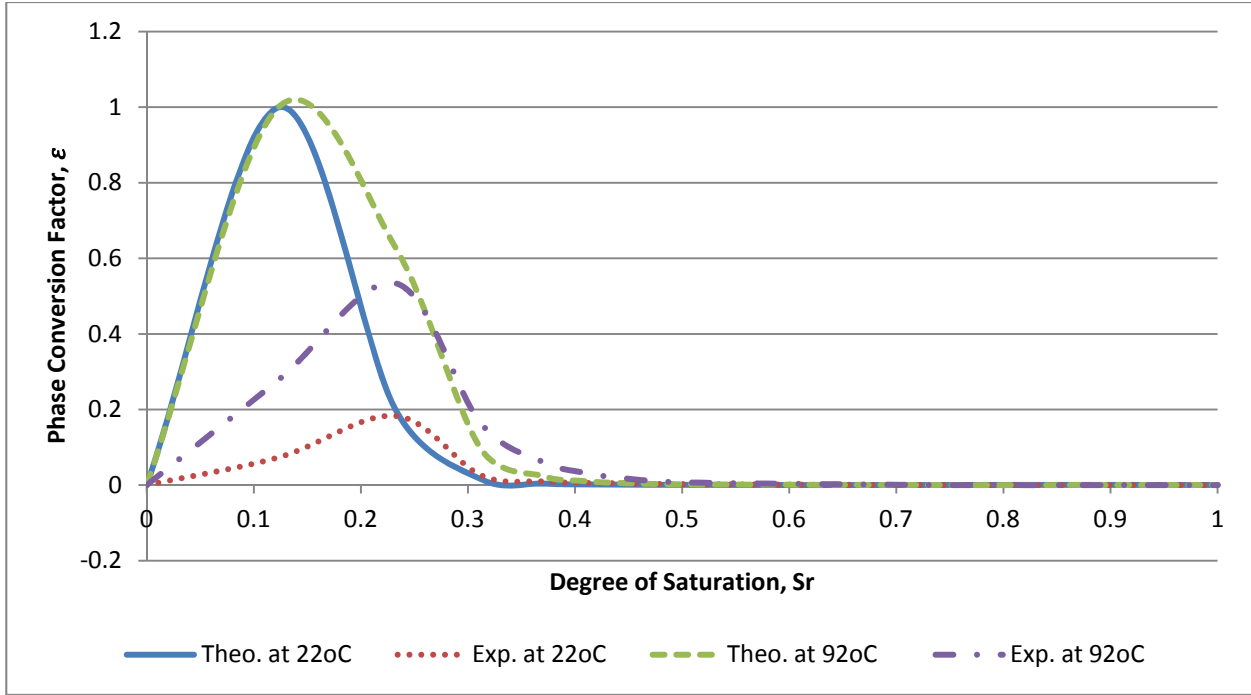


Figure 6.5: Comparison between theoretical and experimental values for ϵ , of Ottawa sand, for two temperatures.

With the available experimental data for the parameter ϵ , an empirical model may be developed, at least for coarse (sandy) soils. More research is needed to develop a suitable empirical model of ϵ and to determine whether the same empirical model for coarse soils can also be applied to medium and fine (silty and clayey) soils. Otherwise, the second set of experimental data for sandy loam by Nikolaev [4] can be used to obtain the experimental ϵ values for medium and fine soils, using the technique described in this thesis.

In light of the findings, it is recommended that the apparent thermal conductivity due to vapour migration developed Thomas and King [11] and appearing in Eq. (6.7) should be replaced by the expression in Eq. (6.3) and used with experimental data for ϵ .

6.4.2 Richmond Hill Results

The phase conversion factor was calculated for the Richmond Hill fine sandy loam soil, with the results presented in Table 6.2.

Table 6.2: Values of experimental phase conversion factor ε for Richmond Hill fine sandy loam soil.

T [°C]	θ [m ³ /m ³]											
	0	0.069	0.138	0.1706	0.2023	0.232	0.2684	0.302	0.369	0.436	0.504	0.571
2	0	0	0	0	0	0	0	0	0	0	0	0
12	0	0	0	0	0.061	0.063	0.113	0.095	0	0	0	0
22	0	0.117	0.075	0.131	0.177	0.155	0.178	0.163	0.004	0.002	0	0
32	0	0.148	0.136	0.204	0.242	0.214	0.221	0.194	0.008	0.004	0	0
42	0	0.135	0.169	0.255	0.300	0.274	0.274	0.228	0.013	0.007	0.001	0
52	0	0.125	0.185	0.287	0.347	0.335	0.317	0.271	0.017	0.010	0.002	0
62	0	0.112	0.182	0.289	0.372	0.388	0.365	0.312	0.023	0.014	0.003	0
72	0	0.092	0.163	0.284	0.384	0.422	0.380	0.348	0.028	0.019	0.005	0
82	0	0.070	0.145	0.260	0.375	0.420	0.385	0.373	0.032	0.022	0.006	0
92	0	0.044	0.103	0.211	0.344	0.391	0.363	0.369	0.035	0.025	0.008	0

In order to observe the impact of soil texture on phase conversion factor, the results for both Ottawa sand and Richmond Hill soil are compared at low water content (0.085 m³/m³ and 0.1706 m³/m³ respectively) as presented in Figure 6.6. As Figure 6.6 shows, the phase conversion factor changes significantly as the soil composition is changed. The difference in phase conversion factor is increased at a faster rate at higher temperature. This is expected since Ottawa sand is a coarse soil and therefore do not retain heat as well as a finer soil such as Richmond Hill fine sandy loam soil. Figure 6.6 shows the results for low volumetric water

content. This significant dependency of ε on soil composition is apparent at medium and high volumetric water content as well.

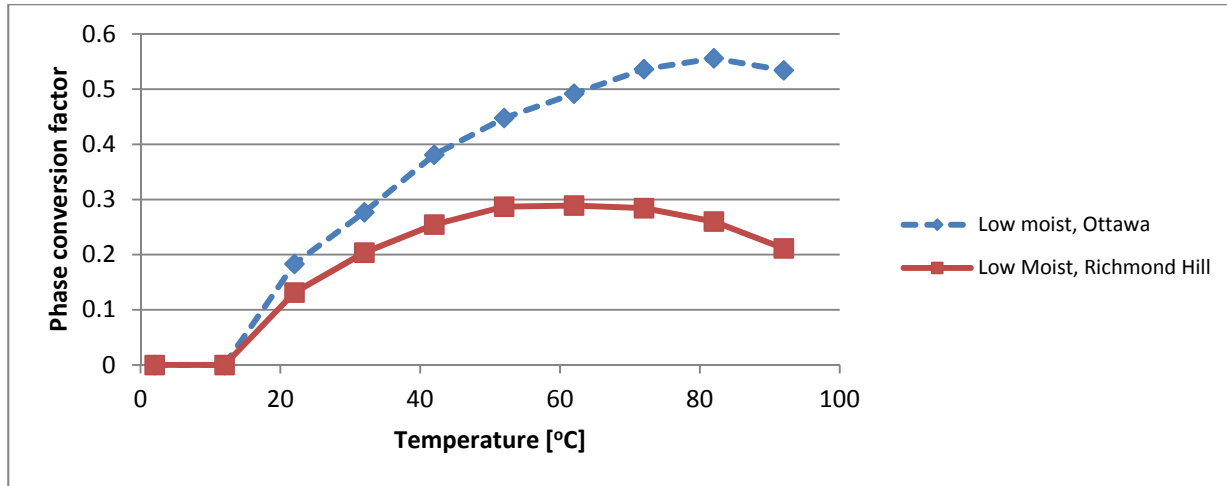


Figure 6.6: Impact of soil texture on the phase conversion factor ε at $VWC = 0.085 \text{ m}^3/\text{m}^3$ and $0.1706 \text{ m}^3/\text{m}^3$, for Ottawa sand and Richmond Hill fine sandy loam soil respectively, for a range of temperatures.

CHAPTER 7 COMPUTER SIMULATION OF A GROUND SOURCE HEAT PUMP SYSTEM USING EXPERIMENTAL SOIL THERMAL CONDUCTIVITIES FOR THREE SOIL TEXTURES

7.1 Introduction

Once the experimental results for all three soil samples were obtained, it was important to investigate their effect on an actual ground source heat pump (GSHP) system. Hence, a computer simulation model of a GSHP system was developed using the TRNSYS simulation studio. TRNSYS is a transient system simulation software which allows a HVAC system to be modeled and simulated under real world conditions. The soil parameters investigated were soil thermal conductivity, composition, and water content. As the results, the experimental soil thermal conductivity of Ottawa sand, Richmond Hill soil and Kortright Centre soil were implemented in the simulation, to investigate the impact of variation in temperature, water content, and soil type on the GSHP performance from cost and electricity consumption perspective. The model was tested for one year (8760 hours) to be able to properly include changes in ground condition throughout the year. The system under investigation is described in the next section.

7.2 Description of the GSHP under Investigation

The HVAC system under investigation is installed at an experimental house, called the Archetype House B, which is located at the Kortright Centre in Vaughan, Ontario. The system is providing space heating and cooling for the three story residential house, with an attached guest suite. Since this is an experimental house, it is unoccupied throughout the year except at times when various researchers come to the house to work on the equipment. The house is equipped with all the appliances and includes all the internal loads of a normal house, such as washer/dryer, fully operational shower and lavatories, fully equipped kitchen with dish washer and fridge, as well as lighting system.

The HVAC system includes a GSHP which provides heating and cooling to the house, connected to a buffer tank in the basement and two horizontal-looped pipes buried in the yard area at 6 feet under the ground. Heating is provided by in-floor heating at each floor and cooling is by a multi-zone air handling unit (AHU). The buffer tank is connected to both in-floor heating system and the AHU. During winter season, the GSHP provides hot water to the buffer tank, which is connected to the in-floor heating system, and during summer season the GSHP provides chilled water to the buffer tank, which is switched and connected to the AHU. A glycol solution is used as the heat transfer medium to prevent any freezing and damage to the buried pipes during winter season. Table 7.1 provides detailed specifications of this HVAC system.

Table 7.1: Detailed specifications of the HVAC equipment under investigation [48].

Equipment	Technical Specification
Buffer tank	270 litres (80 USG)
Ground source heat pump (GSHP)	<p>a) Heating capacity : 13.3 kW¹</p> <p>COP: 3.0</p> <p>b) Cooling capacity: 12.66 kW²</p> <p>COP: 2.86</p> <p>EER: 12.86</p> <p>c) Length of horizontal loop: 152.39m (500')</p> <p>d) Number of loop: 2</p> <p>e) Depth of ground level: 1.83m (6')</p>
Air handling unit (AHU)	<p>a) Maximum heating capacity: 28 kW (95MBH)³</p> <p>b) Cooling capacity: 5.27-12.3 kW (1.5-3.5 tons)</p> <p>c) Nominal air flow rate: 660 L/s (1400 CFM)</p>

1) At 0°C (32°F) EWT, and flow rate of 1.04 L/s (16.5GPM).

2) At 25°C (77°F) EWT, and flow rate of 1.04 L/s (16.5 GPM).

3) At 82°C (180°F) EWT.

Sensors have been installed throughout the house and within the HVAC system to monitor relevant loads and system performance throughout the year. To ensure accuracy of the developed model, results from the model have been compared to the actual data collected from the house. The collected data are from December 1 to 19/2010 for heating and August 23 to September 14/2010 for cooling.

7.3 Simulation Details

In order to investigate the impact of soil properties on the performance of the GSHP system, a transient simulation software, called TRNSYS, was used to model the HVAC system described in section 7.2. Since the GSHP is connected to two different systems for house cooling (air handling unit) and heating (in-floor heating), two separate computer models are first developed, one for cooling and one for heating. Once calibrated, the two models are combined to develop one complete model to simulate the actual HVAC system, with simulation time of one year (8760 hours). Figure 7.1 shows the complete HVAC model with all the program components used in the simulation. Since the program screen was small, the overall screen was very dense; as the result, three relevant components have been snipped and enlarged as presented in Figure 7.2, with a description included in Table 7.2.

To ensure an accurate model, actual data collected from the GSHP, such as heating and cooling performance curves, are used to develop the computer model. Results from computer simulation are compared to the actual data and the model is calibrated to ensure its accuracy.

To ensure simulated results are as realistic as possible, the ground temperature component (Table 7.2) is used within the model to obtain the average ground temperature, at a

depth of 6ft and over 8760 hours, and the thermal conductivity results closest to the ground temperature are used for three moisture levels (complete dryness, field capacity, and full saturation), for the three soil types (Ottawa sandy soil, Richmond Hill sandy loam soil, and Kortright Centre loam soil) under investigation.

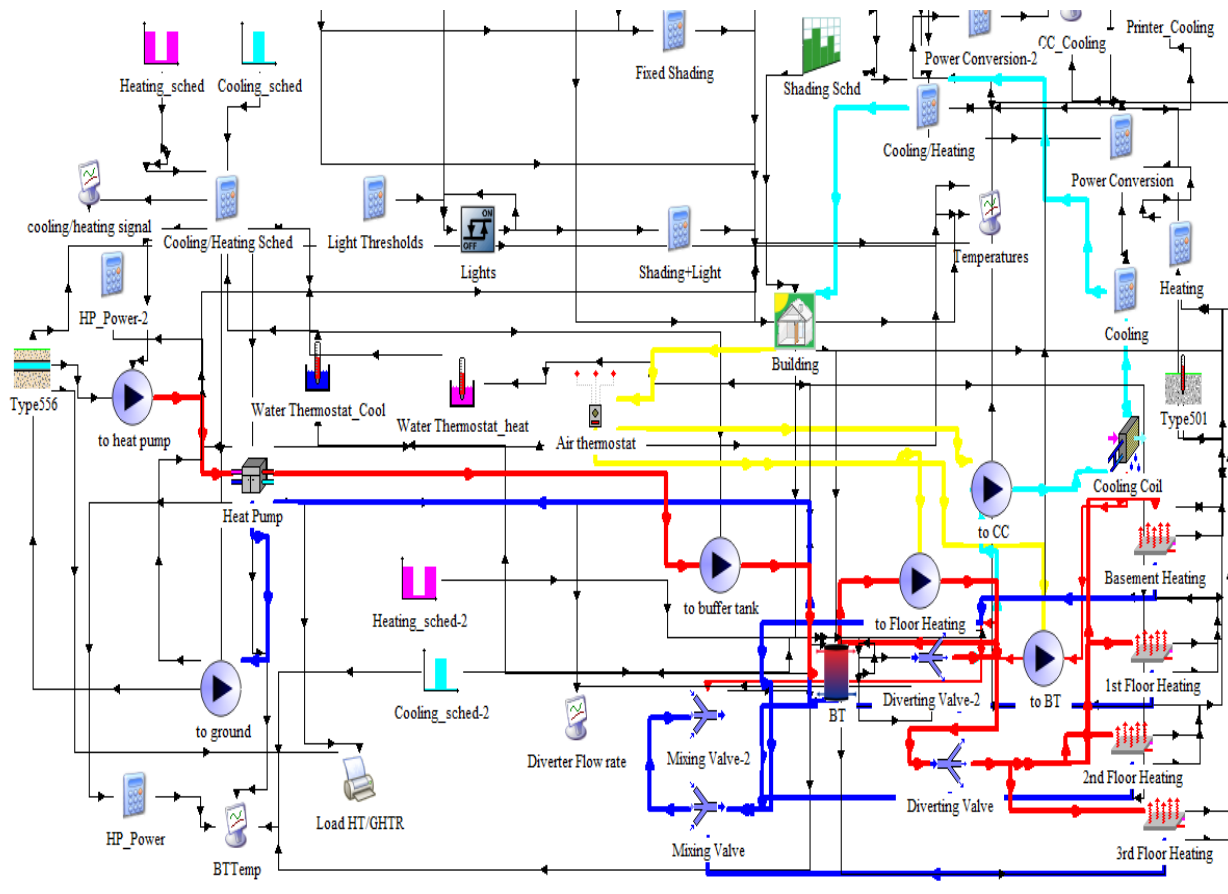
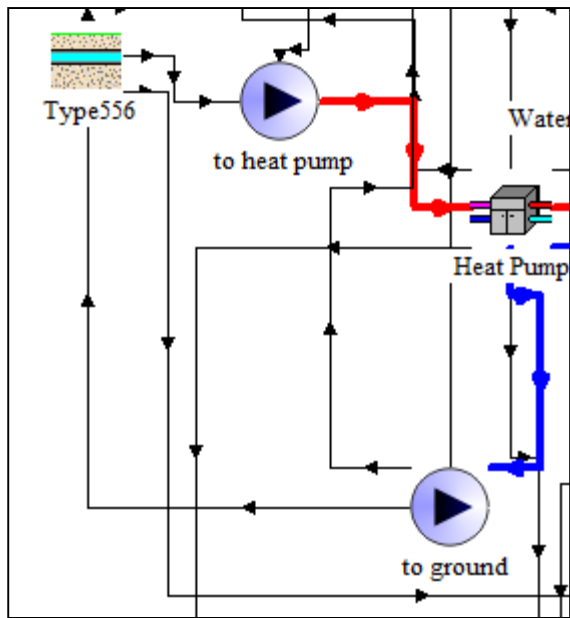
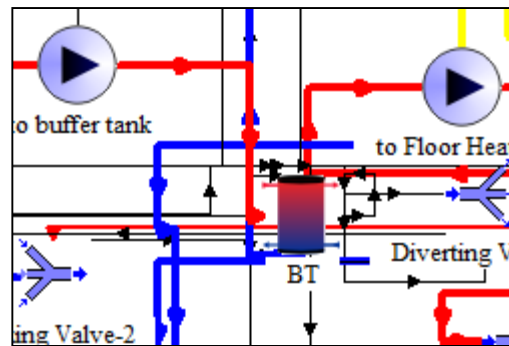


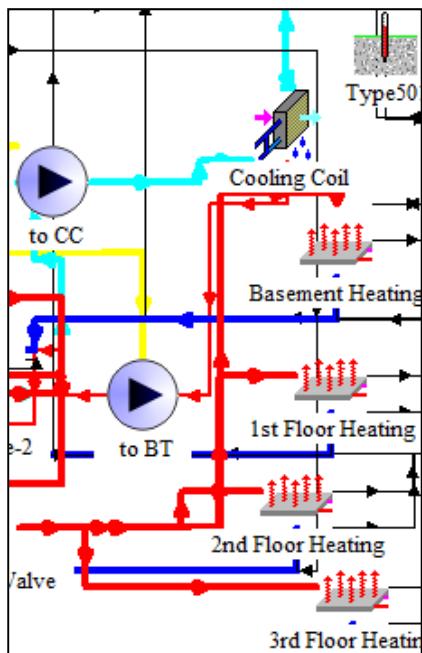
Figure 7.1: An overview of the TRNSYS model of the complete HVAC system.



a)



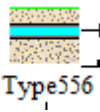
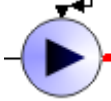


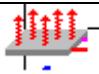

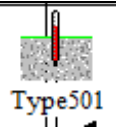
b)



c)

Figure 7.2: Three major components of the HVAC system as modeled in TRNSYS. a) Heat pump-to-ground loop. b) Heat pump-to-buffer tank loop. c) Buffer tank-to-AHU/in-floor heating loop.

Table 7.2: TRNSYS Component Description.

Component	Description
	Buried horizontal pipe component
	Circulation pump component
	Ground source heat pump (GSHP) component
	Buffer tank component
	In-floor heating component
	Air handling unit (AHU)
	Ground temperature component

The parameters under investigation are soil type and water content. Since TRNSYS does not currently consider volumetric water content and soil type in its calculations, the soil thermal conductivity was changed within the model to account for these two parameters in the analysis. Hence, the simulation was performed nine times, i.e., at three different soil types and three volumetric water contents, as presented in Tables 7.3 through 7.5.

Table 7.3: Simulated data for Ottawa Sand.

Volumetric Water content, θ [m³/m³]	Thermal Conductivity [W/m·K] (% change w.r.t. dry state)
0	0.338
0.183 (FC) ¹	1.806 (434)
0.366 (FS) ²	3.329 (885)

1) Field Capacity.

2) Full Saturation

Table 7.4: Simulated data for Richmond Hill soil.

Volumetric Water content, θ [m³/m³]	Thermal Conductivity [W/m·K] (% change w.r.t. dry state)
0	0.223
0.2684 (FC)	0.665 (198)
0.571 (FS)	1.318 (491)

Table 7.5: Simulated data for Kortright Centre soil.

Volumetric Water content, θ [m³/m³]	Thermal Conductivity [W/m·K] (% change w.r.t. dry state)
0	0.253
0.260 (FC)	0.883 (249)
0.520 (FS)	1.495 (491)

For comparison purposes, cooling degree day (CDD) and heating degree day (HDD) from the same period were extracted from the model as well as the actual data from Environment Canada (49), which are presented in Tables 7.6 and 7.7. The base temperature is selected as 18°C for HDD and CDD, based on Environment Canada [50]. Table 7.8 represents percent difference between the two data sets.

Table 7.6: Cooling degree day comparison between actual and simulated data for Aug. 23 – Sep. 14/2010.

	Environment Canada Data		TRNSYS Data	
Day	Outdoor Air [°C]	CDD	Outdoor Air [°C]	CDD
1	19.8	1.8	17.6	0.0
2	19.6	1.6	17.8	0.0
3	20.5	2.5	19.4	1.4
4	16.8	0.0	22.2	4.2
5	17.3	0.0	19.7	1.7
6	21.5	3.5	21.9	3.9
7	23.2	5.2	21.2	3.2
8	27.3	9.3	19.1	1.1
9	27.7	9.7	20.7	2.7
10	27.1	9.1	22.4	4.4
11	26.5	8.5	19.4	1.4
12	20.4	2.4	19.9	1.9
13	14	0.0	20.4	2.4
14	14.8	0.0	22.5	4.5
15	17.1	0.0	21.5	3.5
16	22.8	4.8	18.4	0.4
17	16.8	0.0	11.8	1.8
18	14.6	0.0	13.0	3.0
19	16.3	0.0	10.8	0.8
20	15.4	0.0	10.1	0.1
21	17.9	0.0	8.5	0.0
22	18.5	0.5	8.9	0.0
23	15.1	0.0	11.4	1.4

Table 7.7: Heating degree day comparison between actual and simulated data for Dec. 01-20/2010.

	Environment Canada Data		TRNSYS Data	
Day	Outdoor Air [°C]	HDD	Outdoor Air [°C]	HDD
1	3.8	14.2	-0.2	17.8
2	-0.1	17.9	-5.9	12.1
3	0.4	17.6	2.6	15.4
4	-3.4	14.6	1.9	16.1
5	-2.7	15.3	-1.8	16.2
6	-4	14	-2.8	15.2
7	-4.5	13.5	-2.1	15.9
8	-7	11	-0.9	17.1
9	-8.5	9.5	-4.0	14.0
10	-0.3	17.7	-3.4	14.6
11	2.3	15.7	-7.8	10.2
12	-2.4	15.6	-1.2	16.8
13	-11.1	6.9	-4.7	13.3
14	-9.6	8.4	0.4	17.6
15	-8.5	9.5	1.1	16.9
16	-4.9	13.1	6.8	11.2
17	-2.4	15.6	0.2	17.8
18	-5.1	12.9	5.1	12.9
19	-4.7	13.3	3.5	14.5
20	-3.7	14.3	0.7	17.3

Table 7.8: Total HDD and CDD for the actual and simulated data.

Total	Environment Canada Data	TRNSYS Data	Difference [%]
CDD	59	43.8	38%
HDD	271	303	12%

As shown in Table 7.8, there is a 38 percent and 12 percent difference between the actual and simulated CDD and HDD data sets respectively. The operation of a heat pump is directly related to the outdoor temperature; the lower the outdoor temperature, the higher the heating load and vice versa. Hence, the heat pump must come on more often to meet the required heating or cooling demand. As the result, based on the data provided in Table 7.8, it would be expected for the GSHP system modeled in TRNSYS to operate less frequently and consume less energy by 38 percent, compared to actual performance during summer season. Similarly, it would be expected for the GSHP system to operate more frequently and consume more energy by about 12 percent, during the winter season.

7.4 TRNSYS Simulation Result

Figure 7.3 and 7.4 present the comparison between the actual heat pump electrical energy consumption, obtained from Kortright Centre, and the simulated data from TRNSYS, for cooling and heating seasons, respectively.

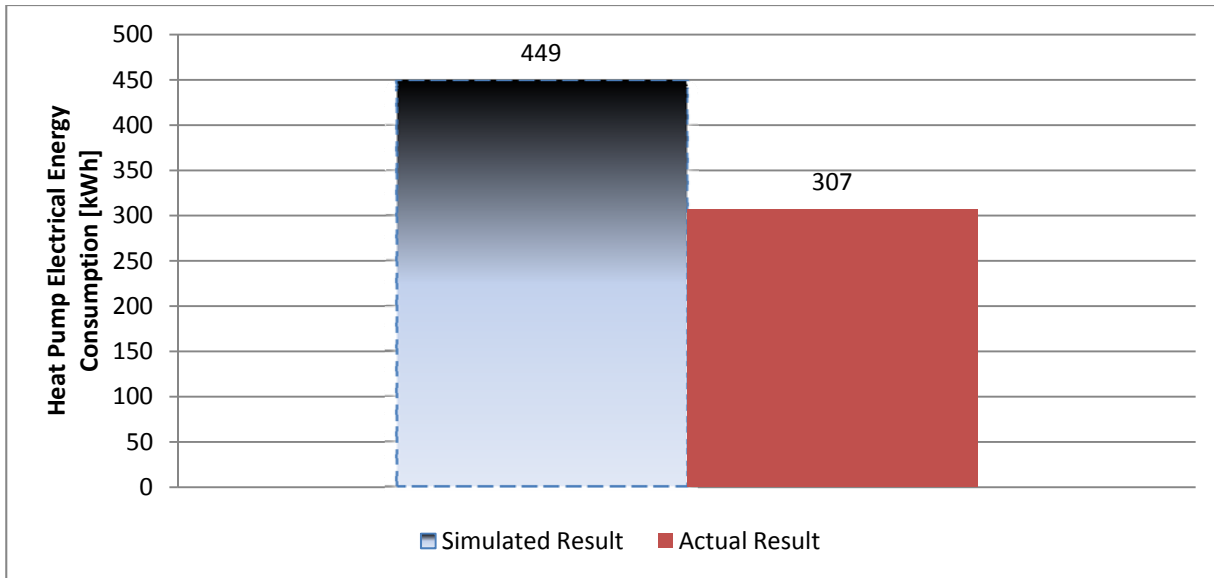


Figure 7.3: Comparison between actual and simulated heat pump electrical energy consumption for the cooling period from August 23rd to September 14th, 2010.

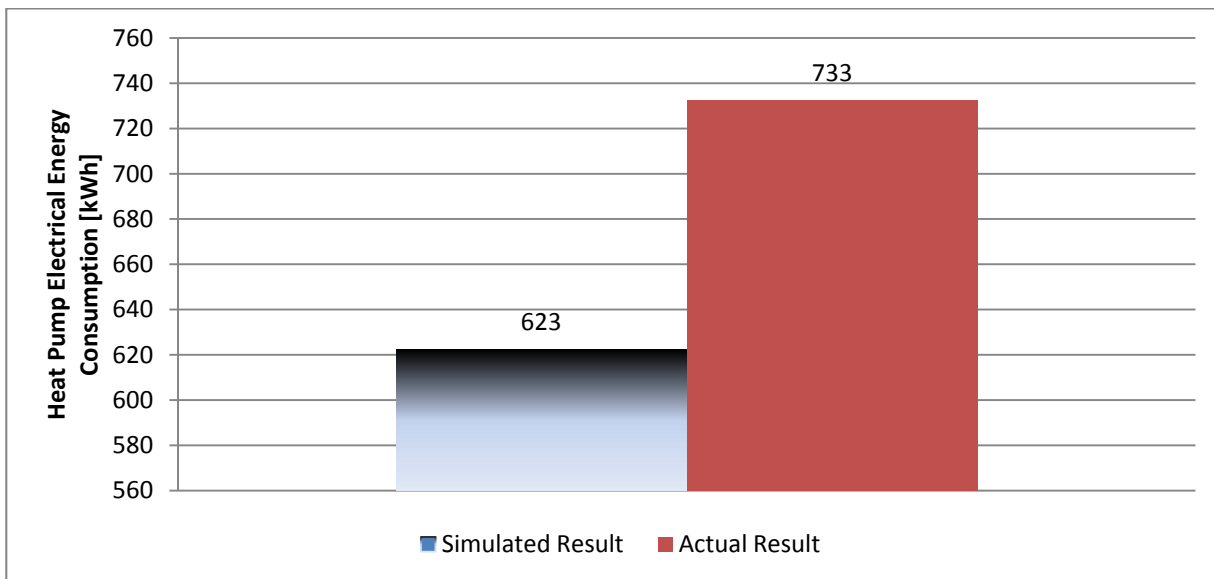


Figure 7.4: Comparison between actual and simulated heat pump electrical energy consumption for the heating period from December 1st to December 20th, 2010.

The comparison between the actual and simulated heat pump electrical energy consumption shows a difference of 46 percent and 15 percent for the cooling and heating results, respectively.

The simulation was performed for all three soil specimens (Ottawa sand, Richmond Hill fine sandy loam, and Kortright Centre loam) for one year (8760 hrs) with a simulation time step of 1 hour. The heat pump electrical energy consumption has been presented in Figures 7.5 through 7.7.

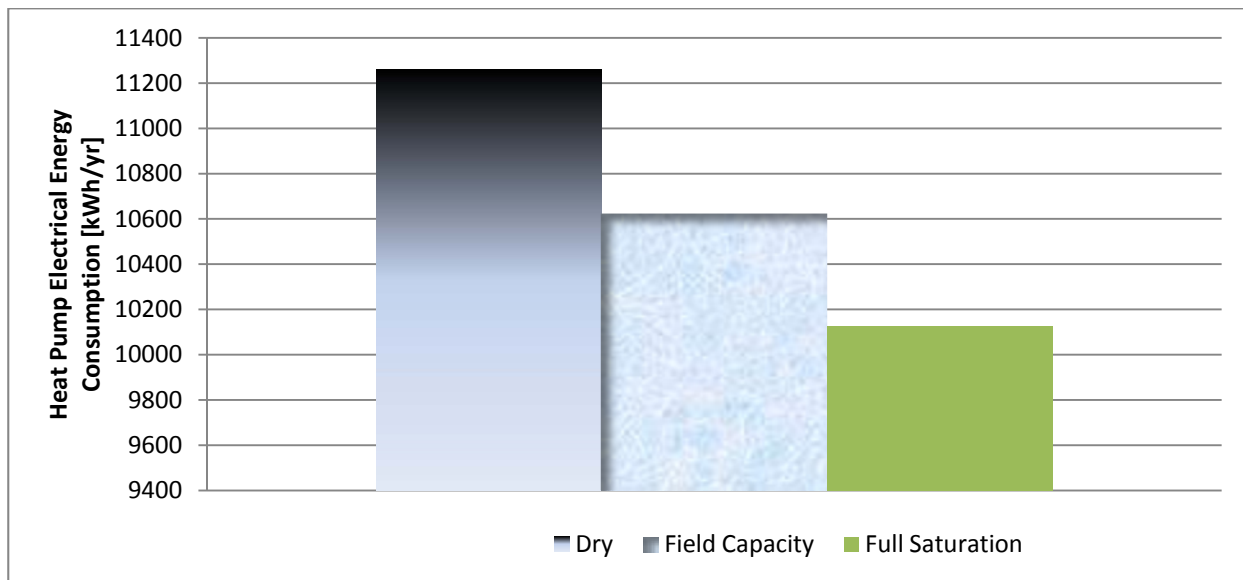


Figure 7.5: Variation in the heat pump energy consumption for Ottawa sand with change in volumetric water content.

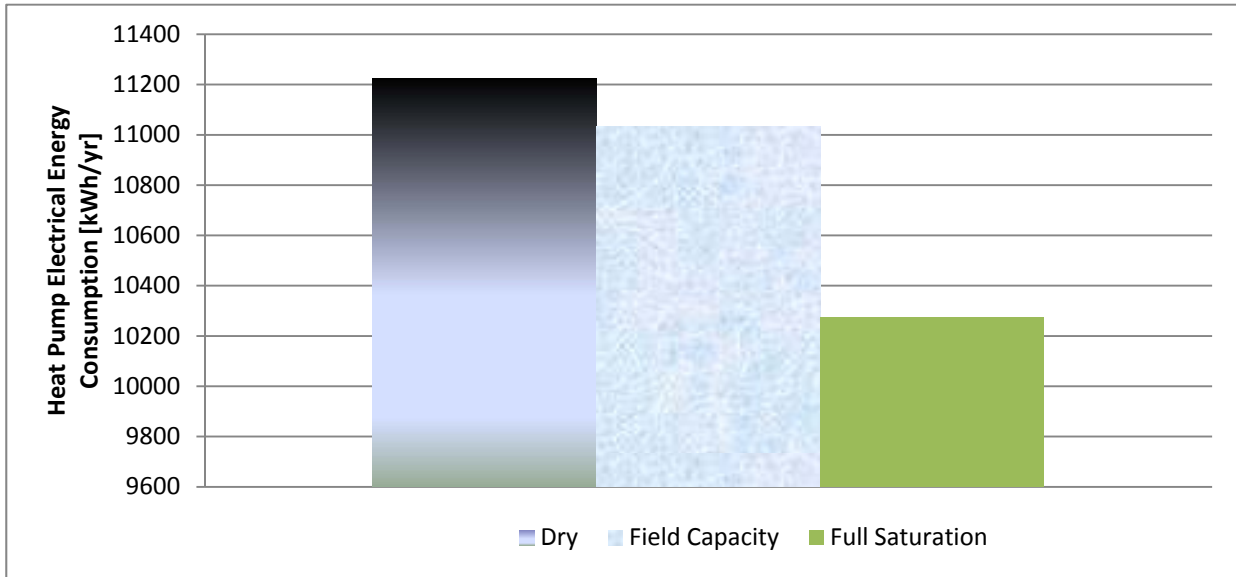


Figure 7.6: Variation in the heat pump energy consumption for Richmond Hill fine sandy loam with change in volumetric water content.

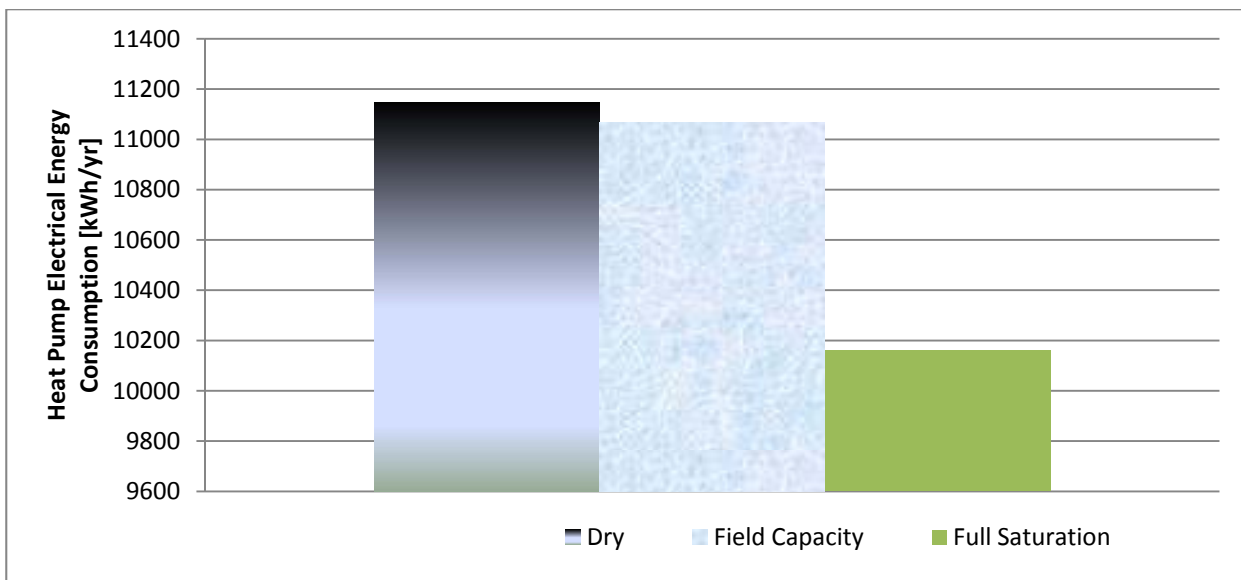


Figure 7.7: Variation in the heat pump energy consumption for Kortright Centre loam with change in volumetric water content.

Figures 7.5 through 7.7 show a decrease in heat pump energy consumption as the soil thermal conductivity increases due to increase in the volumetric water content. The increase in soil thermal conductivity results in better heat transfer between the buried pipes and the surrounding soil. Hence, the GSHP can be operated more efficiently because it is easier to reject heat to the ground (resulting lower entrance fluid temperature to the heat pump) during summer and extract heat from the ground (resulting higher entrance fluid temperature to the heat pump) in winter season, thereby resulting in a reduction of heat pump electrical energy consumption.

In addition to annual electrical energy consumption, the simulated results were divided into cooling (May 01 to October 30) and heating (November 01 to April 31) seasons to observe how heat pump energy consumption would differ between the two seasons. Figures 7.8 through 7.13 present the heat pump electrical energy consumption for cooling and heating seasons, respectively.

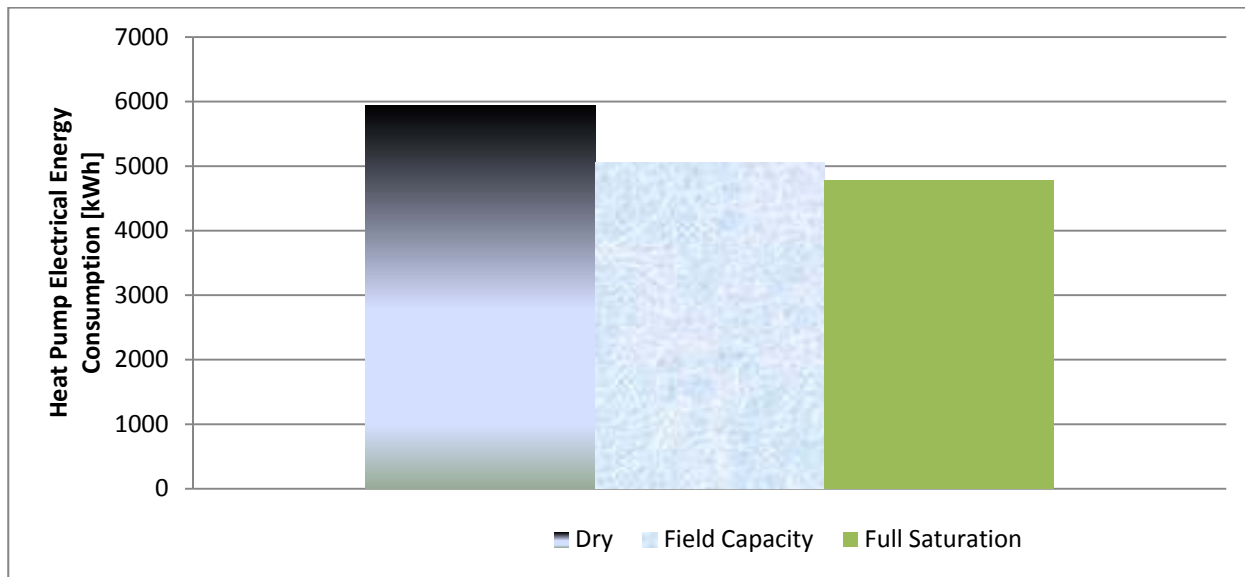


Figure 7.8: Variation in heat pump electrical energy consumption during cooling season (May 01 to October 31) for Ottawa sand at three different water contents.

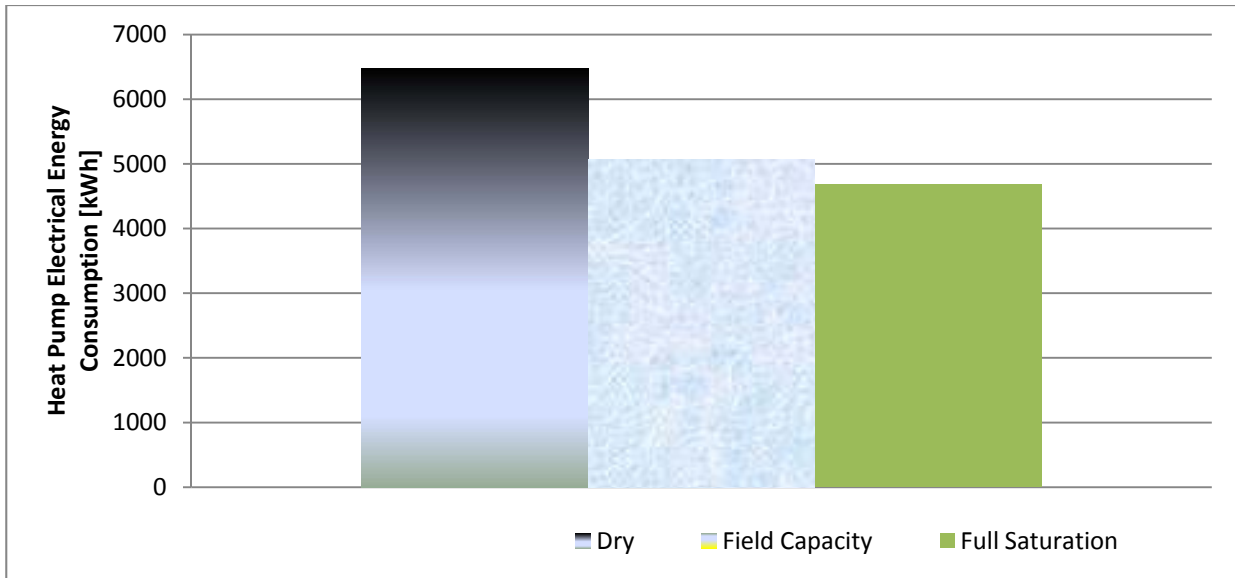


Figure 7.9: Variation in heat pump electrical energy consumption during heating season (November 01 to April 30) for Ottawa sand at three different water contents.

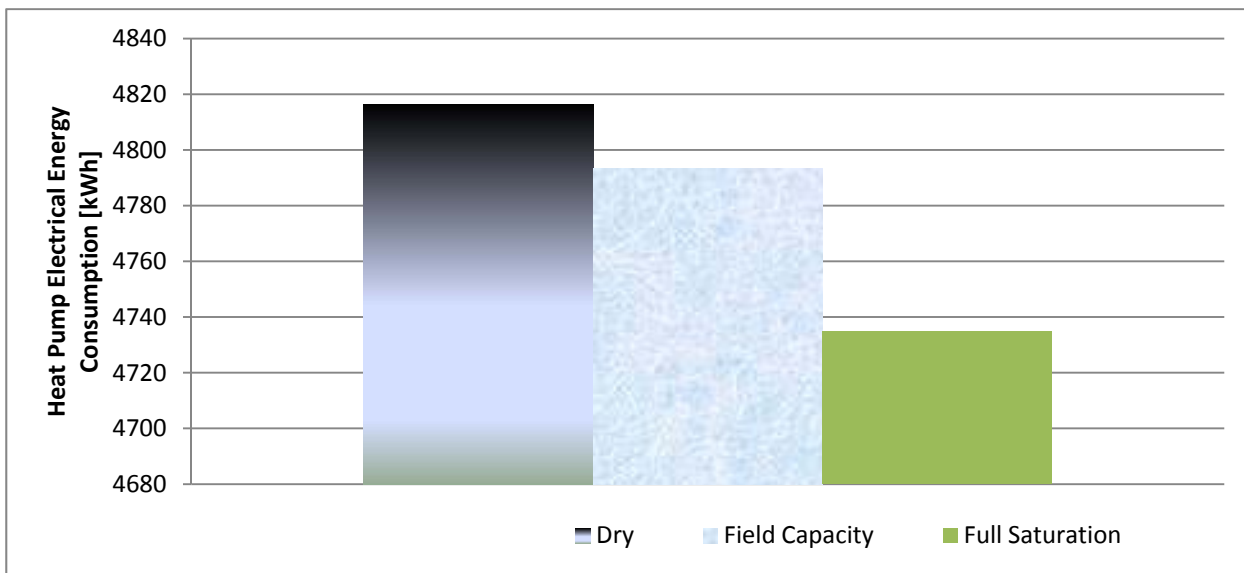


Figure 7.10: Variation in heat pump electrical energy consumption during cooling season (May 01 to October 31) for Richmond Hill fine sandy loam at three different water contents.

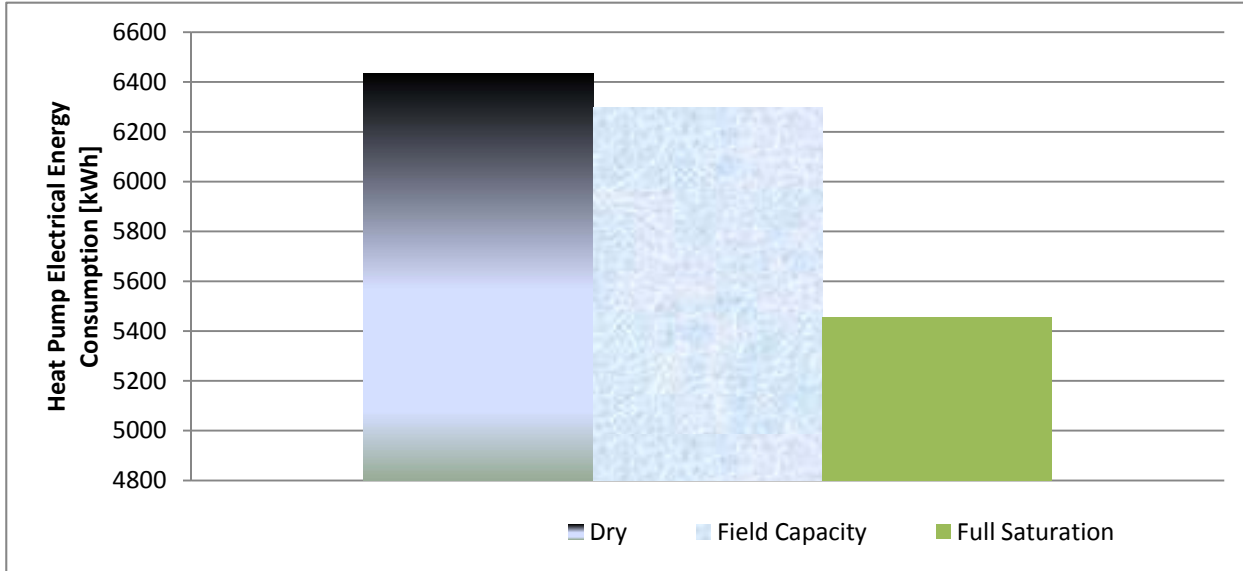


Figure 7.11: Variation in heat pump electrical energy consumption during heating season (November 01 to April 30) for Richmond Hill fine sandy loam at three different water contents.

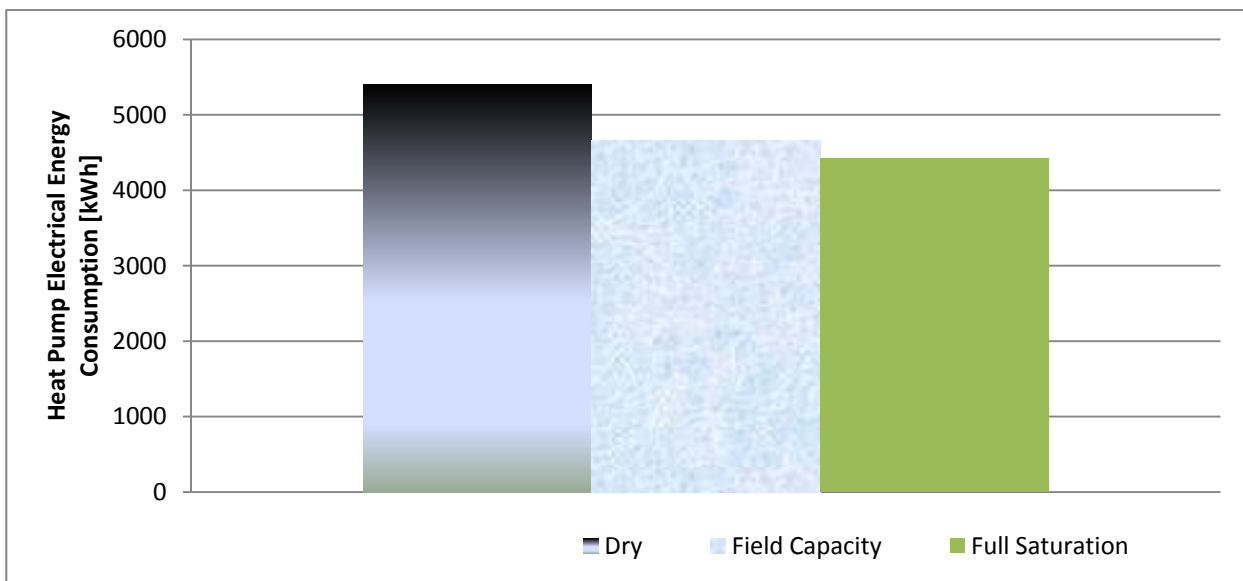


Figure 7.12: Variation in heat pump electrical energy consumption during cooling season (May 01 to October 31) for Kortright Centre loam at three different water contents

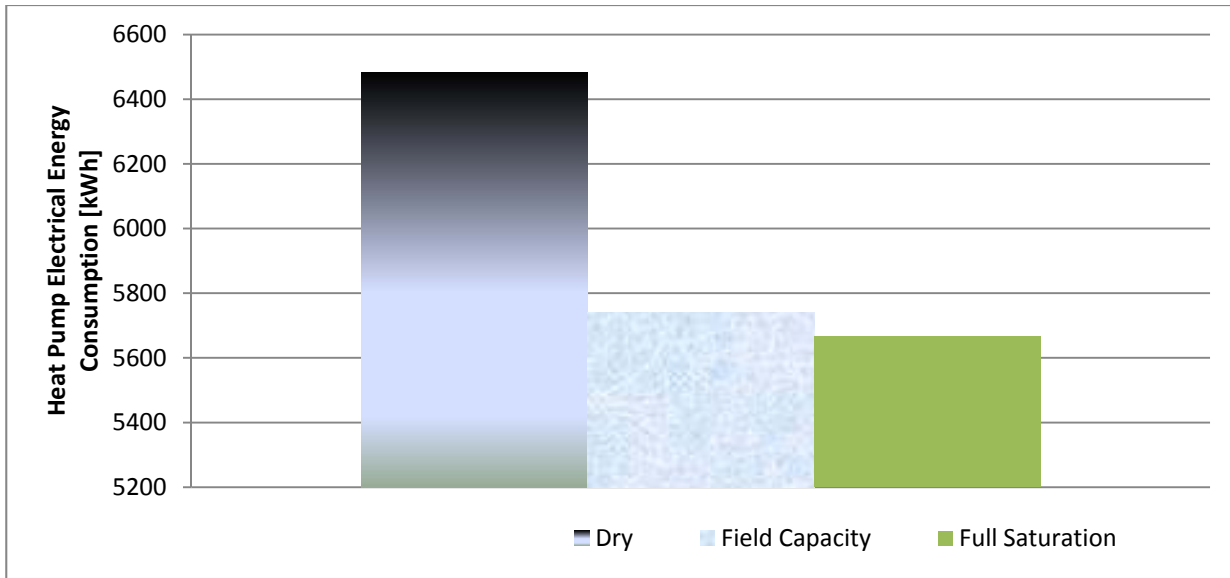


Figure 7.13: Variation in heat pump electrical energy consumption during heating season (November 01 to April 30) for Kortright Centre loam at three different water contents.

As shown in Figures 7.8 to 7.13, the heat pump energy consumption is lower in cooling season than in heating season, which is expected since the heating season is much longer in Toronto. In addition, the variation in the GSHP electrical consumption, for the three water content levels presented here, is different among the three soil types, due to the variation in their thermal conductivities, which might be the result of variation in their texture. In order to better understand the impact of soil type on the GSHP's energy consumption, however, more soil type, such as clay or silt, need to be examined.

The decrease in energy consumption obtained from the numerical model suggests that the impact of variation in soil thermal conductivity becomes significant with a significant change in water content. Hence, the impact of variation in soil thermal conductivity due to water content, on the heat pump performance and consumption becomes significant in regions with significant changes in their weather patterns. For cities that have several months of complete dryness and several months of significant rainfall, soil water content will play a significant role in designing

underground thermal energy storage (UTES) systems. Figure 7.14 presents the monthly rainfall in Toronto from January 2009 to December 2011⁸. As evident in this graph, there is a large variation in rainfall in Toronto from January to December. As the result, for a project in Toronto involving UTES, the impact of soil water content on such system's performance becomes a significant factor.

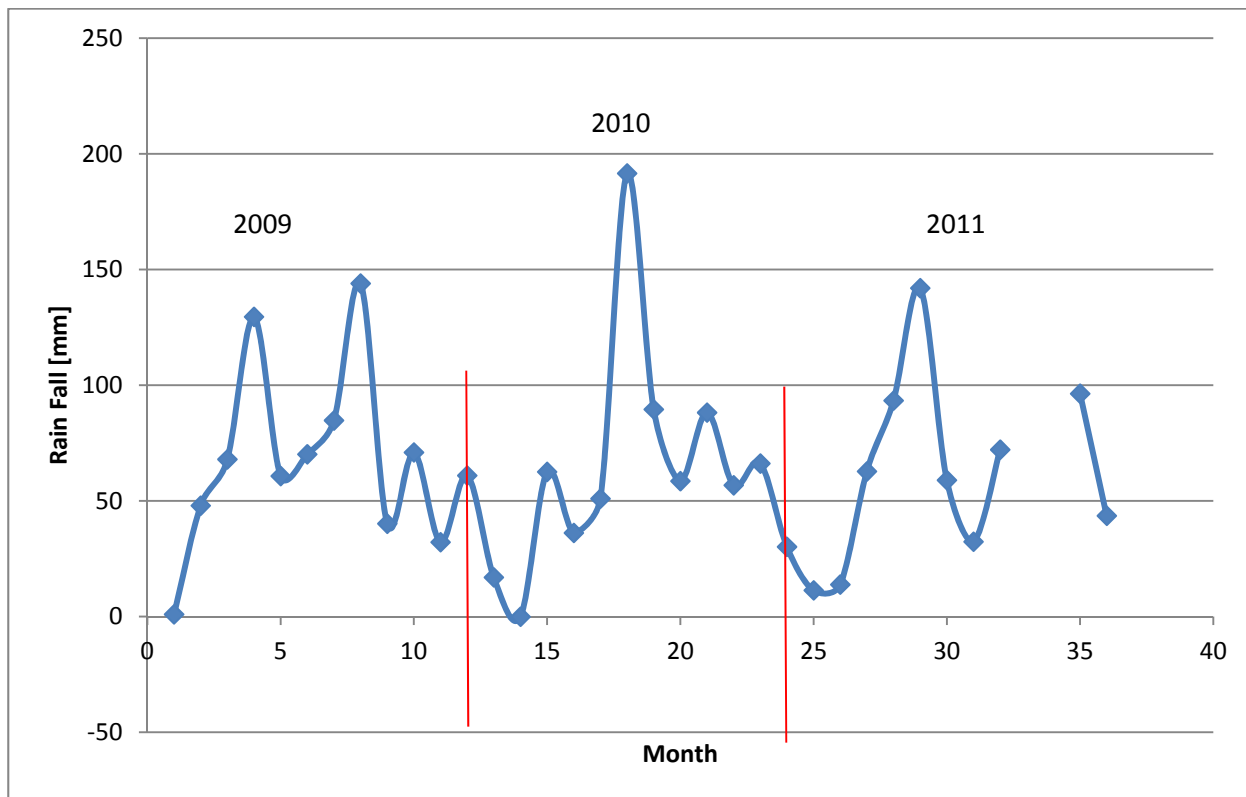


Figure 7.14: Monthly variation in amount of rainfall for the city of Toronto from 2009 to 2011, starting with January 2009 as month 1 [50].

In addition to investigating impact of soil water content on ground source heat pump performance, the impact of soil texture was also investigated. Table 7.9 presents the GSHP electrical energy consumption at three water content levels (dry, field capacity, and full

⁸ Data was not available for September and October 2011.

saturation), for Ottawa sand, Richmond Hill fine sandy loam, and Kortright Centre loam. As shown in Table 7.9, the best performance for a GSHP system can be achieved when it is located in a region with high levels of water content, and surrounded by a soil with similar characteristics as Ottawa sand.

It can be concluded from the results presented in Table 7.9 that the soil water content has higher impact on the heat pump energy consumption than soil type. The change in energy consumption due to the moisture variation can reach as much as 10% with respect to dry soil condition. But among the three soil types, the change in energy consumption due to soil type can only reach as much as 4.2% with respect to Ottawa sand at field-capacity condition. For both dry and fully saturated conditions, the changes in energy consumption due to soil type are not significant, in the order of 1% or less with respect to Ottawa sand.

Table 7.9: Variation in the GSHP energy consumption at three different moisture levels for Ottawa sand, Richmond Hill fine sandy loam, and Kortright Centre loam.

Soil Type	GSHP Energy Consumption [kWh/year] (% change w.r.t. dry state) [% change w.r.t. Ottawa sand]		
	Dry	Field Capacity	Full Saturation
Ottawa sand	11259	10616 (-5.7)	10128 (-10.0)
Richmond Hill fine sandy loam	11226 [-0.3]	11034 (-1.7) [3.9]	10273 (-8.5) [1.4]
Kortright Centre loam	11148 [-1.0]	11067 (-0.7) [4.2]	10160 (-8.9) [0.3]

CHAPTER 8 CONCLUSIONS AND RECOMMENDATIONS

8.1 Summary of Results

The purpose of this research was to investigate various soil parameters and their impact on soil thermal conductivity, to evaluate a well-known theoretical model for predicting the soil apparent thermal conductivity due to vapour migration using experimental results, and to develop more extensive datasets of soil thermal conductivity that could be used for various applications involving heat and moisture transfer in soil. Thus, a study on soil thermal conductivity was undertaken.

As a first step, the soil specimen was obtained from the Kortright Centre, in Vaughan, Ontario. The sample was gathered close to the horizontal ground heat exchanger of a GSHP system, and at a depth of about 30 cm, to minimise any contamination of the samples with biological and organic matter.

Secondly, a reliable and consistent sample preparation technique, developed by Nikolaev [4], was followed to prepare 12 soil samples, which were divided into three categories completely dry, barely-to-moderately moist, and highly-to-fully saturated.

Thirdly, the Kortright Centre soil sample was sent to the Agricultural and Food Laboratory at the University of Guelph, where its texture composition was determined to be a loam soil. In addition, the sample was sent to the Bavarian Environment Agency Laboratory in Marktredwitz, Germany, to determine its mineral content.

Fourthly, the soil samples were tested using the GHPA under temperature variation from 5°C to 92°C. Upon obtaining the thermal conductivity data, the effects of variation in water content and temperature were analyzed and a summary of the findings are included here:

- At low water content, up to the permanent wilting point, the thermal conductivity of the specimens increased at a very slow rate. As the water content increased further, up to the field capacity, the thermal conductivity increase at a much higher rate.
- At low temperatures (5 ~ 30°C), the heat transfer is dominated by conduction, and thus the increase in heat transfer due to vapour migration was very limited. At temperatures higher than 30°C, however, vapour migration has more significant effect on heat transfer rate through soil.

Fifthly, based on the experimental data obtained by Nikolaev [4] for Ottawa sand and Richmond Hill soil, a well-known model of heat and mass transfer in soils was used to evaluate the soil apparent thermal conductivity due to vapour migration, and experimental values of the soil phase conversion factor were developed for each of the soil textures. The relations used in this research for capillary potential vs. soil water content ($\psi-\theta$) and unsaturated hydraulic conductivity vs. soil water content ($K-\theta$) were the closest that this author could obtain from literature. In the future, the results for the phase conversion factor should be re-evaluated if new relations for the soils can be obtained experimentally or from literature.

Lastly, based on the gathered experimental data for all three soil textures, a computer simulation model was developed using TRNSYS. A GSHP system was modeled based on a similar system implemented at an archetype house in Kortright Centre, in Vaughan, Ontario.

The impact of variation in soil water content and texture on the performance of the GSHP system was investigated. A summary of the findings are given, as follows:

- The GSHP electrical energy consumption decreases more prominently (up to 10% decrease with respect to dry-soil conditions) from complete dryness to full saturation of each soil, for all three soil types.
- A change in GSHP electrical energy consumption was observed with variation in soil texture as well; however, it is less prominent. The finer textured soils cause higher GSHP electrical energy consumption (up to 4.2% increase with respect to Ottawa sand).
- These results suggest that for regions with significant rainfall variation throughout the year, soil water content becomes an important factor to consider, when designing an underground thermal energy storage system.

8.2 Conclusions

The following conclusions can be drawn based on the results presented in this thesis:

- A new experimental data set of soil effective thermal conductivity has been obtained over the full range of soil water content (from dryness to full saturation) and a wide range of temperature (from 5°C to 92 °C) by using a guarded hot plate apparatus for a loam soil (Kortright Centre soil).
- The experimental phase conversion factor developed in this thesis can be used to improve the accuracy of the existing model to predict the soil apparent thermal conductivity due to vapour migration. A designer could look through the tables

(Tables 6.1 and 6.2) with different ranges of soil water content and temperature, to obtain the values of phase conversion factor for evaluating the soil apparent thermal conductivity, for the soils similar to Ottawa sand and Richmond Hill fine sandy loam. In addition, a modeling software developer could implement the soil effective or apparent thermal conductivity into their ground thermal energy storage model, to increase the accuracy of their simulation and design.

- When modeling a ground source heat pump system, variations in soil water content and soil type are two important factors that a ground thermal energy storage system modeller needs to consider, in order to obtain more realistic results.

8.3 Recommendations

To utilize the work presented in this research in the industry, a data set could be created for the soil thermal conductivity, based on soil type, soil water content and temperature, so that engineers can refer to such tables while designing their thermal energy storage systems. In addition, modeling software developers, such as eQUEST or TRNSYS, could utilise the soil effective or apparent soil thermal conductivity obtained in this thesis, to improve their GSHP modeling and simulation results. It is recommended to energy system modellers to use the experimental thermal conductivity results obtained in this research, when modeling a ground source heat pump system dealing with similar types of soils.

To improve on this research, it is recommended to measure the capillary potential and unsaturated hydraulic conductivity as a function of soil water content for all three soils, in order to obtain more accurate relations for the evaluation of the phase conversion factor studied in Chapter 6. In addition, it is recommended to modify the TRNSYS model developed in this

research, to be able to use parameters such as soil texture, soil water content, and the phase conversion factor as variables within the model to significantly increase its accuracy.

To extend on the work presented in this research, the experimental thermal conductivity data obtained for Kortright Centre loam soil could also be used to study the apparent soil thermal conductivity and developed the experimental phase conversion factor for loam soil type, to complement those developed for the sandy soil (Ottawa sand) and sandy loam soil (Richmond Hill fine sandy loam). In addition, more soils with varying textures such as silt and clay could be collected and their thermal conductivity variation with temperature and soil water content should be tested to expand the data sets and further extend the study of the apparent soil thermal conductivity due to vapour migration. In addition, it is recommended to extend the minimum and maximum temperatures to around -20°C to 160°C to increase the experimental thermal conductivity data sets, which could potentially improve any existing or future models.

As an extension to the simulation results presented in this research, it is recommended to modify the TRNSYS simulation model by replacing the current horizontal ground loop of the GSHP system with that of a vertical ground loop. This will also allow the impact of variation in soil thermal conductivity on the GSHP system performance with a vertical ground loop to be compared with the one with horizontal ground loop.

APPENDIX A: DETAILED PARAMETERS OF HEAT AND MASS TRANSFER EQUATIONS

One parameter appeared in the governing equation for heat transfer as shown in Eq. (6.1), which is not used in this study, is defined here for reference [9]:

$$K_\varepsilon = L\varepsilon\rho_l D_\theta D_T \quad (\text{A.1})$$

The governing equation for heat transfer presented in Eq. (4.7) contains three parameters $C_{T\psi}$, C_{TT} and $K_{T\psi}$, which are defined here for reference as well [11]:

$$C_{T\psi} = L \frac{\rho_v}{\rho_l} \left[\frac{(\eta - \theta_l)}{R_v T} g - \frac{\partial \theta_l}{\partial \psi} \Big|_T \right] \quad (\text{A.2})$$

$$C_{TT} = \frac{C}{\rho_l} + L \frac{(\eta - \theta_l)}{\rho_l} h \left[\frac{\partial \rho_{vs}}{\partial T} - \frac{\rho_{vs} \psi g}{R_v T^2} \right] - \frac{\rho_v}{\rho_l} \frac{\partial \theta_l}{\partial T} \Big|_\psi \quad (\text{A.3})$$

$$K_{T\psi} = f(\theta_a) L \frac{D_{atm}}{\rho_l} \frac{p}{p - p_v} \frac{\rho_v g}{R_v T} \quad (\text{A.4})$$

where

$$C = (1 - \eta) \rho_s C_{ps} + \theta_l \rho_l C_{pl} + (\eta - \theta_l) \rho_v C_{pv} \quad (\text{A.5})$$

$$h = \exp\left(\frac{\psi g}{R_v T}\right) \quad (\text{A.6})$$

APPENDIX B: EXPERIMENTAL THERMAL CONDUCTIVITY RESULTS

Table B.1: Effective thermal conductivity (W/m·K) of Ottawa sand [4].

T (°C)	θ_l (m³/m³)										
	0	0.045	0.085	0.114	0.1352	0.1492	0.1631	0.183	0.270	0.333	0.366
2	0.336	0.529	0.729	0.916	1.114	1.266	1.443	1.696	2.695	3.190	3.300
12	0.338	0.536	0.766	0.992	1.200	1.367	1.547	1.806	2.800	3.220	3.329
22	0.340	0.552	0.835	1.090	1.316	1.494	1.713	1.996	2.928	3.270	3.364
32	0.343	0.568	0.890	1.190	1.477	1.701	1.954	2.287	3.090	3.340	3.416
42	0.346	0.601	0.967	1.318	1.692	1.976	2.282	2.673	3.238	3.410	3.463
52	0.350	0.630	1.051	1.471	1.954	2.300	2.655	3.059	3.382	3.490	3.537
62	0.353	0.663	1.148	1.658	2.230	2.633	3.069	3.400	3.556	3.600	3.619
72	0.357	0.713	1.282	1.900	2.528	2.989	3.449	3.722	3.759	3.724	3.689
82	0.359	0.800	1.459	2.195	2.879	3.345	3.770	4.052	3.986	3.886	3.811
92	0.363	0.920	1.725	2.632	3.440	3.904	4.248	4.446	4.292	4.078	3.956

Table B.2: Thermal conductivity for pure conduction (W/m·K) of Ottawa sand.

T (°C)	θ_r (m³/m³)										
	0	0.045	0.085	0.114	0.1352	0.1492	0.1631	0.183	0.27	0.333	0.366
2	0.336	0.529	0.729	0.916	1.114	1.266	1.443	1.696	2.695	3.190	3.300
12	0.338	0.536	0.766	0.992	1.193	1.335	1.486	1.718	2.769	3.220	3.329
22	0.340	0.548	0.790	1.018	1.214	1.358	1.512	1.747	2.811	3.270	3.364
32	0.343	0.554	0.800	1.033	1.234	1.381	1.538	1.780	2.873	3.340	3.416
42	0.346	0.557	0.808	1.046	1.252	1.404	1.565	1.814	2.944	3.410	3.463
52	0.350	0.560	0.815	1.058	1.27	1.426	1.593	1.850	3.02	3.490	3.537
62	0.353	0.563	0.821	1.070	1.287	1.448	1.620	1.886	3.101	3.596	3.619
72	0.357	0.566	0.826	1.081	1.305	1.470	1.648	1.924	3.186	3.691	3.689
82	0.359	0.569	0.831	1.092	1.322	1.492	1.676	1.962	3.275	3.791	3.811
92	0.363	0.573	0.836	1.103	1.339	1.515	1.705	2.001	3.367	3.895	3.956

Table B.3: Apparent thermal conductivity due to vapour migration (W/m·K) of Ottawa sand.

T (°C)	θ_l (m³/m³)										
	0	0.045	0.085	0.114	0.1352	0.1492	0.1631	0.183	0.27	0.333	0.366
2	0	0	0	0	0	0	0	0	0	0	0
12	0	0	0	0	0.007	0.032	0.061	0.088	0.031	0	0
22	0	0.004	0.045	0.072	0.102	0.136	0.201	0.249	0.117	0	0
32	0	0.014	0.090	0.157	0.243	0.320	0.416	0.507	0.217	0	0
42	0	0.044	0.159	0.272	0.440	0.572	0.717	0.859	0.294	0	0
52	0	0.070	0.236	0.413	0.684	0.874	1.062	1.209	0.362	0	0
62	0	0.100	0.327	0.588	0.943	1.185	1.449	1.514	0.455	0.004	0
72	0	0.147	0.456	0.819	1.223	1.519	1.801	1.798	0.573	0.033	0
82	0	0.231	0.628	1.103	1.557	1.853	2.094	2.090	0.711	0.095	0
92	0	0.347	0.889	1.529	2.101	2.389	2.543	2.445	0.925	0.183	0

Table B.4: Effective thermal conductivity (W/m·K) of Richmond Hill fine sandy loam soil [4].

T (°C)	θ_l (m³/m³)											
	0	0.069	0.138	0.171	0.203	0.232	0.268	0.302	0.369	0.436	0.504	0.571
2	0.221	0.240	0.285	0.349	0.435	0.503	0.620	0.737	0.816	0.998	1.126	1.301
12	0.223	0.246	0.305	0.376	0.466	0.545	0.665	0.778	0.857	1.031	1.150	1.318
22	0.225	0.253	0.328	0.410	0.511	0.594	0.720	0.835	0.914	1.080	1.186	1.332
32	0.227	0.260	0.351	0.447	0.560	0.650	0.786	0.906	0.985	1.124	1.220	1.357
42	0.229	0.268	0.376	0.492	0.624	0.726	0.880	0.997	1.071	1.180	1.278	1.388
52	0.232	0.278	0.404	0.545	0.703	0.827	0.992	1.120	1.180	1.263	1.334	1.426
62	0.234	0.289	0.433	0.598	0.793	0.955	1.139	1.271	1.327	1.368	1.402	1.447
72	0.237	0.300	0.463	0.665	0.902	1.105	1.280	1.451	1.485	1.496	1.492	1.489
82	0.239	0.312	0.511	0.744	1.034	1.263	1.447	1.658	1.650	1.624	1.594	1.546
92	0.242	0.325	0.568	0.844	1.223	1.459	1.622	1.861	1.827	1.774	1.712	1.613

Table B.5: Apparent thermal conductivity due to vapour migration (W/m·K) of Richmond Hill fine sandy loam soil.

T (°C)	θ_l (m³/m³)											
	0	0.069	0.138	0.171	0.203	0.232	0.268	0.302	0.369	0.436	0.504	0.571
2	0	0	0	0	0	0	0	0	0	0	0	0
12	0	0	0	0.000	0.012	0.017	0.041	0.045	0	0	0	0
22	0	0.011	0.012	0.027	0.049	0.055	0.085	0.102	0.026	0.014	0	0
32	0	0.020	0.031	0.058	0.088	0.099	0.137	0.155	0.075	0.030	0	0
42	0	0.026	0.051	0.096	0.143	0.163	0.214	0.228	0.137	0.070	0	0
52	0	0.034	0.074	0.142	0.212	0.252	0.308	0.333	0.222	0.119	0	0
62	0	0.043	0.098	0.188	0.293	0.368	0.437	0.465	0.343	0.190	0	0
72	0	0.052	0.124	0.248	0.392	0.506	0.560	0.626	0.476	0.284	0	0
82	0	0.061	0.167	0.320	0.514	0.652	0.710	0.815	0.615	0.378	0	0
92	0	0.072	0.219	0.413	0.694	0.835	0.868	0.999	0.766	0.496	0	0

Table B.6: Effective thermal conductivity (W/m·K) of Kortright Centre loam soil.

T (°C)	θ_l (m³/m³)											
	0	0.043	0.086	0.13	0.163	0.195	0.228	0.26	0.325	0.39	0.455	0.52
5	0.245	0.266	0.316	0.387	0.482	0.557	0.687	0.816	0.904	1.106	1.247	1.441
12	0.253	0.279	0.346	0.427	0.529	0.618	0.754	0.883	0.972	1.169	1.304	1.495
22	0.260	0.293	0.379	0.474	0.591	0.687	0.833	0.966	1.057	1.249	1.372	1.541
32	0.273	0.313	0.422	0.538	0.674	0.782	0.946	1.090	1.185	1.352	1.468	1.633
42	0.283	0.331	0.465	0.609	0.772	0.898	1.088	1.233	1.325	1.459	1.581	1.655
52	0.287	0.344	0.499	0.674	0.869	1.022	1.226	1.385	1.459	1.561	1.649	1.763
62	0.302	0.374	0.560	0.773	1.025	1.235	1.472	1.643	1.715	1.768	1.812	1.871
72	0.326	0.413	0.638	0.916	1.243	1.522	1.763	1.999	2.046	2.061	2.055	2.051
82	0.338	0.441	0.723	1.052	1.462	1.786	2.046	2.345	2.333	2.297	2.254	2.186
92	0.353	0.475	0.830	1.233	1.786	2.131	2.369	2.718	2.668	2.591	2.500	2.356

APPENDIX C: GRAIN SIZE DISTRIBUTION AND MINERAL COMPOSITION OF RICHMOND HILL SOIL

Table C.1: Richmond Hill soil texture composition by percent weight.

Soil Texture	Particle Size [μm]	Mass Fraction [wt%]
Sand (total)	53 – 2000	52.3
Very Fine Sand	53 – 100	13.7
Fine Sand	100 – 250	19.7
Medium Sand	250 – 500	10.2
Coarse Sand	500 – 1000	5.4
Very Coarse Sand	1000 – 2000	2.8
Silt	2 – 53	32.2
Clay	< 2	15.5

Table C.2: Major elements and element oxides for the Richmond Hill soil specimen.

Element Content	Composition
LOI*	13.8 [wt%]
SiO ₂	51.15 [wt%]
Al ₂ O ₃	8.97 [wt%]
Fe ₂ O ₃	3.18 [wt%]
MgO	0.07 [wt%]
MnO	1.49 [wt%]
CaO	16.99 [wt%]
Na ₂ O	1.74 [wt%]
K ₂ O	1.92 [wt%]
TiO ₂	0.45 [wt%]
P ₂ O ₅	0.15 [wt%]
Ce	53 [mg/kg]
Cr	34 [mg/kg]
Nb	< 7 [mg/kg]
Ni	15 [mg/kg]
Sr	373 [mg/kg]
V	52 [mg/kg]
Zn	59 [mg/kg]
Zr	259 [mg/kg]

* LOI = Loss of Ignition. It represents the amount (weight percent) of carbon elements within the specimen, which is lost by heating the specimen for 1.5 hours in an oven at 1050°C.

Table C.3: Richmond Hill soil mineral composition.

Mineral Content	Composition [wt%]
Quartz	33
K-Feldspar (microcline-dominated)	7
Plagioclase (albite-dominated)	20
Actinolite	2
Chlorite	29
Clay Minerals (illite-dominated)	3

REFERENCES

- [1] **Maggio, G. and Cacciola, G.** *When Will Oil, Natural Gas, and Coal Peak*. 2012, Fuel, pp. 111-123.
- [2] **Dincer, I., Dost, S. and Li, X.** *Performance Analysis of Sensible Heat Storage Systems for Thermal Applications*. 1997, International Journal of Energy Research, pp. 1157-1171.
- [3] **Dincer, I. and Rosen, M. A.** Thermal Energy storage (TES) Methods. *Thermal Energy Storage: Systems and Applications*. West Sussex : John Wiley & Sons Ltd., 2002, pp. 93-94.
- [4] **Nikolaev, I. V.** *An Experimental Study of Soil Thermal Conductivity Using a Guarded Hot Plate Apparatus*. Department of Mechanical and Industrial Engineering, Ryerson University. Toronto : s.n., 2007.
- [5] **Chapuis, S. and Bernier, M.** *Seasonal Storage of Solar Energy in Borehole Heat Exchangers*. 2009. Eleventh International IBPSA Conference. pp. 599-606.
- [6] **de Vries, D. A.** *Simultaneous Transfer of Heat and Moisture in Porous Media*. 1958, Trans. America Geophysical Union, Vol. 30, pp. 909-916.
- [7] **Luikov, A. V.** *Heat and Mass Transfer in Capillary Porous Bodies*. Oxford : Pergamon, 1966.
- [8] **Rieder, W. G. and Prunty, L. D.** *An alternative modeling procedure for describing coupled heat and mass transfer in semi-dry porous media samples*. 1997. ASME Fluids Eng. Division. Vol. 244, pp. 389-399.

- [9] **Thomas, H. R.** *Modeling two dimensional heat and moisture transfer in unsaturated soils, including gravity effects.* 1985, Int. J. Numerical and Analytical Methods in Geomechanics, pp. 573-588.
- [10] **Philip, J. R. and de Vries, D. A.** *Moisture movement in porous materials under temperature gradient.* 1957, Trans. America Geophysical Union, Vol. 38, pp. 222-232.
- [11] **Thomas, H. R. and King, S. D.** *Coupled heat and mass transfer in unsaturated soil—a potential-based solution.* 1992, Int. J. Numerical and Analytical Methods in Geomechanics, Vol. 16, pp. 757-773.
- [12] **Yonge, R. N., Xu, D. M., Mohamed, A. M. O., and Cheung, S. C. H.** *An analytical technique for evaluation of coupled heat and mass flow coefficients in unsaturated soil.* 1992, Int. J. Numerical and Analytical Methods in Geomechanics, Vol. 16, pp. 233-246.
- [13] **Thomas, H. R. and Ferguson, W. J.** *A Fully Coupled Heat and Mass Transfer Model Incorporating Contaminant Gas Transfer in an Unsaturated Porous Medium.* 1999, Vol. 24, pp. 65-87.
- [14] **Reddy, G. B.** *Analysis of Heat Transfer Characteristics of an Unsaturated Soil Bed: a Simplified Numerical Method.* 2001, International Journal of Energy Research, Vol. 25, pp. 1333-1344.
- [15] **Lee, I. M., Lee, H. J., Cheon, J. Y., and Reddi, L. N.** *Evaporation Theory for Deformable Soils.* 11, 2003, Journal of Geotechnical and Geoenvironmental Engineering, Vol. 129, pp. 1020-1027.

- [16] **Yu, M., Peng, X. and Fang, Z.** *Water transport in porous media at pore scale*. 2005, Laboratory of Phase Change and Interfacial Transport Phenomena, pp. 181-185.
- [17] **Dos Santos, G. H. and Mendes, N.** *Unsteady combined heat and moisture transfer in unsaturated porous soils*. 2005, J. Porous Media, Vol. 5, pp. 493-510.
- [18] **Prabhu, S. M. and Krishnan, S.** *Nonlinear two dimensional potential based study of coupled heat and mass transfer in a porous medium*. 2006, Microporous and Mesoporous Materials, Vol. 95, pp. 241-247.
- [19] **Balghouti, M., Kool, S., Farhat, A., Daghari, H., Belghith, A.** *Experimental investigation of thermal and moisture behaviors of wet and dry soils with buried capillary heating system*. 2005, Solar Energy, Vol. 79, pp. 669-681.
- [20] **Chen, Y., Shi, M. and Li, X.** *Experimental investigation on heat, moisture and salt transfer in soil*. 2006, International Communications in Heat and Mass Transfer, pp. 1122–1129.
- [21] **Bittelli, M., Ventura, F., Campbell, G. S., Snyder, R. L., Gallegati, F. and Rossi Pisa, P.** *Coupling of heat, water vapor, and liquid water fluxes*. 2008, Journal of Hydrology, pp. 191–205.
- [22] **Olguín, M. C., Salvadori, V. O., Mascheroni, R. H. and Tarzia, D. A.** *An analytical solution for the coupled heat and mass transfer during*. 2008, International Journal of Heat and Mass Transfer, pp. 4379–4391.
- [23] **dos Santos, G. H. and Mendes, N.** *Simultaneous heat and moisture transfer in soils combined*. 2006, Energy and Buildings, pp. 303-314.

- [24] **Heitman, J. L., Horton, R., Ren, T. and Ochsner, T. E.** *An Improved Approach For Measurment of Coupled Heat and Water Transfer in Soil Cells*. 2007, Soil Science Society of America Journal, pp. 872-880.
- [25] **Arfaei Malekzadeh, F. and Pak, A.** *A discretized analytical solution for fully coupled non-linear simulation of heat and mass transfer in poroelastic unsaturated area*. Tehran : s.n., 2009, International Journal of Numerical and Analytical Methods of Geomechanics, Vol. 33, pp. 1589-1611.
- [26] **Santander, R. E. and Bubnovich, V.** *Assessment of Mass and Heat Transfer Mechanisms in Unsaturated Soils*. 4, 2002, Int. Comm. Heat Mass Transfer, Vol. 29, pp. 531-545.
- [27] **Florides, G. A., Christodoulides, P. and Pouloupatis, P.** *An Analysis of Heat Flow Through a Borehole Heat Exchanger Validated Model*. 2012, Applied Energy, Vol. 92, pp. 523-533.
- [28] **Jalaluddin and Miyara, A.** *Thermal Performance Investigation of Several Types of Vertical Ground Heat Exchangers With Different Operation Modes*. 2012, pp. 167-174.
- [29] **Pertzborn, A., Nellis, G. and Klein, S.** *Impact of Weather Variation on Ground-Source Heat Pump Design*. 2, 2011, HVAC&R Research, Vol. 17, pp. 174-185.
- [30] **Lu, S., Lv, Y. and Zhang, X.** *Thermal Comfort Assessment and Energy Consumption Analysis about the System of Ground Source Heat Pump Combined with Radiant Heating/Cooling*. Zhenjiang : s.n., 2008, pp. 1158-1166.

- [31] **Choi, J. C., Lee, S. R. and Lee, D. S.** *Numerical Simulation of Vertical Ground Heat Exchangers: Intermittent Operation in Unsaturated Soil Conditions*. 2011, Computers and Geotechnics, Vol. 38, pp. 949-958.
- [32] **Dehdezi, P. K., Hall, M. R. and Dawson, A. R.** *Enhancement of Soil Thermo-physical Properties Using Microencapsulated Phase Change Materials for Ground Source Heat Pump Applications*. s.l. : Trans Tech Publications, 2012, pp. 110-116.
- [33] **Wang, H. and Qi, C.** *A Laboratory Experimental Study of High-Temperature Thermal Storage in the Unsaturated Soil Using A Vertical Borehole Heat Exchanger*. 2011, International Journal Of Low-Carbon Technologies, Vol. 6, pp. 187-192.
- [34] **Reuss, M., Bech, M. and Muller, J. P.** *Design Of A Seasonal Thermal Energy Storage In The Ground*. 4-6, 1997, Solar Energy, Vol. 59, pp. 247-257.
- [35] **Gauthier, C., Lacroix, M. and Bernier, H.** *Numerical Simulation Of Soil Heat Exchanger-Storage Systems For Greenhouses*. 1997, Solar Energy, Vol. 60, pp. 333-346.
- [36] **Reid, D.** *Guarded Hot Plate Apparatus Design and Construction For Thermal Conductivity Measurements*. Mechanical and Industrial Engineering, Ryerson University. Toronto : s.n., 2005. pp. 1-98, Thesis Report.
- [37] **Dadey, K. A., Janecek, T. and Klaus, A.** *Dry Bulk Density: It's Use and Determination*. 1992. Vol. 126, pp. 551-554.
- [38] **Soil Science Society of America**. [Online] 2012. [Cited: 01 24, 2012.] www.soils.org.
- [39] **Banin, A. and Amiel, A.** *A Correlation of Chemical Physical Properties of a Group of Natural Soils of Israel*. 1970, Vol. 3, pp. 185-198.

- [40] **Dahiya, I. S., Dahiya, D. J., Kuhad, M. S. and Karwasra, S. P. S.** *Statistical Equations for Estimating Field Capacity, Wilting Point, and Available Water Capacity of Soils From Their Saturation Percentage*. 1988, Journal of Agricultural Science, Vol. 110, pp. 525-520.
- [41] **Horton, R., Wierenga, A. and Nielsen, D. R.** *A Rapid Technique for Obtaining Uniform Water Content Distributions in Unsaturated Soil Columns*. June 1982, Soil Science, Vol. 133, pp. 397-399.
- [42] **Eching, S. O., Hopmans, J. W. and Wendroth, O.** *Unsaturated Hydraulic Conductivity from Transient Multistep Outflow and Soil Water Pressure Data* . 1994, Soil Science Society of America, Vol. 58, pp. 687-695.
- [43] **Salvas, R. J.** Standard Compaction Test. *Manual for The Measurement of Soil Properties In The Laboratory*. Toronto : s.n., 1991, pp. 43-45.
- [44] **de Vries, D. A.** *The Theory of Heat and Moisture Transfer in Porous Media Revisited*. 1987, International Journal of Heat and Mass Transfer, Vol. 30, pp. 1343-1350.
- [45] **Walker, W. R. and Sabey, J. D.** *Studies of Heat Transfer and Water Migration in Soils*. 1981, Colorado State University.
- [46] **Endo, A. and Hara, M.** *Simultaneous Measurement of Water Flux Density Vectors and Thermal Properties Under Drainage Condition in Soil*. 2007, Paddy Water Environ., Vol. 1, pp. 171-180.
- [47] **Endo, A. and Hara, M.** 2007, Paddy Water Environ, Vol. 5, pp. 171-180.
- [48] **Barua, R.** *Assessment and Energy Benchmarking for Two Archetype Sustainable Houses Through Comprehensive Longterm Monitoring*. Toronto : s.n., 2010. pp. 1-86.

[49] Daily data Report. *Environment Canada National Climate Data and Information Archive*. [Online] 2010.

http://www.climate.weatheroffice.gc.ca/climateData/dailydata_e.html?Prov=ON&StationID=5097&Year=2010&Month=8&Day=4&timeframe=2.

[50] Monthly Data Report. *Environment Canada National Climate Data and Information Archive*. [Online] 2011.

http://www.climate.weatheroffice.gc.ca/climateData/monthlydata_e.html?Prov=ON&StationID=5097&Year=2011&Month=6&Day=30&timeframe=3.